A Low Volume Oxygenator for Open Well Liver-on-a-Chip Tissue Culture

by

Daniel Rodion Rathbone

B.S., Yale University (2014)

Submitted to the Department of Mechanical Engineering
in partial fulfillment of the requirements for the degree of

Master of Science in Mechanical Engineering

at the

MASSACHUSETTS INSTITUTE OF TECHNOLOGY

February 2018

Author .....
Department of Mechanical Engineering
January 23, 2018

Certified by .....
David L. Trumper
Professor, Mechanical Engineering
Thesis Supervisor

Accepted by .....
Rohan Abeyaratne
Chairman, Department Committee on Graduate Theses
Graduate Officer

A Low Volume Oxygenator for Open Well Liver-on-a-Chip Tissue Culture

by

Daniel Rodion Rathbone

Submitted to the Department of Mechanical Engineering
on January 23, 2018, in partial fulfillment of the
requirements for the degree of
Master of Science in Mechanical Engineering

Abstract

MicroPhysiological Systems (MPS) show significant promise in speeding drug development and advancing basic research. They may serve better than animal models for obtaining accurate human response data and thereby reducing failed clinical trials. The CN Bio LiverChip is one such commercial MPS device which cultures liver cells on a perforated polystyrene scaffold and actively circulates cell culture medium through them. Reducing the total circulating volume is desirable to increase the concentration of difficult-to-detect compounds, improve autocrine signaling, and achieve more physiologically relevant drug decay times. However, achieving adequate oxygenation at lower volumes is challenging due to surface tension effects.

This thesis describes an open-well, flow-through MPS platform with a low-volume oxygenator, at a total circulating volume of approximately 500 µL. The oxygenator uses the interior corner of a hydrophillic spiral to constrain the circulating fluid and to create a thin fluid region, which decreases the diffusion depth relative to exposed surface area, thereby improving oxygenation. The oxygenator performs equivalently to the LiverChip at a fraction of the volume, and features a downward slope that prevents fluid from accumulating in the oxygenator, which could deplete the cell culture well. The fluidic configuration and other design considerations are described, as well as hardware testing results and improved methods for preventing fluid from bypassing the scaffold.

This project was supported by NIH grant number UH3-TR000496.

Thesis Supervisor: David L. Trumper
Title: Professor, Mechanical Engineering

Acknowledgments

I would like to express my gratitude for the assistance and good company provided by my lab-mates, both biological and mechanical. Specifically: Pierre S. Phabmixay introduced me to the LiverChip and its use, and ran the experiments which provided reference oxygen consumption data. Brij Bushan shared his indispensable experience with the existing hardware, and our discussions about oxygenation modeling directly informed the models presented here. Jun Young Yoon provided valuable comments to drafts of the manuscript. Timothy Kassis was generous with his time and experience, sharing institutional knowledge, relevant literature, and useful perspective.

I am particularly grateful to Professor Linda Griffith, for her vision and support, and to Professor David Trumper, for his experienced guidance, direct openness, and fruitful conversations.

Finally, I thank my parents, for modeling a practical, curious, and intellectually alive engagement with the world, and Ning Dai, for her enduring inspiration and support.

Contents

List of Figures

List of Tables

Chapter 1

Introduction

This thesis describes the process of developing an actively perfused cell culture platform capable of providing adequate oxygenation to 600k human liver cells in a 500 μL circulating media volume, as shown in Figure 1-1. The project is an extension of work done in the Griffith lab at MIT [1, 2, 3] that led to the LiverChip platform (CN Bio Innovations, Welwyn Garden City, UK), a commercial device with a circulating volume of 1.2 mL. The primary contributions of our new work are: (1) the development of a volume-limited free-surface oxygenator that maintains a defined fluid path even at very low volumes, (2) fluid flow configurations that allows this oxyygenator to interface with a cell culture scaffold, and (3) concepts and prototyping of sealing methods to prevent fluid from bypassing the scaffold in a more robust manner than in the existing LiverChip system.

This chapter provides motivation for the project and background relevant to the design, gives an overview of the design and preliminary testing that make up this thesis work, and describes the system-level requirements that apply to all of the subsystems described in subsequent chapters. Chapter 2 describes design and testing of the oxygenator, the design challenge central to this work. Chapter 3 describes development of the flow circulation configuration that connects the oxygenator to the cell culture environment. Methods considered for fixing the cell scaffold in place and preventing media from bypassing the cells are outlined in Chapter 4, and the integrated platform design is discussed in Chapter 5. Finally, in Chapter 6 we conclude

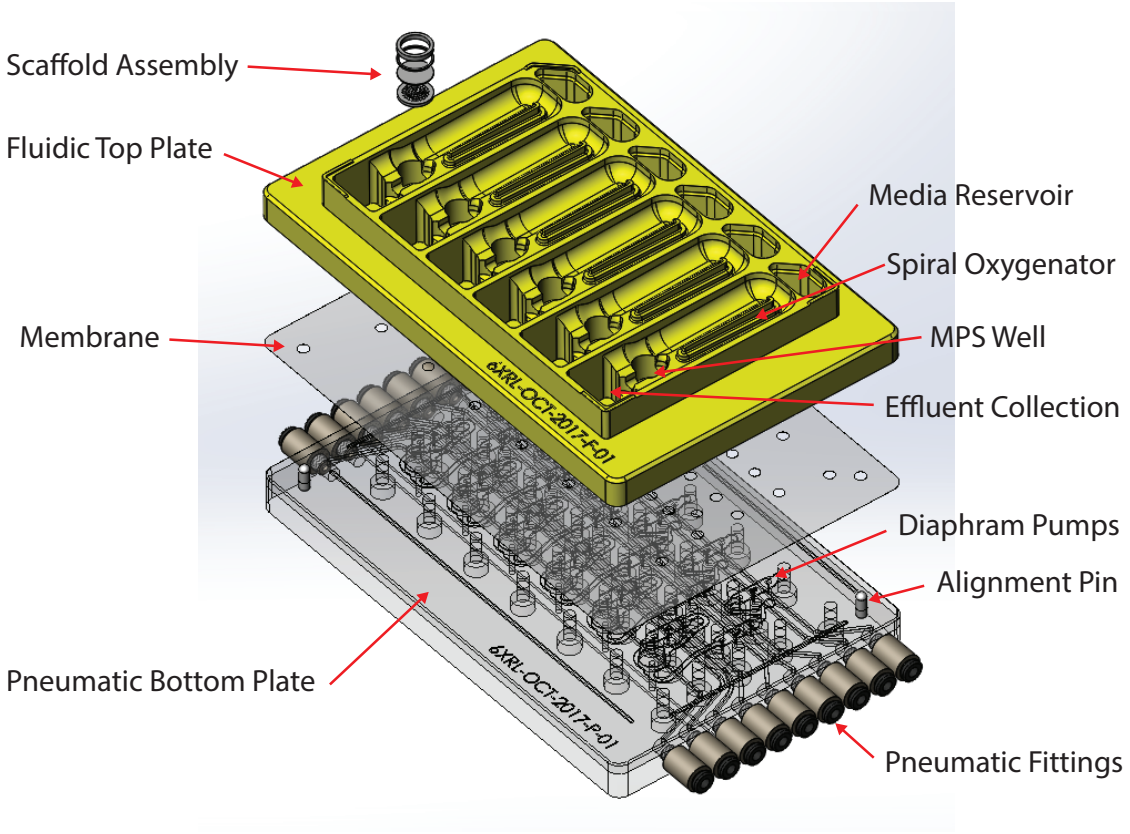

Figure 1-1: This CAD rendering shows the platform consists of a fluidic top plate (polysulfone) and a pneumatic bottom plate (acrylic) separated by an elastomeric polyurethane membrane. Each of six replicate lanes consists of an oxygenator spiral, an MPS well, and a supply and effluent reservoir for the programmable media exchange. Three diaphragm pumps per lane control media exchange, oxygenator flow rate, and the MPS flow rate (perfusion rate through the scaffold), respectively. The pneumatic channels are coupled across lanes, so the flow rates in each lane are nominally the same for a given one of the three functions. A standard tissue culture lid (not shown) covers the wells to reduce contamination risk.

with specific suggestions for future development, including a fluidically closed system that would allow further reduced circulating volumes.

1.1 Open-Well MicroPhysiological Systems

In the long and costly process of developing a new drug, an important challenge is screening drugs for toxicity and efficacy before clinical trials. Animal models are limited in their translation to human physiology, which has caused failures in clini-

cal trials and may cause viable drugs to be rejected [4]. MicroPhysiological Systems (MPS), or small-scale *in-vitro* systems that recapitulate some aspect of human physiology with human cells, show significant promise for drug screening assays as well as applications in basic research [4, 5].

Open-well systems culture cells in a manner that allows ready access to the cells, and has an unconstrained fluid-air interface. Closed-volume systems, by contrast, offer contained volumes that allow easier fluid handling, but access to the cells is often more difficult.

The Griffith Lab has developed multiple open-well platforms with on-board pumping that allow easy access to the cells for seeding, sampling, or transfer to and from the platform, using either standard Transwell-type cell culture inserts or an actively perfused scaffold [1, 2, 6]. CN Bio Innovations has commercialized one of these platforms as the LiverChip, which consists of 12 replicate lanes, each perfusing media through a polystyrene scaffold on which the hepatocytes (liver cells) are grown.

1.2 Motivation for Low Circulating Volumes

The LiverChip perfuses the cells with a circulating volume of 1.2 mL of growth medium, which contains nutrients and growth factors, and which transports oxygen from the free air-liquid interface to the cells. A smaller circulating volume is desirable to avoid the dilution effect of larger liquid volumes for three reasons: (1) biomarkers produced in low quantities will be easier to detect; (2) intercellular communication will be promoted if autocrine compounds are less dilute; (3) less drug mass will be required to achieve the same initial concentration, and the drug exposure over time will be closer to that for humans *in vivo*.

The main challenge with reducing volume in an open well format is the dominance of surface tension at small length-scales. Simply putting less medium in the LiverChip causes the fluid to wet the corners of the oxygenator channels, no longer providing the surface area required to adequately oxygenate the cells. A 500 μL target is less than half the LiverChip circulating volume, and we estimated this is about as low as

we could achieve in an open-well format. Circulating volumes less than 500 μL will likely require moving to a closed-volume format, concepts for which are presented in Chapter 6.

1.3 Oxygenation Approaches

Oxygenating cell culture media can be broadly divided into two approaches: 1) solid-liquid interface, such as membrane oxygenation, and 2) gas-liquid interface, such as culturing in a static dish or bubbling a gas through the liquid (sparging). Microcarriers that simulate the oxygen-storing capacity of hemoglobin in the blood have been described [7, 8]; while these allow greater oxygen storage density, the oxygen must still be replenished for long-term culture.

1.3.1 Solid-Liquid Interface

Many microfluidic and organ-on-chip systems are fabricated from PDMS (Polydimethylsiloxane, a silicone rubber). PDMS can be poured into 3D printed molds with fine feature resolution, which allows for faster prototyping than with materials that require machining or etching. It can be bonded to itself and to glass by plasma surface activation, it is relatively biologically and chemically inert, and it is highly permeable to oxygen relative to other polymers [9]. This last property has led to the use of thin PMDS membranes in extracorporeal membrane oxygenators (ECMO) used in medical contexts to oxygenate blood [10, 11]. Many microfluidic oxygenators and cell culture devices also use PDMS as the bulk material, membrane material, or both [12, 13, 14].

While its fabrication and gas transport properties are favorable, PDMS is severely limited in contexts where measurement or control of lipophillic drug, drug metabolite, or biomarker concentrations are important, as required in many MPS devices [5]. These compounds both adsorb onto and absorb into PDMS, making the concentration in the local cell environment difficult to predict, measure, or interpret [15]. The platform described in this thesis is ultimately intended for experiments where

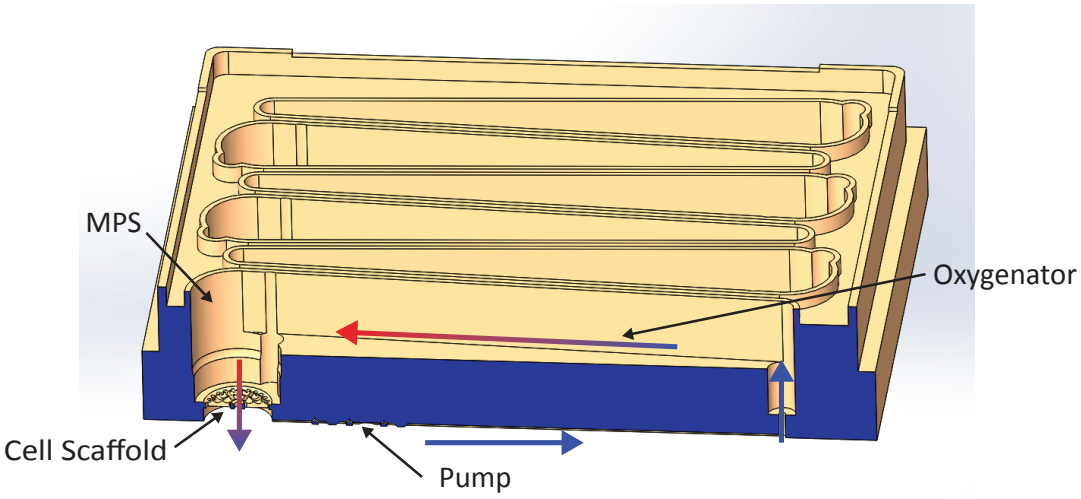

Figure 1-2: Cross-section showing inline circulation on the CN Bio LiverChip during downward flow. The oxygenator consists of a wide channel with enough exposed surface area to oxygenate the media as it travels back to the MPS.

such binding is not acceptable. For our purposes, oxygenation membrane materials are therefore effectively constrained to nano-porous Polycarbonate [16], micro-porous polypropylene or PTFE [17], or diffusive Dupont Teflon AF [17], which are minimally interactive.

1.3.2 Gas-Liquid Interface

The standard approach for oxygenation of open-well static culture is by passive diffusion through an exposed surface. A culture lid increases sterility but allows oxygenation by overhanging the edge of the dish or well-plate; oxygen diffuses up the vertical air column, but bacteria, which sink in still air, are passively excluded. The primary factor affecting oxygenation is then the surface area of the air-medium interface relative to the depth of diffusion.

This passive interface oxygenation method has been used for open well systems with active circulation and mixing [6], as well as active perfusion through cell scaffolds [2]. The LiverChip platform uses a "tail," a shallow elongated channel that increases the exposed surface area, to provide oxygenation (see Figure 1-2). Inman [1] describes the development of these oxygenator channels in more detail.

Several methods have been described to increase oxygen uptake in a free-surface

cell culture environment, such as roller bottles, shakers, other agitation methods [18], but these are not feasible options for very low fluid volumes. Sparging (bubbling gas through a reservoir of the fluid to be oxygenated) can increase gas-liquid surface area by introducing small bubbles, but this also requires a reservoir of medium and a method of containing the foaming that can be produced.

1.4 Project Summary

The objective of the work described in this thesis is to **design an organ-on-chip platform capable of adequately oxygenating and culturing at least 250k rat or 600k human liver cells in a flow-through, open-well environment with a total circulating volume of 500 μL or less.** Specific functional requirements of the system are described in Section 1.5, after the following overview.

1.4.1 System Overview

The Six-replicate Reduced-volume Liver (6xRL) platform developed for this thesis is shown in the photographs in Figure 1-3. This new platform uses a format similar to other devices from the Griffith lab [2, 6], with a non-sterile acrylic pneumatic plate and a sterile polysulfone fluidic plate separated by a sterile polyurethane membrane, which allows circulation of the media in the fluidic plate by means of pneumatic diaphragm pumps, shown in Figure 1-4. A media exchange system, consisting of a fresh media reservoir, a pump, and passive spilling into an effluent collection reservoir, replenishes nutrients and flushes out waste products. The platform configuration is shown in Figure 1-1, and the integration of the system components is discussed in Chapter 5.

To oxygenate the media through a free air-liquid interface while constraining the fluid path and limiting the volume that can collect in the oxygenator, we invented a spiral oxygenator that captures the fluid in the corner of a spiral cut into hydrophillic polysulfone, as shown in Figure 1-5. The corner serves to limit the maximum thickness of fluid that oxygen must diffuse into, and the spiral provides enough length in a small

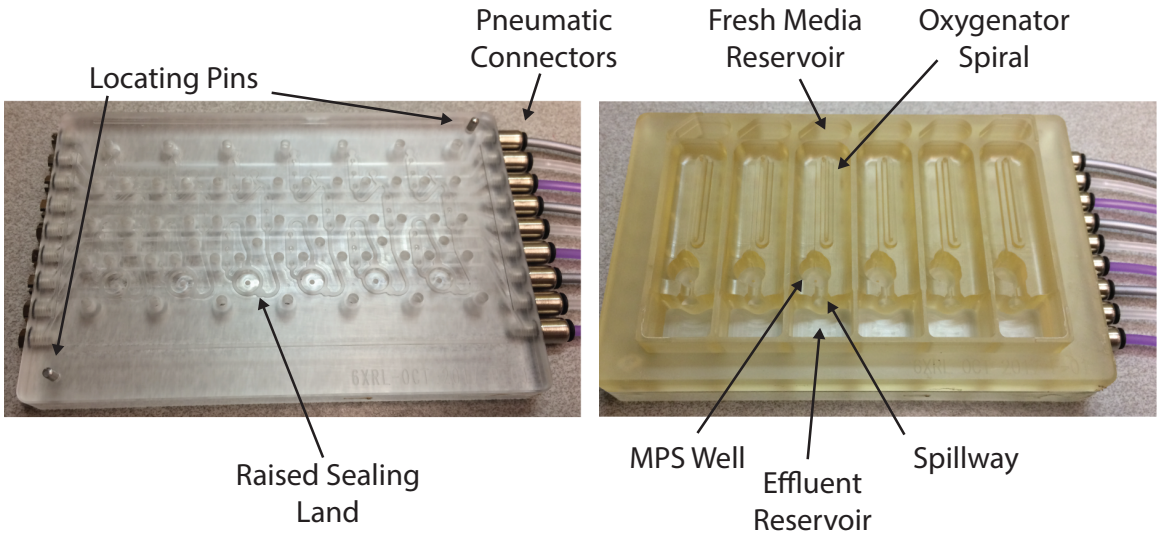

Figure 1-3: A photograph of the 6xRL revision 2 platform. The acrylic pneumatic plate is shown at left, and the fluidic top plate is shown at right.

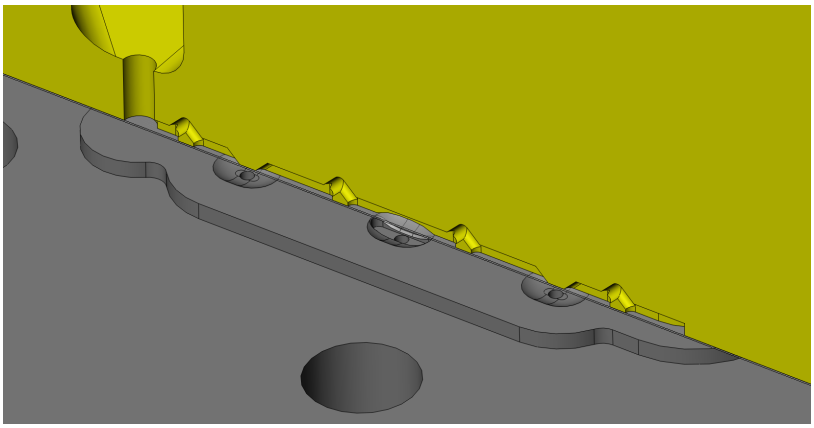

Figure 1-4: A section of the diaphragm pump geometry. A central pump chamber and two valves allow for bi-directional volume-determined flow. See Inman [19] for detail on the pump operating principle.

footprint for the fluid to exit the spiral adequately oxygenated. The oxygenator is discussed in detail in Chapter 2.

The cell seeding protocol requires that flow be down through the cell scaffold, which is shown in Figure 1-6, for the first eight hours to allow cells to attach, and then upwards for the remainder of the experiment to prevent the cells from occluding the scaffold channels. To allow the oxygenator to self-empty (thereby preventing volume from accumulating in the oxygenator and allowing the cells to dry out), the oxygenator

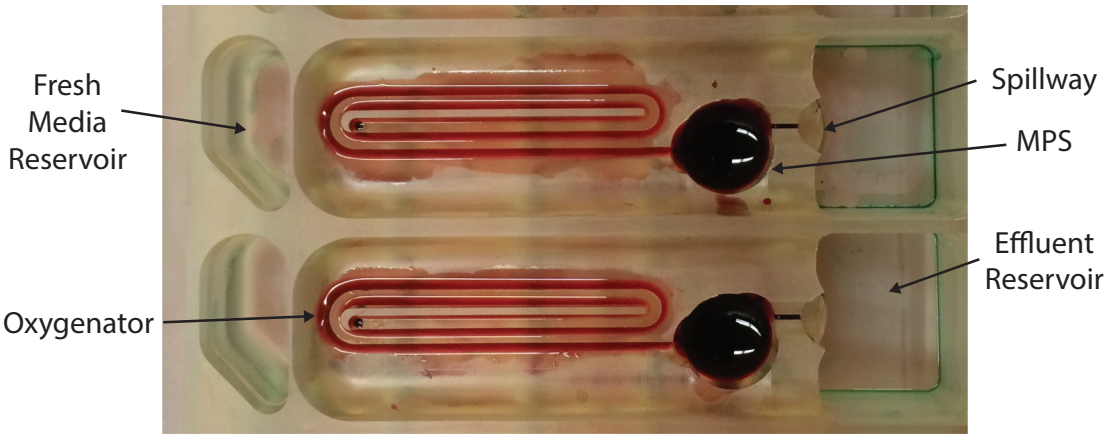

Figure 1-5: The revision 2 oxygenator. Fluid (dyed red) enters the oxygenator through the hole at left and flows counter-clockwise down a descending spiral through a channel formed by surface tension forces pulling fluid into a corner. The fluid spills over into the MPS well, and the continuous fluidic connection ensures a pressure drop ρgh that prevents fluid from accumulating in the oxygenator, and also serves to thin out the fluid profile, thereby decreasing diffusion depth and improving oxygenation.

is used in unidirectional flow circuit which is separated from the bidirectional scaffold perfusion flow circuit. To maximize the oxygenation of the media going to the cells during upward flow, the media intake is placed directly under the oxygenator output. To maximize the oxygen uptake in the oxygenator, the oxygenator intake is located on the opposite end of the MPS, where the concentration is expected to be lower. A schematic of this "selective sourcing" flow configuration is shown in Figure 1-7. This and other configurations we considered are discussed in Chapter 3.

On the LiverChip, the scaffold is held in place with a polypropylene retaining ring that is slightly larger in diameter than the well it sits in (see Figure 1-6 on the left). Because this ring does not create any defined seal, fluid has been observed to flow around the scaffold when using scaffolds of higher flow resistance than the standard one. This is resolved in our new design by using a chamfered retaing ring and a Viton gasket, a configuration which can seal up to 40 kPa, well above the anticipated pressure drop. Alternative designs for securing the scaffold, including promising non-elastomeric methods worth future consideration, are discussed in Chapter 4.

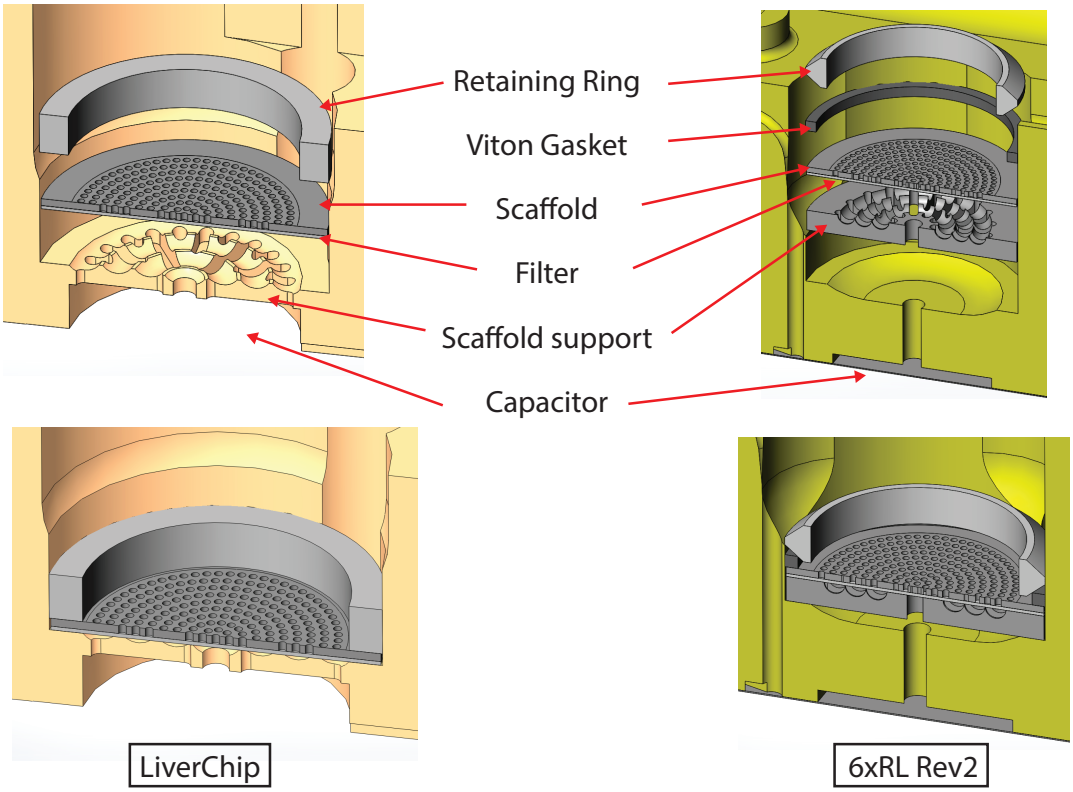

Figure 1-6: The scaffold assembly for the LiverChip (left) and reduced volume Rev2 platform (right). Both platforms use the same polystyrene scaffold (CN Bio Innovations, Welwyn Garden City, UK) and filter (Durapore 5 μm SVPP membrane filter, MilliporeSigma). Cells are initially seeded above the scaffold while the fluid is flowing downward and collect in the scaffold pores where the filter prevents them from passing through. The scaffold support prevents the filter from deflecting, which would allow the cells to move in between the filter and scaffold. After eight hours, the cells have attached to the scaffold walls and the flow is reversed to prevent cell growth from clogging the pores. The retaining ring holds the assembly in place and is intended to prevent fluid from flowing around the scaffold and bypassing the cells. The Rev2 assembly improves this sealing function by using a Viton gasket. The membrane capacitor, in combination with the filter and scaffold resistance, reduces the pulsatility of the flow, reducing the peak pressure below the scaffold (the membrane is not shown for the LiverChip on the left).

1.4.2 Results

Full characterization of the device is not yet possible due to the pneumatic channels fracturing during manufacturing. A revised version that is expected to solve this problem is not yet fabricated at the time of writing. Characterization of the

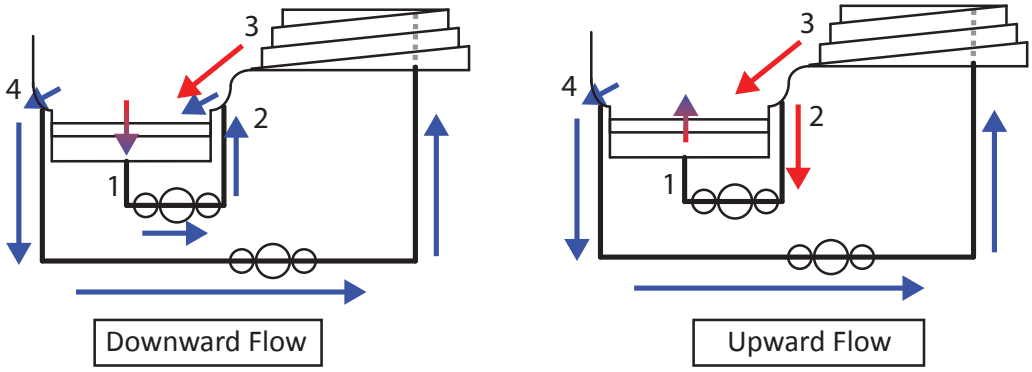

Figure 1-7: Selective sourcing. During seeding, media flows down through the cells, where oxygen is consumed, then from 1 to 2. A mixture of media from 3 (high oxygen concentration) and 2 (low concentration) then flow both back through the cells, and also to 4, which feeds the oxygenator. After flow reversal, the cells are fed by media sourced from 2, which is a mix of high concentration from 3 and low concentration from the cells. The position of 2 directly under the oxygenator output 3 increases the ratio of high to low concentration media, so the cells see an oxygen concentration above the bulk average in the well. At the input to the oxygenator (4), the opposite occurs, pulling media that is below average oxygen concentration.

oxygenator and selective sourcing layout were, however, possible.

The 6xRL revision 2 oxygenator performed better or the same as the CN Bio LiverChip, but with better control of the fluid at less than a quarter of the volume held in the oxygenator (we estimate closer to one eighth). The oxygen concentration that actually reaches the cells, however, depends the flow direction. For downward flow, a conservative fully mixed model in Chapter 3 suggests that the oxygen concentration going to the cells in steady-state will be a maximum of 125 μM, which does not meet the 150 μM requirement. After 8 hours, when upward flow begins, an experiment with the revision 1 6xRL prototype indicates that the requirement will be met and oxygenation will be better than on the LiverChip for the remainder of the experiment. The circulating volumes are within 50 μL of the 500 μL target.

Several methods of sealing the scaffold were explored. The elastomeric approach was chosen as the best initial solution, as it is readily implemented and satisfies the sealing requirement of 40 kPa. However, experiments involving compounds that

adsorb to Viton may require a different sealing approach.

The other design requirements described in this thesis were met either by our new designs or by using existing approaches that have been proven on similar platforms, such as the pneumatic pumping or existing sterile technique.

1.5 System Design Requirements

Together with the background presented above, the requirements presented in this section provide context for the platform design. These requirements relate to the overall function of the device, and hold across the different sub-systems.

1. ***Device must be cell- and drug-compatible***

   The need to avoid cytotoxicity and absorption of lipophilic drugs narrows the range of allowable materials for media-contacting components. Further, the platform material must be sterilized; steam (autoclave) is preferable for its convenience and speed, but other methods may be used if required. The existing reusable organ-on-chip platforms used by the Griffith lab are machined from autoclavable Polysulfone (PSU) with a thermoplastic polyurethane (TPU) membrane sterilized by ethylene oxide gas (EtO); other acceptable materials include teflon/PTFE, polystyrene, COC, and stainless steel.

2. ***The total circulating volume should be less than 500 μL***

   Given the benefits of lower media volume described above, 500 μL is chosen as close to the minimum volume achievable with an open-well platform.

3. ***The platform should provide controlled media exchange with at least 500 μL capacity***

At lower volumes, the depletion of nutrients by the liver cells and accumulation of waste products becomes more significant, and batch media exchange (full removal and replacement of media at one time, as is done on the LiverChip), may cause unwanted spikes in metabolic activity. Continuous or programmable media exchange is therefore desired to replace the media more frequently. 500 μL would allow for replenishment of the media reservoir daily.

4. ***Sterility of media must be maintained during operation***

   Cell seeding and media exchange can be done in a sterile Biological Safety Cabinet (BSC) with standard precautions. The platform will therefore need to be transported between incubator and BSC without contamination, as is required with the earlier platform designs.

5. ***The platform should be compatible with a standard tissue culture lid***

   If no oxygen measurement is required, the platform should be compatible with standard pre-sterilized lids. The current lid used with the LiverChip platform is the Costal universal lid (Corning Product #3099).

6. ***The platform should integrate with existing pneumatic infrastructure***

   To simplify use in the Griffith lab, the platform should be compatible with 1/8th inch OD pneumatic tubing and driven by the existing pneumatic controllers, as used in earlier platforms.

These requirements constrain the materials and workflow of the design, as well as how the different subcomponents integrate with each other. In the following chapters, we present the different subsystems and their own specific requirements, beginning with the requirements, design, and testing of the oxygenator.

Chapter 2

Low-Volume Oxygenator

The oxygenator design is the central challenge of this thesis, and is critical to the goal of culturing hepatocytes at low circulating volumes. In this chapter, requirements for the oxygenator are listed (Section 2.1), followed by concepts (Section 2.2), concept selection (Section 2.3), prototyping (Section 2.4), modeling of the oxygen diffusion process within the oxygenator (Section 2.5), and testing (Section 2.6).

2.1 Oxygenator Requirements

The requirements that informed the oxygenator design processes are described below.

1. ***Oxygenation Potential (ϕ) greater than 0.8 at 1 μL/s***

   This requirement aims to ensure that the oxygenator performs as well as, or better than, the CN Bio LiverChip oxygenation channel, which is taken as a benchmark. The oxygenation potential ϕ, described in more detail in Section 2.5, is defined as the change in oxygen concentration ($C_{high} - C_{low}$) across the oxygenator, normalized by the maximum possible change ($C_{sat} - C_{low}$):

$$\phi \equiv \frac{C_{high} - C_{low}}{C_{sat} - C_{low}}. \tag{2.1}$$

Here, C_{low} is the oxygen concentration at the oxygenator inlet, C_{high} is the concentration at the outlet, and C_{sat} is the fully saturated concentration. The parameter ϕ is a non-dimensional measure of oxygenator efficiency that varies from 0 to 1. It will be demonstrated in Section 2.5 that ϕ is flow-rate dependent, but independent of inlet concentration. In an experiment with 250,000 rat hepatocytes (described in appendix C), the oxygenation potential of the LiverChip was determined to be 0.8 at 1 μL/s. This value is used as a benchmark. After the oxygenator design was developed it became clear that during the initial eight hour cell seeding period, $Q\phi \geq 4$ μL/s is a better equivalency requirement, while the $\phi \geq 0.8$ requirement is appropriate after seeding. See Sections 3.4 and 3.6 for more details, and a discussion of mixed vs. inline configurations).

2. ***Bubble clearing***

   Gas bubbles trapped under the scaffold can cause cell death by displacing media and therefore starving the cells, and can also cause increased fluid shear stresses, as the same volume flow rate of liquid passes through a smaller area. To lower this risk, the media exiting the oxygenator should be bubble-free.

3. ***Flow should resume without depleting the MPS volume after stopping for 5 minutes***

   During an experiment, the oxygenator will not be stopped for more than approximately one minute. The cells must remain oxygenated, so transportation of the chip between incubator and bio-safety cabinet must be brief, and both locations must have pumping capability. The cells' need for oxygen therefore limits the duration that the oxygenator can be stagnant. Five minutes is chosen as a requirement with an acceptable safety margin.

Spontaneous wetting of a dry oxygenator path is ideal, but not strictly necessary. Propagation of the fluid path along a dry channel is a constant balance of forces. If advancing the fluid front requires substantial pressure behind it due to hydrophobicity, the advancing channel of fluid can hold significant volume and potentially spill in undesired directions. This volume must also not be so great as to deplete the MPS and dry out the cells. Further, after an initial priming, the oxygenator must not run dry, even after a five minute duration of stopped flow.

4. ***Volume-limited***

   To avoid storing fluid volume and therefore depleting the MPS and risking cell death, the oxygenator must not allow excess volume to accumulate.

2.2 Oxygenator Concepts

The following concepts were considered as methods to oxygenate media before returning it to the cells. General considerations are listed for each concept in this section. In Section 2.3, the concepts are compared against both system-level and oxygenator-specific requirements .

2.2.1 Oxygen Permeable Membrane

Many oxygenation methods for closed systems use permeation of oxygen through a membrane interface that contains the fluid and separates it from an external environment. The membrane can be flat, with shallow channels guiding fluid against it, or tubular, with fluid either inside or outside the tube. Extracorporeal membrane oxygenation (ECMO) and existing microfluidic devices [10, 11, 20] offer inspiration for possible configurations.

Cross-membrane and free-surface oxygenation approaches are limited by the effective diffusion distance and by the surface area of the interface. Membrane oxygenation is additionally limited by the rate of oxygen permeation through the membrane material, which must be biologically inert, non-sorptive of a wide range of drugs and biomarkers, non-permeable to liquid, and highly permeable to oxygen. One such material that has been used in cell culture applications is DuPont Teflon AF-2400 [17], but at a cost of approximately $30,000 per kg for raw material (quoted June, 2017 by Biogeneral, San Diego, CA) plus tooling costs. Alternatively, using a polyurethane membrane currently in the platforms developed by the Griffith Lab [2, 6] offers an opportunity to reduce cost and complexity, but the thickness required for pumping and sealing leads to very slow permeation. Pressurized air or pure oxygen could accelerate oxygen permeation across a membrane, but introduces other setup and safety concerns.

2.2.2 Interior Corner

The interior corner concept (Figure 2-1) makes use of the tendency of a wetting fluid to pin to interior corners. In the LiverChip, where the oxygenator is simply a wide, open channel, if the fluid height is decreased past a certain threshold, the fluid clings to the corners, dramatically reducing the surface area available for oxygenation, and creating unpredictable performance. This concept takes advantage of this phenomenon to constrain the fluid in a predictable geometry, so that the oxygenator length can be designed deterministically to meet the system needs. One additional requirement for predictable geometry is the downward slope of the flow path: the negative pressure pulls the fluid tightly into the corner, rather than expanding arbitrarily outward.

The interior corner was originally conceived as a grooved switchback path carved into a downward sloping ramp, but the fluid behavior at the switchbacks is difficult to predict, and was thought to be less robust than the corner path itself. A spiral ramp (Figure 2-2) resolves this issue, allowing a long, continuous corner to fit in a more contained footprint.

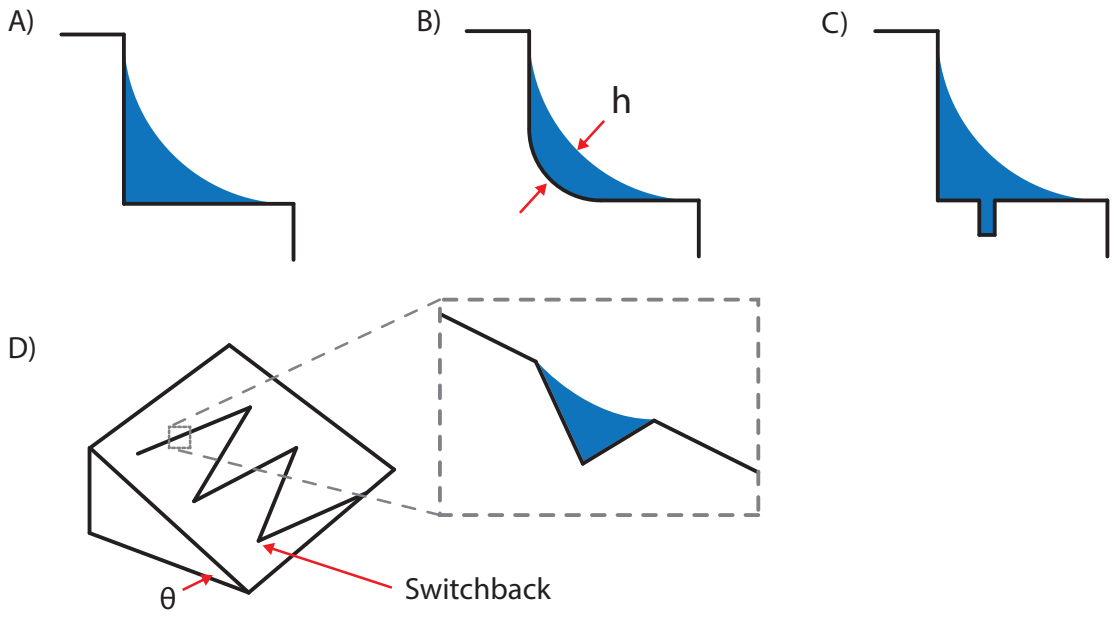

Figure 2-1: *A)* As fluid wets an inside corner of a hydrophillic surface, surface tension thins the fluid into a curved profile, both limiting diffusion distance h and constraining the fluid path. *B)* A radius on the internal corner can reduce the effective diffusion length even further. *C)* If the material is not sufficiently hydrophillic to fill spontaneously, a groove causing spontaneous capillary flow can aid rapid wetting of the full surface. *D)* The corner can be cut into a downward sloping surface, ensuring that the oxygenator is self-emptying. For compact packaging, the path may need to double back on itself with some sort of switchback, but it is difficult to manage flow at the switchback corner.

The aim in making an efficient oxygenator is to decrease the diffusion path relative to the interface area. The diffusion length scale can be further reduced in this configuration by introducing a corner radius that is smaller than the fluid interface radius.

Spontaneous capillary flow (SCF), if not achieved by the contact angle and corner geometry alone, can potentially be achieved through a narrow triangular groove such that the groove half-angle and the fluid contact angle sum to less than 90 degrees [21]. As an alternative, the conditions for an SCF channel are described by Berthier et al. [22].

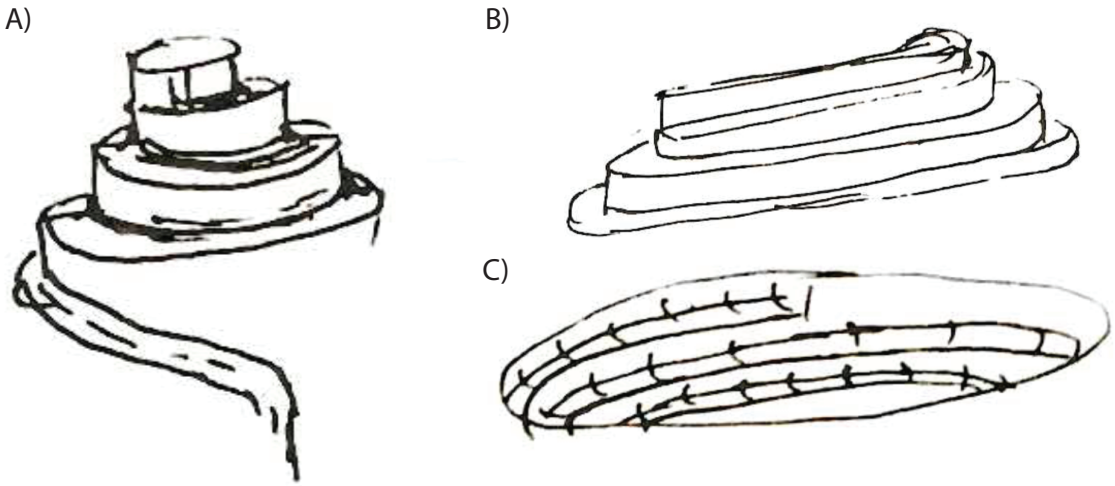

Figure 2-2: To avoid the potential instabilities associated with switchbacks, the interior corner can be packaged in a spiral. *A)* An exterior spiral maintains fluid continuity, and a pressure drop from top to bottom keeps the fluid profile tight in the corner. *B)* The exterior spiral can be elongated to improve packaging. *C)* An interior spiral is an alternate configuration, though there may be a tendency for fluid to pool at the bottom.

2.2.3 Exterior Corner

The phenomenon of a wetting fluid being contained by a sharp edge [23] can be used to create a fluid path suitable for oxygenation, as shown in Figure 2-3. One potential risk is spilling over the edge of the corner. This might be mitigated with an inverted configuration, where the fluid is suspended from a sharp-edged protrusion. In either case, this concept seemed less robust than others, and so was not pursued in detailed designs.

2.2.4 Channel

The LiverChip uses a channel with a free surface to oxygenate the circulating media, though with over two times the volume targeted for this project. Doing so at lower volumes might be accomplished with a long, shallow channel (Figure 2-4). However, there are several drawbacks. The channel cannot be much wider than the capillary length (approximately 2.5 mm) or fluid will separate and cling to the corners. Additionally, the height of fluid in the channel (and therefore diffusion length) is

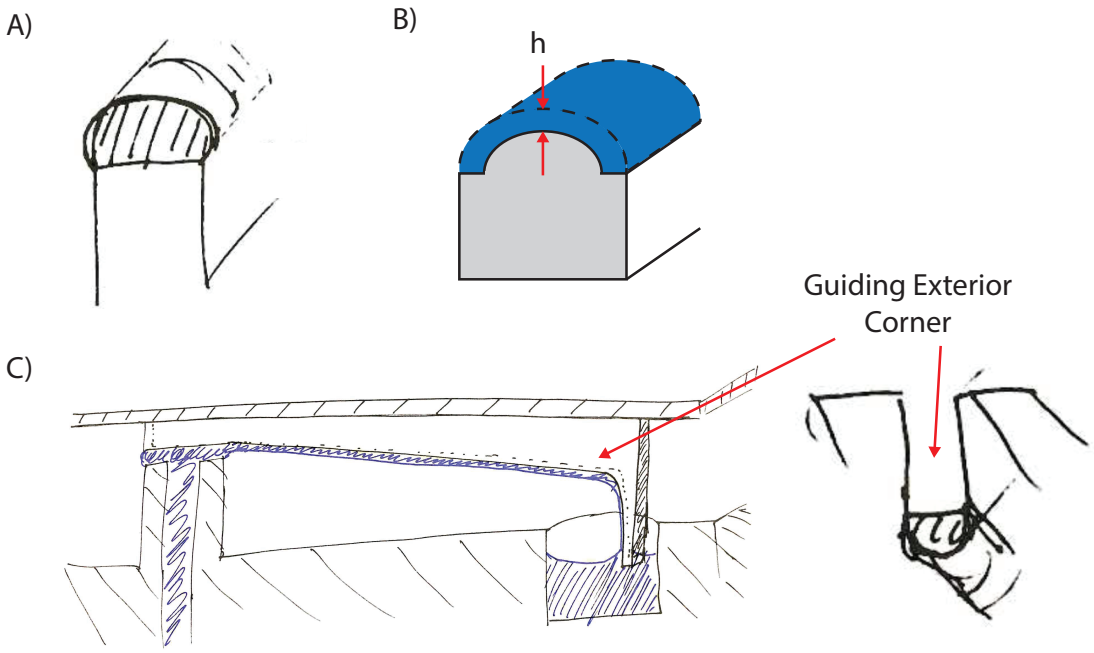

Figure 2-3: *A)* The exterior corner concept uses a sharp exterior edge to contain fluid expansion and guide it along an oxygenation path. *B)* As with the interior corner, a feature could be introduced to the flow path to reduce the effective diffusion length. *C)* The concept could also be inverted, suspending the flow from a guiding path on the lid.

difficult to define, especially if the fluid pins to the top edges of the channel. The diffusion length is likely to be larger relative to the air contacting surface area than for the interior or exterior corner, reducing the oxygenation effectiveness relative to those concepts.

2.2.5 Filament

If fluid can be arranged to flow down a wetted filament (Figure 2-5, similar to condensation running down the exterior of slanted pipes and eventually dripping at a local minimum), the potential to spiral the filament may enable a more compact design than other concepts. The filament could be formed into the desired geometry, and either removed for sterilization or disposed of after each use. However, this concept does require an additional component, marginally increasing cost, logistical overhead, and setup time, similar to a membrane (though attachment could be much

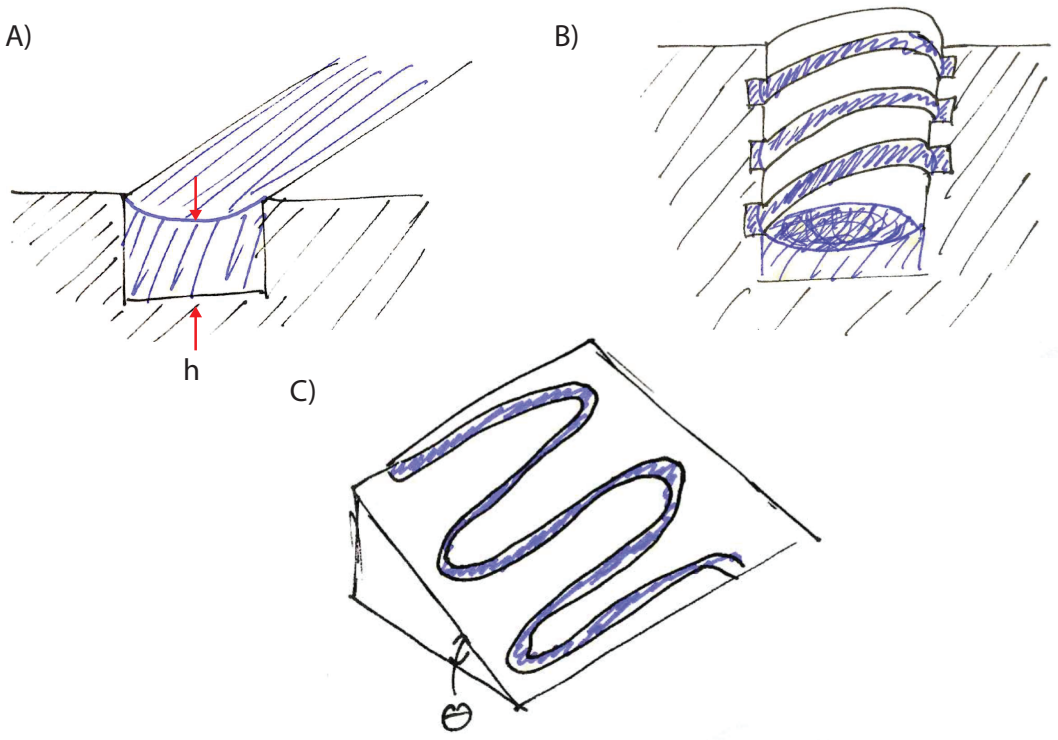

Figure 2-4: *A)* The channel concept uses a channel to guide the fluid flow. *B)* This channel could be spiraled around the interior of a well. *C)* The channel could snake back and forth down a ramp inclined anywhere from 0 degrees (flat) to 90 (vertical wall) to 180 (suspended upside-down).

simpler than sealing a membrane, and priming the fluid path to ensure wetting could be accomplished by dipping the apparatus in sterile BSA solution).

2.2.6 Gap-spanning

Similar to the filament concept, if two filaments are placed in closer together than the capillary length the fluid paths may join to form a fluid bridge (Figure 2-6). This would increase further the exposed interface area relative to the diffusion depth for a given length of the oxygenator. The angle of each gap edge should be chosen with the contact angle of culture medium on that material in mind so as to make a fluid bridge energetically favorable, and thus make it form reliably.

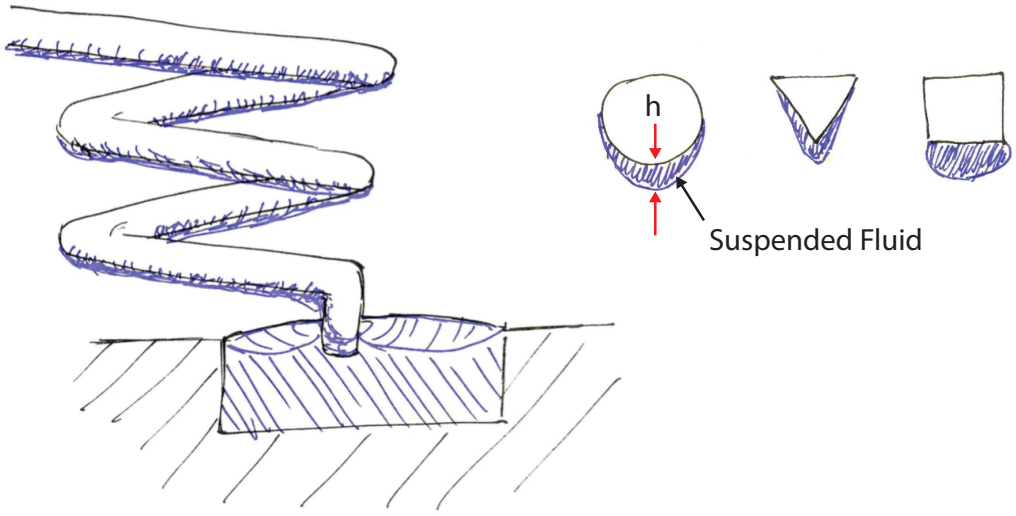

Figure 2-5: The filament concept, similar to the inverted exterior corner concept in Figure 2-3-C, uses the suspension of fluid from a feature to constrain the fluid path and provide oxygenation. The filament has the advangage of wrapping over itself in a spiral (left), allowing for tighter packaging. The filament cross section (right) could be round or angular.

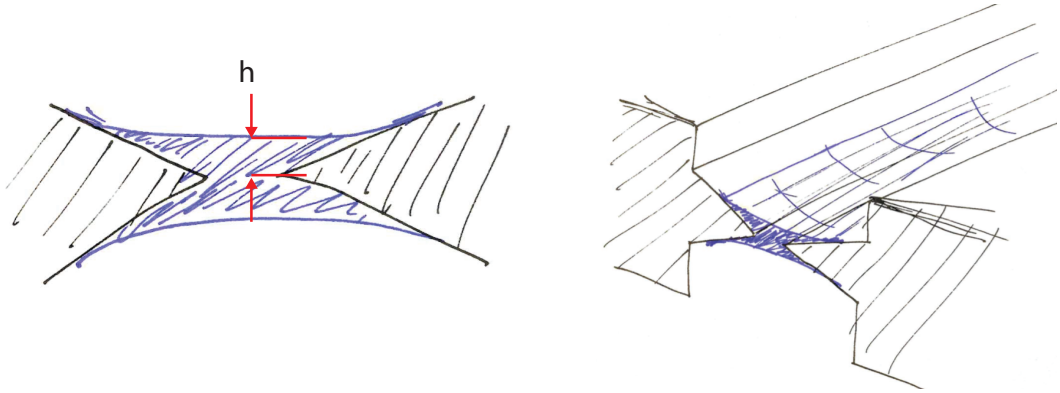

Figure 2-6: The gap-spanning concept consists of two hydrophillic angled features with a gap between them. When fluid bridges this gap, surface tension pulls it into a tight profile (right). The maximum diffusion distance h is further reduced by symmetry, if the fluid is oxygenated from both sides (left).

2.2.7 Droplets

The diffusion length of oxygen through the culture media could be limited by forming small droplets which then drip into a collector and feed back into the cell culture well (Figure 2-7). To keep pace with the oxygen consumption of the hepatocytes, an

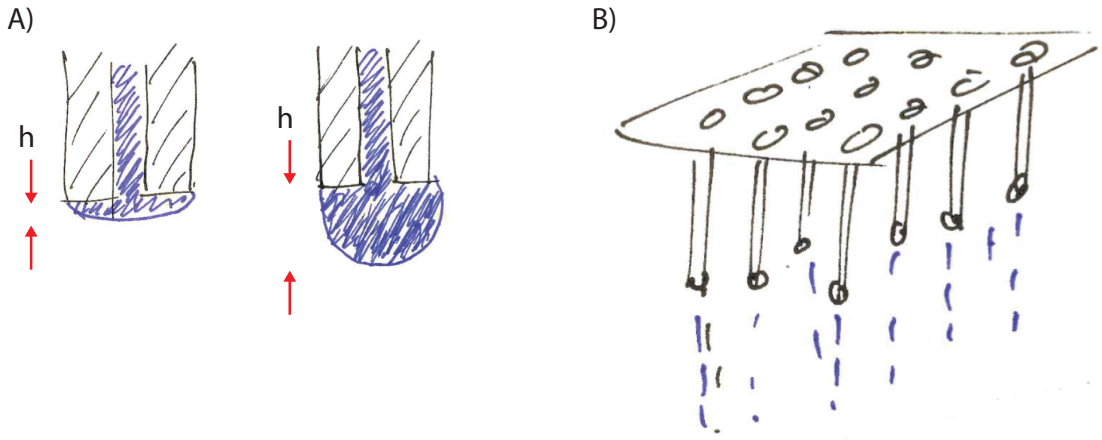

Figure 2-7: The droplets concept relies on the short diffusion distance during the initial formation of a droplet (left). The maxiumum diffusion distance over time will be the droplet radius. To maintain small droplets while allowing reasonable flow rates, an array of many droplet generating outlets could be used (right).

array of multiple sources might be required as shown in Figure 2-7-B. However, this concept involves substantially more manufacturing and sterilization complexity than the others.

2.2.8 Surface Modification

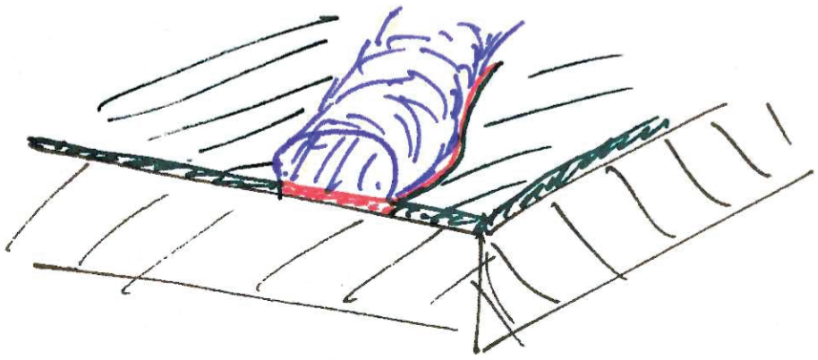

Figure 2-8: Fluid could concievably be constrained and guided by an interface between hydrophillic surface treatment (red, under the fluid path) and hydrophobic surface treatment (green).

A barrier between hydrophillic and hydrophobic regions by some method of surface

modification could be used as a method of steering fluid in a long path (Figure 2-8). This concept was not pursued due to concerns about robustness and the development effort and compromises involved in the surface treatment. If appropriate surface treatments are developed, perhaps to satisfy other requirements, this concept may become compelling.

2.2.9 Successive Barriers

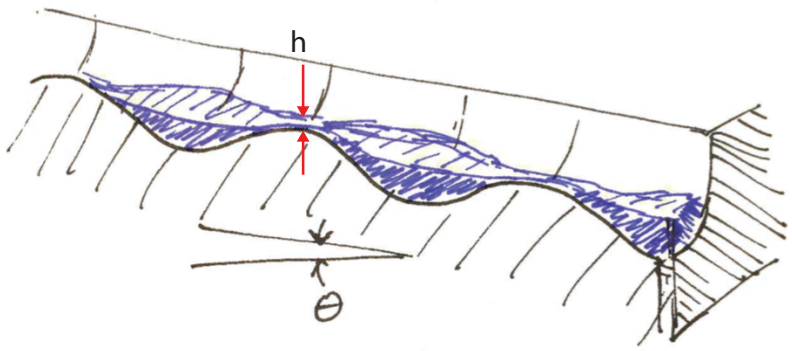

Figure 2-9: This concept uses successive barriers to thin out the fluid profile, reducing diffusion distance at the barrier, while using intermediate reservoirs to stabilize the flow, since a thin film longer than the capillary length (2-4 mm) will not be stable.

If the fluid could be limited to a very thin film in even just a few regions, the overall oxygenation rate would increase. This might be accomplished by introducing barriers between deeper segments, as shown in Figure 2-9. The barriers force a thin film over a distance shorter than the fluid capillary length, while the deeper segments provide stability to the overall flow path. One challenge might be reducing the volume required by the intermediate deeper regions.

2.3 Concept Selection

The corner flow oxygenation concept was selected for implementation based on the anticipated performance relative to the requirements and anticipated development/manufacturing time as expressed in table 2.1. Integration into the platform

itself with no crevices or interfaces requiring adhesive is a significant advantage for sterilization, cell compatibility, and usability over most other concepts. Further, the design is resistant to sloshing, and bubbles stay trapped at the top of the oxygenator without being passed on to the cell culture well.

2.4 Prototyping

Designing an open-well system at very low volumes requires careful attention to surface tension effects, which can be difficult to predict by modeling alone. The design process relied heavily on quickly iterating prototypes and breadboard models to test individual components of the system.

Two surrogates were used in the process: (1) a 1% bovine serum albumin (BSA) solution in phosphate buffered saline (PBS) was used as a less-expensive substitute for the cell culture medium, (2) and stereolithography (SLA) resin prototypes were plasma-treated to approximate the wetting properties of polysulfone (PSU) [24]. Polysulfone is highly inert, autoclavable, and minimally adsorbing of a wide range of drug compounds. For these reasons, it has been used in previous Griffith Lab platforms [2, 6] and was chosen as a suitable material for the top plate of the platform developed for this project. However, it is expensive and time-consuming to fabricate PSU prototypes, and SLA prototyping allowed much faster and less expensive development and testing of protoypes.

To validate plasma-treated SLA as a surrogate prototyping material, an equal volume of of BSA solution was pipetted onto the two surfaces and compared (Figure 2-10). Absent equipment for measuring contact angle accurately, comparing the footprint of the two equal-volume droplets is a reasonable indication of how close the contact angles are. The drop on the polysulfone appears larger, indicating that the contact angle of 1% BSA solution on PSU is lower than that on plasma treated SLA, but they are relatively close, and plasma-treated SLA should work as a prototyping surrogate for observing surface tension effects.

The simple SLA breadboard model shown in Figure 2-11 is an initial tool to assess

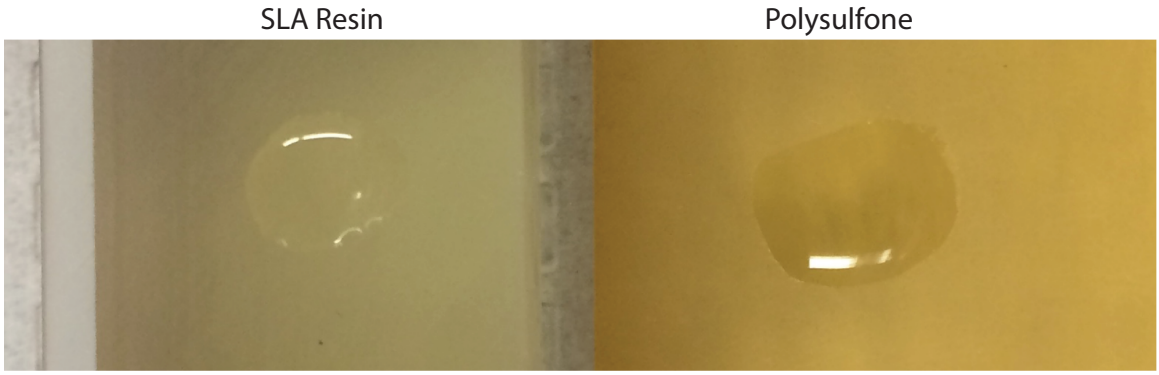

Figure 2-10: To evaluate plasma treated SLA (Clear v2 Resin, Formlabs, Somerville, MA) surface as an easily prototyped surrogate for machined polysulfone (PSU), an equal volume of fluid was pipetted onto clean surfaces of plasma treated SLA (left) and untreated PSU (right). The size of the drop is an indication of wetting, and shows rough equivalence between the two surfaces.

Table 2.1: Decision matrix for oxygenator concept selection. Relevant sections for each concept are cited in the headings. Membrane oxygenation is taken as the standard, and the anticipated performance of each concept is ranked as much better (++), better (+), the same (0), worse (-) or much worse (- -) than a membrane oxygenator against the functions and attributes listed at left. The total scores for each concept indicate the appropriateness of pursuing each concept.

	Membrane 2.2.1	Internal Corner 2.2.2	External Corner 2.2.3	Channel 2.2.4	Filament 2.2.5	Gap 2.2.6	Droplet 2.2.7	Surface Mod. 2.2.8	Barriers 2.2.9
Cell/drug compatibility	0	+	+	+	0	+	0	-	+
Vol < 500 μL	0	0	-	-	+	0	-	-	- -
Sterilization/usability	0	++	++	++	0	+	-	+	++
Fit with pneumatic infrastructure	0	0	0	0	0	0	-	0	0
$\phi > 0.8$ @ 1 μL/s	0	+	+	0	+	+	0	+	+
Bubble clearing	0	++	++	0	++	+	0	+	+
Resume after 5 min	0	- -	- -	-	-	-	0	- -	0
Volume-limiting	0	-	- -	- -	-	-	-	- -	- -
Manufacturing complexity	0	+	+	+	0	-	-	-	+
Robustness	0	-	- -	-	-	- -	0	- -	-
Cost	0	++	++	++	+	++	+	0	++
Development risk	0	+	+	+	0	-	-	- -	0
Total	**0**	**+6**	**+3**	**+2**	**+3**	**0**	**-5**	**-8**	**+3**

the scale and viability of flow in a corner as an oxygenator concept. It demonstrates the desired wetting behavior, though not spontaneous capillary filament formation, indicating the contact angle is greater than 45 degrees [21]. Once the channel is wetted, fluid travels in the conduit formed by the corner and the free surface, as long as fluid is being evacuated from the opposite end. If fluid enters one end without being removed from the other, the free surface expands out away from the corner and holds volume. If the inlet is elevated relative to the outlet by tilting the device, the excess fluid accumulates in the exit well, and the free surface tightens into the corner, due to the pressure drop ρgh across the channel.

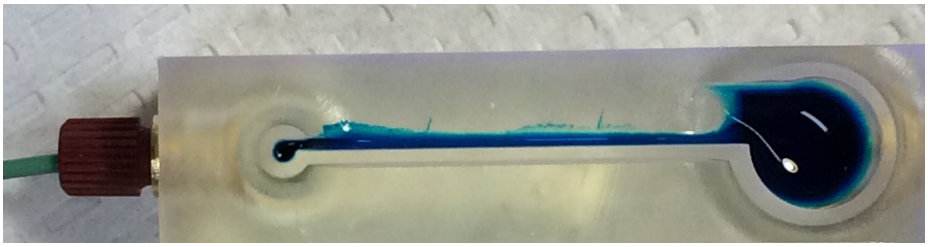

Figure 2-11: One of several preliminary SLA models to evaluate corner wetting behavior. Fluid is introduced through the tube on the left and sinks from the well on the right. The SLA has been plasma treated. Fluid is 1% BSA in PBS with food dye for better visibility.

One challenge involved with achieving adequate oxygenator length on a small platform is how to change the flow-path direction to allow tight packaging. Switchbacks were considered, but the additional exposed surfaces at the switchback corners can allow fluid to spread into other undesired regions or or create fluid instabilities at the corner. A spiral configuration resolves this challenge by maintaining an approximately straight path if the curvature of the spiral is significantly larger than the curvature of the fluid free surface. An interior spiral was evaluated, as shown in Figure 2-12), but an exterior spiral was chosen for two primary reasons. First, with an interior spiral, the cell culture well must sit within the bounds of the spiral, or a secondary collection pool at the base of the spiral must be pumped into the well. It is thus difficult to have passive emptying into the well. Second, if the interior curve is made too tight, fluid pools at the corner as described by the Young-Laplace equation, increasing the diffusion length. For an exterior corner, the path curvature at the corners is negative

relative to the fluid interface curvature, and the Young-Laplace equation forces the radius of curvature of the fluid free surface to become smaller, shortening the diffusion length (see Figure 2-24 in Section 2.5 for elaboration on this phenomenon).

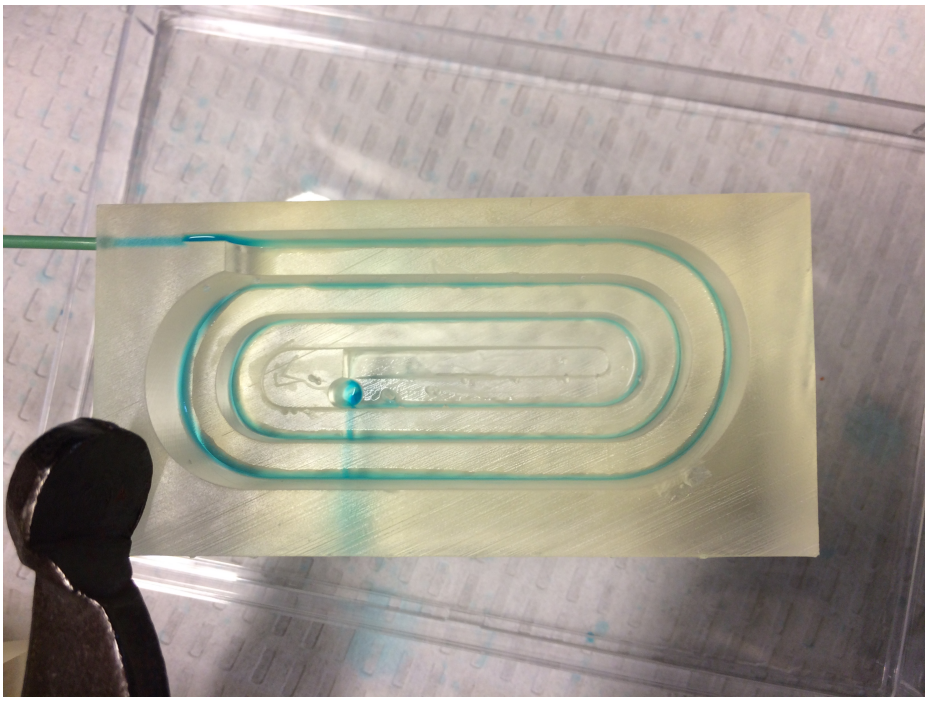

Figure 2-12: Interior spiral breadboard. Plasma treated SLA, flowing 1% BSA solution with food dye.

An exterior spiral breadboard is shown in Figure 2-13. Because there is a feature at the bottom of the spiral that allows fluid to accumulate, the fluid profile is significantly thicker at the base than at the top. This was resolved by including a wetted exit ramp into the cell culture well that provides a continuous fluidic connection to a region at a lower pressure head, thereby evacuating excess fluid from the oxygenator flow path (Figure 2-14).

Once the fluid behaved as desired, the oxygenation potential of an exterior spiral breadboard model was measured using probes (810 μm needle probes, Lucid Scientific, Atlanta, GA) placed at the inlet and outlet (Figure 2-14).

A polysulfone spiral (Figure 2-15) was also fabricated to validate plasma treated SLA as a surrogate, and to present any issues caused by machining the spiral. The oxygenator exit region was cut away to facilitate manufacturing and to enable the

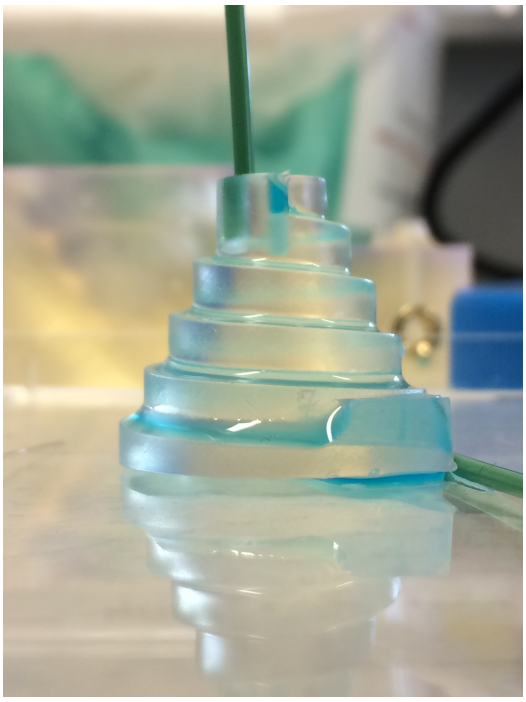

Figure 2-13: An early SLA (sterolithography) exterior spiral breadboard model. The SLA has been plasma treated for 1 min to approximate the wetting properties of polysulfone. Note the undesired accumulation at the exit caused by stable wetting in the exit channel.

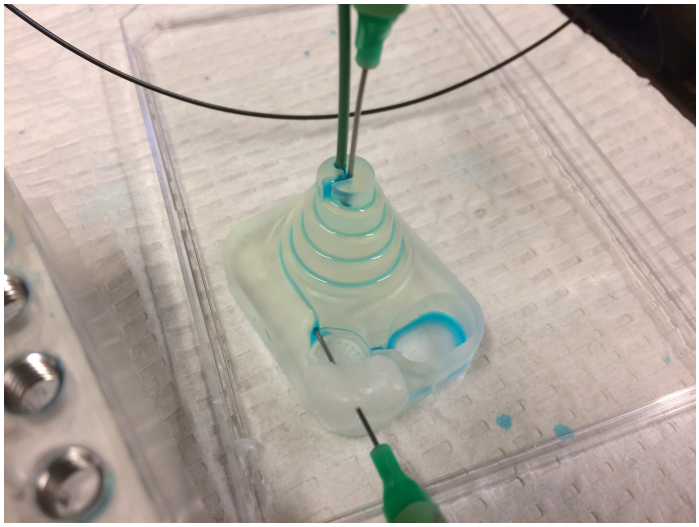

Figure 2-14: A later SLA exterior spiral breadboard with probes in position to measure oxygenation potential. Accumulation at the base of the spiral has been reduced by including a wetted slope into the cell culture well to provide reliable exit flow.

fluid to spill out into a wide plate rather than backing up into the oxygenator. Data presented later in Figure 2-28 show the similarity between SLA and PSU spiral per-

formance, and validate plasma treated SLA as a surrogate prototyping material.

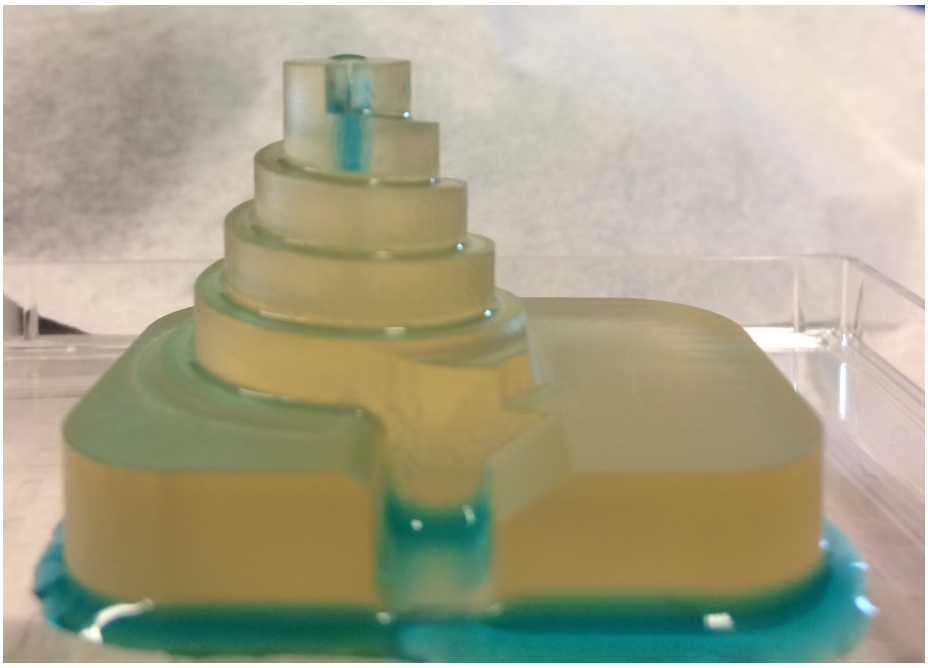

Figure 2-15: The first machined Polysulfone (PSU) spiral oxygenator, to compare wetting behavior between PSU and plasma treated SLA. The corner channel has a radius of 0.5 mm, as machined by the cutting tool.

The next oxygenator iteration, on the revision 1 platform (Figure 2-16), was shorter in height than the previous spirals, in order to reduce the platform height and the thickness of raw polysulfone stock needed for manufacture. This compressed spiral showed an oxygenation potential similar to the taller PSU spiral (Figure 2-21).

For packing multiple replicates on a single platform, it is easiest to have the pump geometry in the same position across all replicates, allowing the pneumatic channels to run straight across the platform without crossing. This led to an elongated spiral design, shown in Figure 2-17. This first SLA breadboard included narrow guidance grooves around the oxygenator curves, intended to facilitate wetting upon initial startup of the oxygenator. These grooves were ineffective (note the buildup of fluid before the first curve in Figure 2-17), though we expect effective guidance channels could be designed with some additional effort. Because the oxygenator can be primed with BSA before operation, and the oxygenator cannot be stopped for longer than tens of seconds, such spontaneous capillary flow channels are not necessary for function,

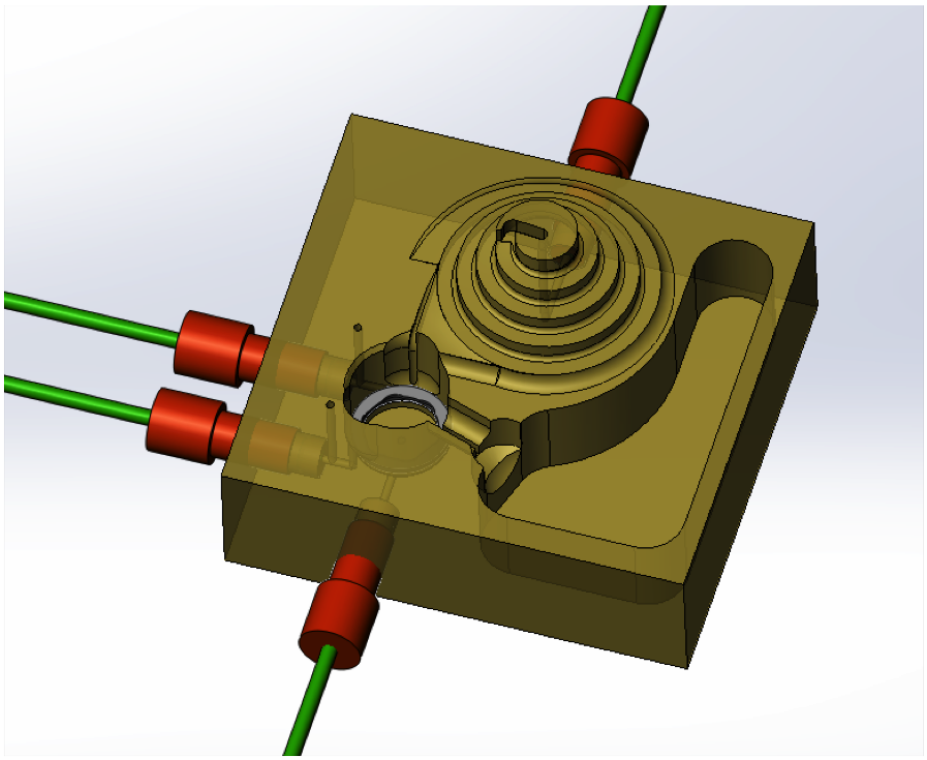

Figure 2-16: The Revision 1 spiral oxygenator, which is shorter than the original PSU spiral. The geometry of the well and the flow tests using this prototype are discussed in Chapter 3

and this development was left for future iterations.

After further SLA validation of the wetting characteristics of an elongated spiral oxygenator without guidance channels, the revision 2 platform was machined from polysulfone (Figure 2-18). This oxygenator was half the height of Rev 1, and one fourth the height of the PSU spiral breadboard. Each lane is surrounded by a barrier to prevent cross-contamination. The flat surfaces are sloped so as to empty to the end of the oxygenator, and the radius at the base of the barrier walls is large enough to prevent fluid accumulation.

2.5 Oxygenator Diffusion Model

This section describes analytic modeling that aims to predict oxygenator performance and highlight its dependence on various physical parameters. The model is compared to measured data, and simple approximations offer both a sanity check and

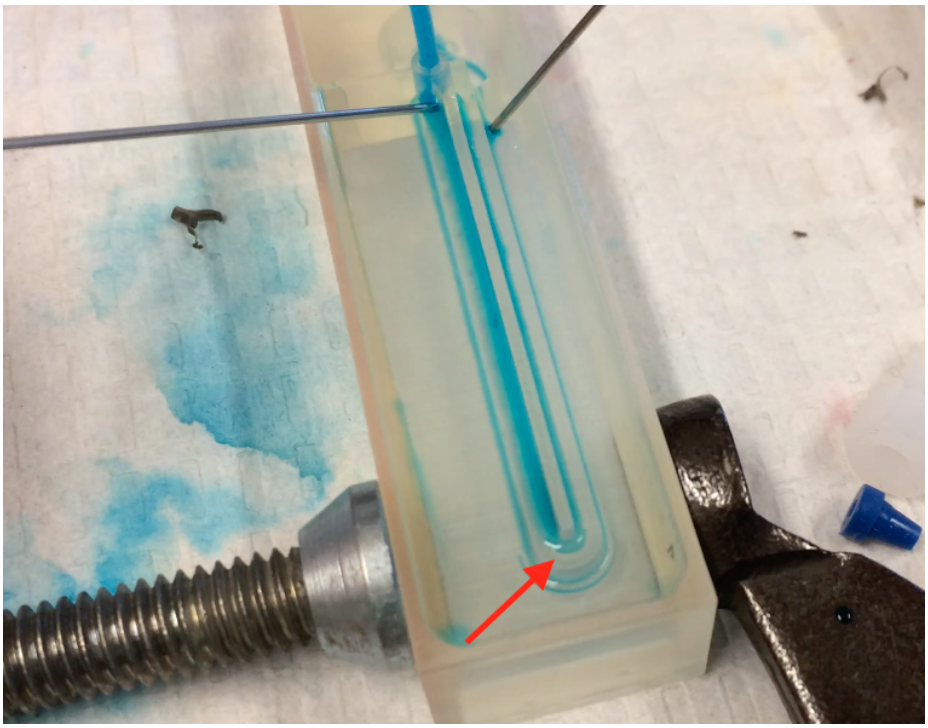

Figure 2-17: The spiral was adapted to an elongated format to facilitate packing replicate loops on the same platform. This SLA model also includes small grooves around the curves intended to facilitate wetting, but which instead seemed to prevent effective emptying (red arrow). Note the fluid has backed up at the curve, preventing the corner from filling down-stream.

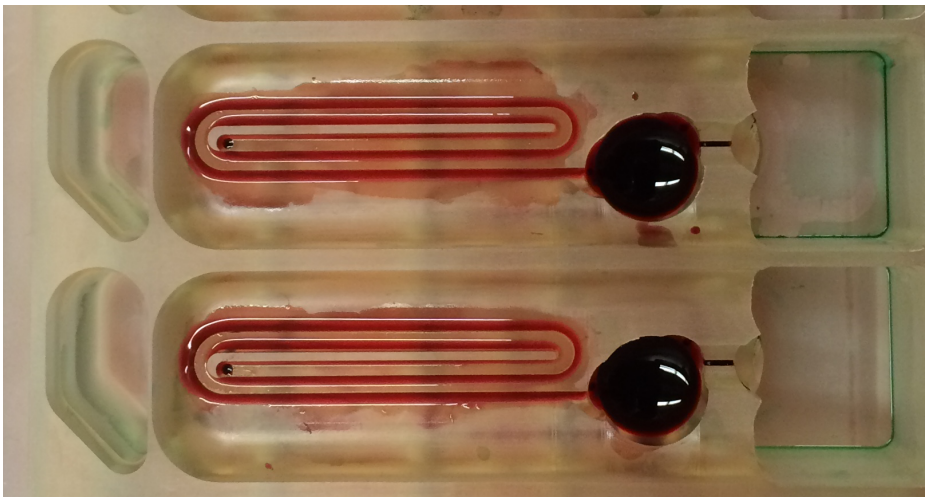

Figure 2-18: The revision 2 oxygenator. The spiral oxygenator is elongated to facilitate packing multiple replicates on the platform, and is half the height. to reduce the cost of the raw polysulfone stock needed to machine the platform.

an order-of-magnitude guide for future designs.

The performance of the oxygenator can be described by an efficiency that Inman [3] calls ϕ, the oxygenation potential:

$$\phi \equiv \frac{C_b - C_a}{C_{sat} - C_a}, \tag{2.2}$$

where the oxygen concentration difference of inlet (C_a) and outlet (C_b) is normalized by the maximum possible oxygenation, that is when the outlet is at saturation C_{sat}. This parameter allows comparison of oxygenators across experiments, where the input concentration is likely to vary, and is independent of cell oxygen consumption activity. Further, it can be directly measured with a probe each at the oxygenator inlet and outlet.

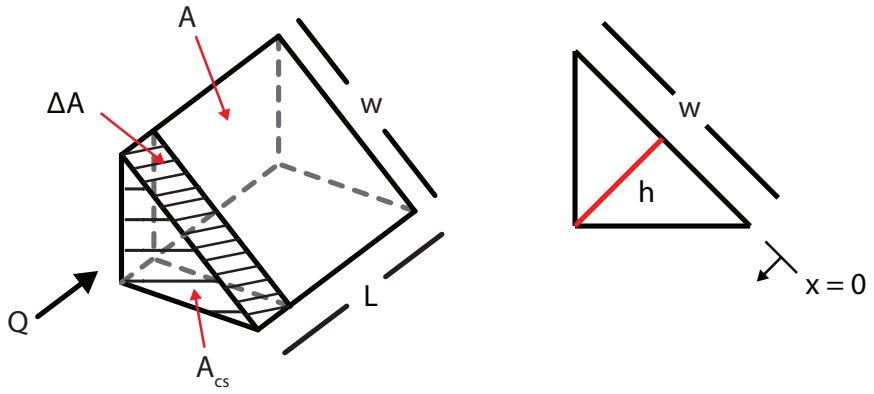

Figure 2-19: Plug flow model used for simplified oxygenator modeling.

The analysis that follows expresses this oxygenation potential in terms of relevant parameters of the system: flow rate Q, diffusion depth h, air-liquid interface area A, and the diffusion coefficient D_{O_2}. We assume plug flow, which requires that (1) there is no diffusion in the direction of advection, i.e. down the length of the oxygenator channel and also that (2) the velocity field is uniform. We can check the validity of the first assumption by estimating the Péclet number, Pe, which compares the advective transport rate to the diffusive transport rate in the direction of advection [25]. The

Péclet number is often expressed as

$$\mathrm{Pe}_L \equiv \frac{\text{adv. rate}}{\text{diff. rate}} = \frac{LU}{D} \tag{2.3}$$

where U is a characteristic velocity, L is a characteristic length, and D is a diffusion coefficent. For the oxygenator we estimate its value using order-of-magnitude values: the characteristic velocity is the flow rate $Q \approx 1$ μL/s divided by the fluid cross sectional area $A_{cs} \approx 1$ mm^2, $L \approx 100$ mm is the length of the oxygenator, and $D_{O_2} = 3 \times 10^{-3}[\frac{\text{mm}^2}{\text{s}}]$ is the diffusion coefficient for oxygen in water at 37 °C. The Pećlet number is then

$$\mathrm{Pe}_L = \frac{LQ}{D_{O_2} A_{cs}} \approx 10^4 \tag{2.4}$$

which indicates that advective transfer dominates, and diffusion along the length of the oxygenator is negligible.. Note that we later use a different Péclet number, Pe_h, which addresses diffusion perpendicular to advection, while Pe_L is only used here to validate the plug flow assumption that diffusion in the direction of advection is negligible.

We first consider the diffusion of oxygen into a plug of fluid over time through the surface ΔA in Figure 2-19. Fick's First Law [25] relates the transport rate of a species across a boundary to the concentration gradient at the boundary. In one dimension, this is expressed as

$$J = -D_{O_2} \frac{dC}{dx} \tag{2.5}$$

where J is the mass flux across the surface in [mol/mm^{2}s] and C is the concentration in [mol/mm^3]. Note that below we will use units of μM, equivalent to [μmol/L]. At that point, the units of concentration will be set by the boundary conditions and μM is more convenient. Here, we use [mol/mm^3] to match the relevant length dimensions.

To find total oxygen entering the plug volume, we need the oxygen flux at the air-liquid interface. As a first approximation, we can linearize the concentration gradient

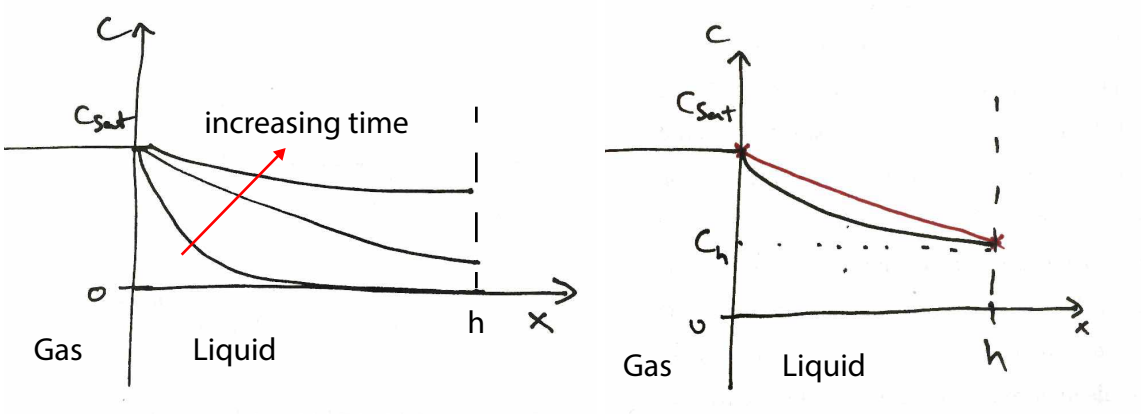

Figure 2-20: *Left)* As oxygen diffuses through the air-liquid interface at $x = 0$, the concentration will decrease exponentially with x. *Right)* We approximate $\frac{dC}{dx}|_{x=0}$ by linearizing the concentration gradient between $x = 0$ and $x = h$.

as shown in Figure 2-20. The oxygen flux at the surface is

$$J|_{x=0} = -D_{O_2}\frac{dC}{dx}|_{x=0} \approx -D_{O_2}\frac{C_h - C_{sat}}{h} \tag{2.6}$$

where C_h is the oxygen concentration at the wall ($x = h$) of the oxygenator opposite the gas-liquid interface ($x = 0$), and the flux is in the direction of decreasing concentration. The linear concentration gradient that we assume means that the oxygen transport rate at the interface is the same as at the wall, and can be written

$$J = \frac{\dot{n}}{\Delta A} \tag{2.7}$$

where $\dot{n}$ is the species transport rate in [mol/s] and ΔA is the area in [mm^2] of the gas-liquid interface for the individual plug. We define a mean concentration C_m as the quantity of species n [mol] in the system divided by the volume V [mm^3]:

$$C_m = \frac{n}{V} = \frac{2n}{\Delta A h} \Rightarrow J = \frac{\dot{n}}{\Delta A} = \frac{h}{2}\frac{dC_m}{dt}. \tag{2.8}$$

Note that with a linear concentration gradient,

$$C_m = \frac{C_h + C_{sat}}{2} \Rightarrow C_h = 2C_m - C_{sat}. \tag{2.9}$$

Using J in (2.8) and substituting 2.9 into (2.6), we obtain

$$\begin{aligned} \frac{h}{2}\frac{dC_m}{dt} &\approx -D_{O_2}\frac{C_h - C_{sat}}{h} \\ -\frac{h^2}{2D_{O_2}}\frac{dC_m}{dt} &= (2C_m - C_{sat}) - C_{sat} \\ \frac{dC_m}{dt} + \frac{4D_{O_2}}{h^2}C_m &\approx \frac{2D_{O_2}}{h^2}C_{sat}. \end{aligned} \tag{2.10}$$

Solving the differential equation in (2.10), we obtain

$$C_m \approx A_1 e^{-\frac{t}{\tau_D}} + A_2 \tag{2.11}$$

where A_1 and A_2 are constants and $\tau_D = \frac{h^2}{4D_{O_2}}$ is the time constant of diffusion. Applying the boundary conditions $C_m = C_o$ at $t = 0$ and $C_m = C_{sat}$ as $t \to \infty$ gives

$$C_m \approx (C_o - C_{sat})e^{-\frac{t}{\tau_D}} + C_{sat}. \tag{2.12}$$

Rearranging,

$$\begin{aligned} C_m &\approx -(C_{sat} - C_o)e^{-\frac{t}{\tau_D}} + (C_{sat} - C_o) + C_o \\ (C_m - C_o) &\approx (C_{sat} - C_o)(1 - e^{-\frac{t}{\tau_D}}) \\ \frac{(C_m - C_o)}{(C_{sat} - C_o)} &\approx (1 - e^{-\frac{t}{\tau_D}}). \end{aligned} \tag{2.13}$$

Equation 2.13 describes the time evolution of the mean concentration of a single plug. If this plug enters the oxygenator at an initial mean concentration $C_o = C_{in}$, it will exit at $C_m = C_{out}$ after a residence time $t = \tau_a = \frac{L}{U}$. At the exit of the

oxygenator,

$$\frac{t}{\tau_D} = \frac{\tau_a}{\tau_D}. \tag{2.14}$$

Recalling the definition of the oxygenation potential (equation 2.2), and using 2.14, equation 2.13 becomes:

$$\phi \equiv \frac{C_{out} - C_{in}}{C_{sat} - C_{in}} \approx (1 - e^{-\frac{\tau_a}{\tau_D}}). \tag{2.15}$$

The residence time τ_a can be estimated by referring to Figure 2-19. For a triangular oxygenator,

$$A = Lw \tag{2.16}$$

$$A_{cs} = \frac{1}{2}hw = \frac{hA}{2L} \tag{2.17}$$

$$U = \frac{Q}{A_{cs}} = \frac{2LQ}{Ah} \tag{2.18}$$

$$\Rightarrow \tau_a = \frac{L}{U} = \frac{hA}{2Q}. \tag{2.19}$$

To relate this residence time τ_a to the diffusion time constant τ_D we use a Péclet number Pe_h, which refers to the rate of diffusion orthogonal to the direction of advection to a depth h (while Pe_L used above refers to diffusion in the direction of advection to a length L). This Pe_h captures how much or how little diffusion can occur in the time that the fluid plug travels through the oxygenator, and depends on the flow rate Q, system geometry as represented by $\frac{h}{A}$, and diffusion coefficient D_{O_2}:

$$\mathrm{Pe}_h = \frac{\text{adv. rate}}{\text{diff. rate}} = \frac{1/\tau_a}{1/\tau_D} = \frac{\tau_D}{\tau_a} = \frac{Qh}{2D_{O_2}A}. \tag{2.20}$$

The flow rate is on the order of 1 μL/s, and the lengths are on the order of 1 mm. Note that for a rectangular oxygenator with $A_{cs} = hw$ and $A = wL$, the Péclet number is also $\frac{Qh}{2D_{O_2}A}$.

Substituting this modified Péclet number into equation 2.15 gives an expression

for the oxygenator efficiency in terms of the geometry and flow rate of the fluid path:

$$\phi = \frac{C_{out} - C_{in}}{C_{sat} - C_{in}} \approx (1 - e^{-\frac{1}{\mathrm{Pe}_h}}) \tag{2.21}$$

Figure 2-21 shows predictions of the oxygenator efficiency ϕ for arbitrary $\frac{h}{A}$ next to measured ϕ values from the LiverChip, an intermediate prototype, and the final revision 2 prototype. Note that equation 2.21 shows that ϕ is a concentration-independent characterization of oxygenator performance and depends only on system geometry, oxygenator flow rate, and the diffusion coefficient.

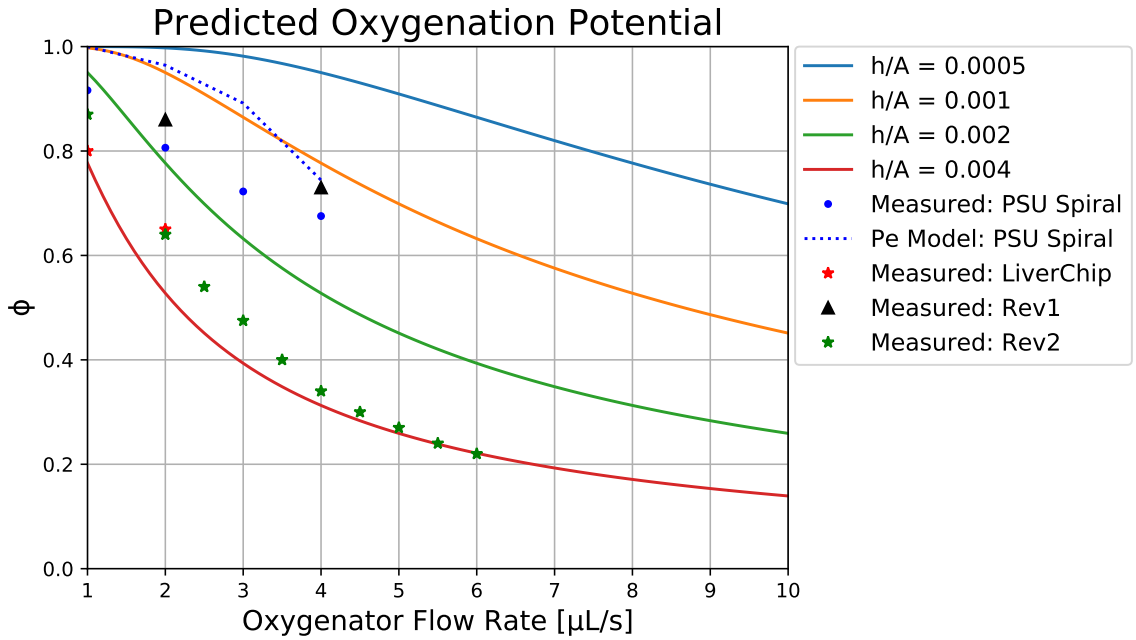

Figure 2-21: Oxygenation potential as a function of flow rate for various $\frac{h}{A}$. Solid lines represent the prediction of equation 2.21 for various geometries, represented by $\frac{h}{A}$. Experimental data are presented for the existing LiverChip, the reduced liver prototypes revision 1 and 2, and an earlier oxygenator prototype (PSU_spiral). The dotted blue line shows values calculated from (2.21), using measured values for $\frac{h}{A}$ as described in Figure 2-22. The LiverChip data are from appendix C. The LiverChip flow rate is limited to 2 μL/s by the on-board pumps, so the LiverChip data are only provided at 1 and 2 μL/s.

Increasing either $\frac{h}{A}$ or Q decreases ϕ; the faster a fluid plug is moving, or the farther the oxygen must diffuse into the system for a given surface area, the farther from C_{sat} the plug will be upon exiting. At these flow rates, the Revision 2 prototype matches

LiverChip oxygenator performance, while the earlier breadboard (PSU_spiral) shows better performance (at the cost of oxygenator height) for reasons discussed below.

To assess the oxygenation model empirically, we imaged the fluid profile under flow (1-4 μL/s) in the incubator (35-37 °C during measurements) using a Dyno-Lite USB microscope (AnMo Electronics Corporation, TWN). The images were processed using ImageJ software (https://imagej.nih.gov/ij/), as shown in Figure 2-22. Because the profile varied with height, the $\frac{h}{A}$ values from position C were used in calculating the PSU Spiral values in Figure 2-21.

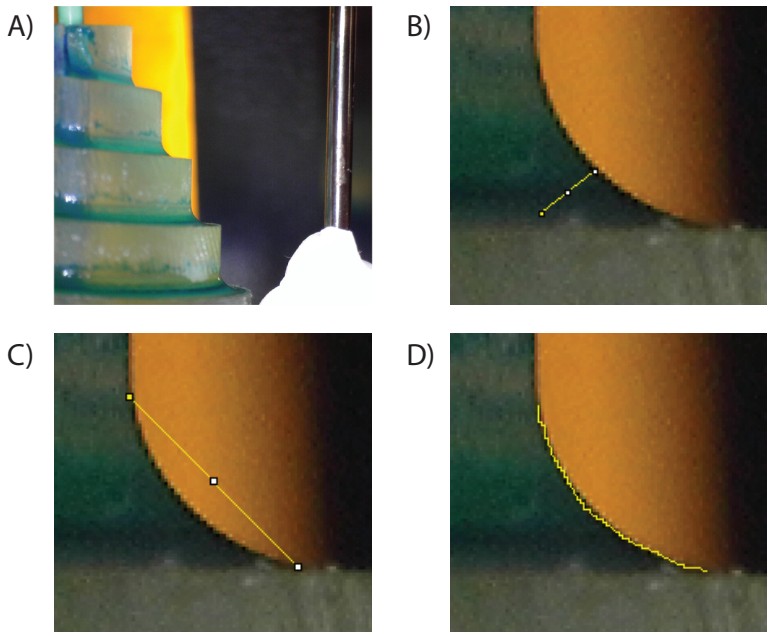

Figure 2-22: The fluid profile in the oxygenator corner is imaged at the locations labeled A through D in Figure 2-27 and measured using ImageJ software. *A)* In an image used to measure the profile at location B at 1 μL/s, a 1/16 in. drill bit in the plane of the profile is used for scale. *B)* The measurement h' is taken from the fluid surface to the corner obtained by extending the PSU edges, and then 0.2 mm is subtracted to account for the corner radius and obtain h. *C)* The value for w is measured two ways, first by a straight line. *D)* The value of w is also found by tracing the fluid interface with a freehand tool and measuring the path length. There is less than a 10% difference between the two methods, and it seems to have little effect on ϕ, but the free-hand method is used for all values presented here.

As shown in Figure 2-21, the model above over-estimates the oxygenation potential. We believe this is partly due to the linearized concentration profile used to

calculate the average concentration C_m. As shown in Figure 2-20 on the right, a linear profile will always over-predict a mean concentration calculated by dividing the area under the curve by h. As shown on the left, the error is particularly large early on in the development of the profile, before the diffusion has reached the distance h.

To describe ϕ in terms of a mean concentration that is integrated over the profile, we can borrow a model described by Glicksman and Lienhard for heat transfer applications [26]. For diffusion into a bulk slab, we can use the first term of a Fourier series to approximate the concentration profile. This model, described in detail in Appendix B, relates the normalized mean temperature, or in this case concentration, to the dimensionless Fourier number, which describes the ratio of diffusive transport to storage rate. In mass transfer, for characteristic time t and length h,

$$\mathrm{Fo}_m = \frac{D_{O_2} t}{h^2}. \tag{2.22}$$

At the end of the oxygenator, $t = \tau_a$. Thus, approximating the triangular geometry as a slab of thickness $h/2$ and using equation 2.19 yields

$$\mathrm{Fo}_m = \frac{D_{O_2}}{h^2}\frac{hA}{2Q} = \frac{DA}{2Qh}. \tag{2.23}$$

Using tabulated coefficients for the slab geometry, we can express the oxygenation potential as

$$\phi = \frac{\bar{C} - C_o}{C_{sat} - C_o} = 1 - 0.8106e^{-2.47\mathrm{Fo}_m} \tag{2.24}$$

where $\bar{C}$ is the spatially averaged concentration in x from the free surface down to $x = h$.

This one-term approximation model, shown in Figure 2-23, better predicts the measured oxygenation potential for the PSU spiral, when the changing $\frac{h}{A}$ values are taken into account. The Rev2 data, however, appear even more divergent than in the Péclet number model when $\frac{h}{A}$ is constant (compare to green line in Figure 2-21).

The remaining discrepancy between the one-term model and the measured values

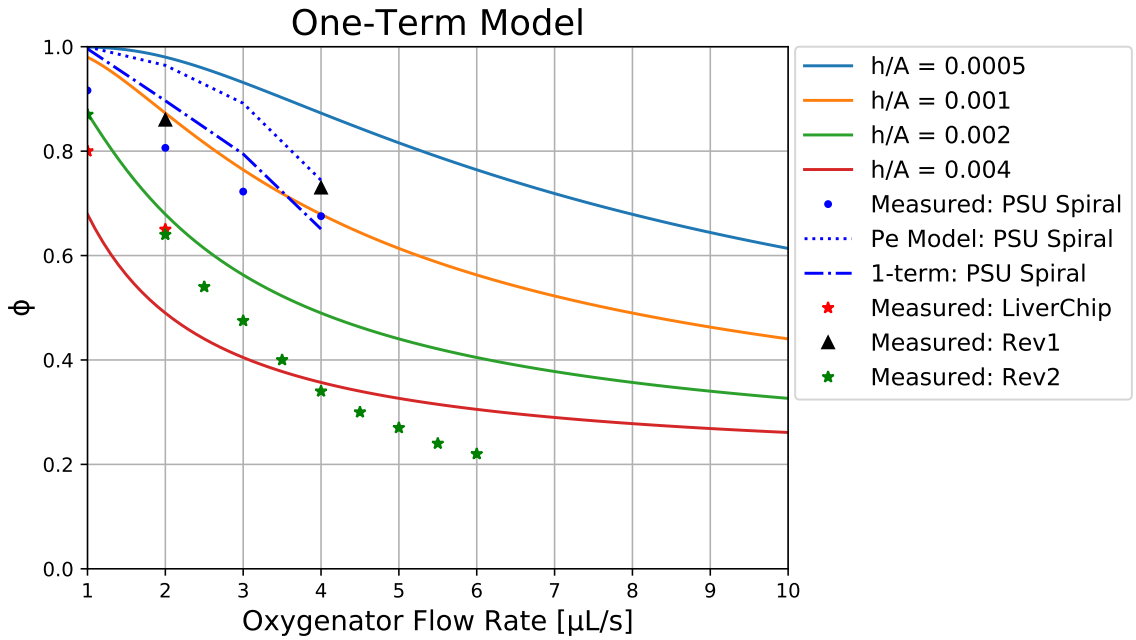

Figure 2-23: The one-term approximation for oxygenation potential. The solid lines are calculated from equation 2.24 for various $\frac{h}{A}$ values, and the 1-term result is calculated from the same model using measured dimensions from the PSU spiral at location C, as shown in Figure 2-22. All other data are the same as in Figure 2-21.

for the PSU Spiral is small enough to be explained by lack of differences between the true geometry and the approximated slab, the plug flow assumption of a uniform velocity profile, or a combination of the two.

The measured values of ϕ for revision 2 decrease more with increasing flow rate than either model predicts if $\frac{h}{A}$ is held constant. This is in contrast to the the models based on the PSU spiral measured geometry, where ϕ was calculated using an $\frac{h}{A}$ value that was specifically measured for each flow rate. As the flow rate increases, the cross sectional area, the radius of curvature, or both must increase to compensate for the higher flow rate. This can be illustrated by combining the Young-Laplace and Bernoulli equations, where the two reference points for the Bernoulli equation are taken one at the top of the oxygenation spiral and the other in the fluid well where the pressure is atmospheric and the velocity is negligible. The Young-Laplace equation can be further simplified by assuming a straight path, where the radius of curvature in the top plate $R_x \rightarrow$ inf. Expressing the velocity as $\frac{Q}{A_{cs}}$ then gives

equation 2.27 (note that A_{cs} is a function of R_y and the fluid path width):

$$\Delta P = \gamma \left(\frac{1}{R_x} + \frac{1}{R_y} \right) \qquad \text{Young-Laplace Eqn.} \qquad (2.25)$$

$$(P_1 - P_2) + \frac{\rho}{2}(v_1^2 - v_2^2) + \rho g(h_1 - h_2) = 0 \qquad \text{Bernoulli Eqn.} \qquad (2.26)$$

$$-\frac{\gamma}{R_y} + \frac{\rho}{2}\frac{Q^2}{A_{cs}^2} + \rho g \Delta h = 0 \qquad (2.27)$$

where ΔP is the pressure difference in [Pa] between the two sides of the interface, γ is the surface tension of the interface in [N/m], and R_x and R_y are orthogonal radii of curvature of the surface (see Figure 2-24). In 2.26, ρ is the fluid density in [kg/m^3], and $g = 9.8$[m/s^s]; $P_{1,2}$ are the pressures in [Pa], $v_{1,2}$ are the average fluid velocities in [m/s], and $h_{1,2}$ are the heights in [m] at points one and two in the system.

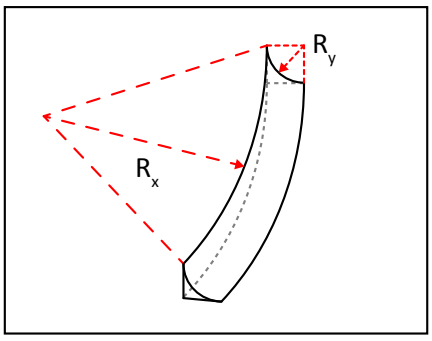

Figure 2-24: An illustration of the radii of curvature of the fluid surface. In this case, R_y is positive and R_x is negative

In practice, the free surface is observed to flatten out at higher flow rates, with a slight increase in the fluid path width until it is limited by the oxygenator edge. As the free surface changes from concave to flat, exposed surface area is decreasing as the diffusion length is increasing, so $\frac{h}{A}$ must increase. This would result in a decreased ϕ as the flow rate increases. This is supported empirically when there is a negative pressure on the fluid from the ρgh height difference, as shown in Figure 2-25.

Figure 2-21 also shows measurements from the revision 1 spiral. These measurements show a significantly higher oxygenation potential than those of revision 2, though the oxygenator length was similar. Two effects can explain this: a fluid path

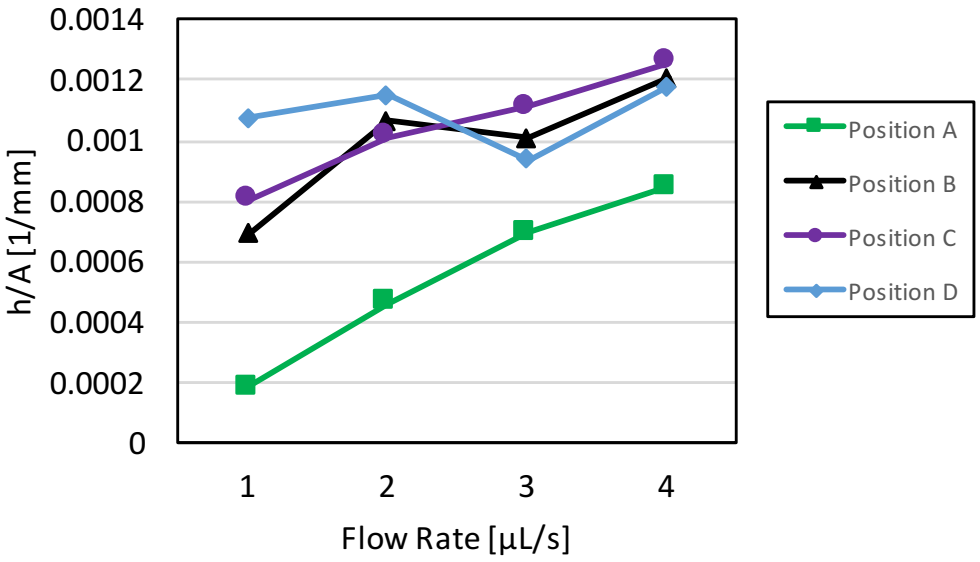

Figure 2-25: The measured geometric ratio h/A generally increased with increasing flowrate, as predicted. The effect was significant at a greater height (position A), while negligible closer to the base of the spiral (position D). Also note that h/A is generally smaller at the higher position, confirming that spiral height plays an indirect role in oxygenation potential ϕ. These measurements were taken from the PSU spiral, as shown in Figure 2-22.

curved in the top plate and a greater height difference. A convex curved path, by equation 2.25, requires a more concave curvature in the fluid profile. This tightens the fluid path against the corner, decreasing $\frac{h}{A}$ and therefore increasing oxygenation potential relative to a straight path. The greater height difference has a similar effect in decreasing the radius of curvature, a relationship described by equation 2.27.

We can estimate the relative contribution of these effects. Comparing two cases with an equal pressure differential at the interface yields

$$\frac{1}{R_x} + \frac{1}{R_y} = \frac{1}{R'_x} + \frac{1}{R'_y} \tag{2.28}$$

$$\frac{R'_y}{R_y} = 1 + \frac{R'_y}{R'_x} - \frac{R'_y}{R_x}. \tag{2.29}$$

Let $R'_y \approx 1$ mm be the radius of curvature of the fluid profile in the cross sectional plane for a corner-channel that has a radius in the top plane of $R'_x \approx -10$ mm (where

curvature is positive if the center is on the air side of the interface, and negative if the center is on the fluid side: see Figure 2-24). If we compare to a straight-path oxygenator ($R_x \to \text{inf}$), $\frac{R'_y}{R_y} \approx 0.9$; we expect at most a 10% change from this curvature effect.

To assess the effect of height, we can rearrange equation 2.27 and compare between two cases, assuming the cross-sectional area stays constant:

$$R'_y - R_y = \frac{\gamma}{\rho g}\left(\frac{1}{\Delta h'} - \frac{1}{\Delta h}\right)$$

approximating

$$\begin{aligned} \Delta h' &= 2\Delta h \approx 0.01 \text{ m} \\ R_y &\approx 0.001 \text{ m} \\ \rho &\approx 1000 \text{ kg/m}^3 \\ g &\approx 9.8 \text{ m/s}^2 \\ \gamma &\approx 0.06 \text{ N/m [27]} \end{aligned}$$

gives

$$\frac{R'_y}{R_y} = 1 - \frac{\gamma}{2\rho g \Delta h R_y} \approx 0.4.$$

This indicates that between the two measured oxygenators, the difference in oxygenation potential derives primarily from the height difference, and the curvature effect is relatively minor.

2.6 Testing and Performance

To measure the oxygenation potential, deoxygenated BSA solution is flowed through the oxygenator, and the dissolved oxygen concentration is measured at the inlet and

outlet. The oxygenation potential, φ, is then calculated using equation 2.2. 1% Bovine serum albumin (BSA) in phosphate-buffered saline (PBS) is deoxygenated by bubbling nitrogen in a glass container. The media is then pumped through PEEK tubing (1/16 in. OD, 1/32 in. ID) with a pneumatic membrane pump. For subsequent tests, at flow rates higher than 2 μL/s, deoxygenated BSA solution is extracted from the bubbler with a syringe and flow is controlled using a syringe pump, as the pump block cannot supply these higher flows. Because the oxygenation potential is concentration-independent, the media does not have to be completely deoxygenated at the inlet. Probes were positioned so as to fully immerse the tip in the fluid path. The setup is allowed to sit in the incubator at 37 degrees C for at least 30 minutes to bring the platform to temperature. The media had sat in the incubator for 1-2 additional hours to deoxygenate and come to temperature. The setup used for the SLA spiral is shown in Figure 2-26.

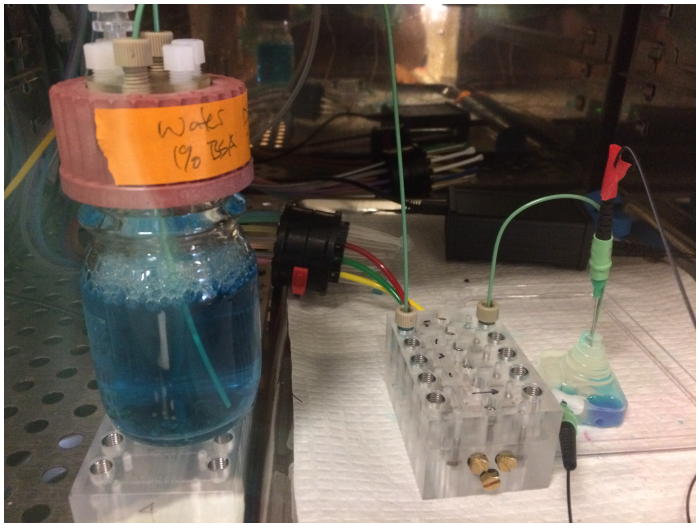

Figure 2-26: Setup for measuring oxygenation potential in an incubator at 37 Celsius. A solution of 1% Bovine Serum Albumin in PBS is deoxygenated at left by bubbling nitrogen. The BSA is then pumped through a pump block and to the top of the spiral, where probes at top and bottom measure the dissolved oxygen concentration difference.

A simple plug flow model predicts that as the oxygenator length increases for a constant flow rate, the outlet concentration will approach saturation with a decaying exponential as a function of length (see Section 2.5, equation 2.21). This was exper-

imentally assessed by probing the oxygen concentration at various locations on the spiral, as shown in Figure 2-27.

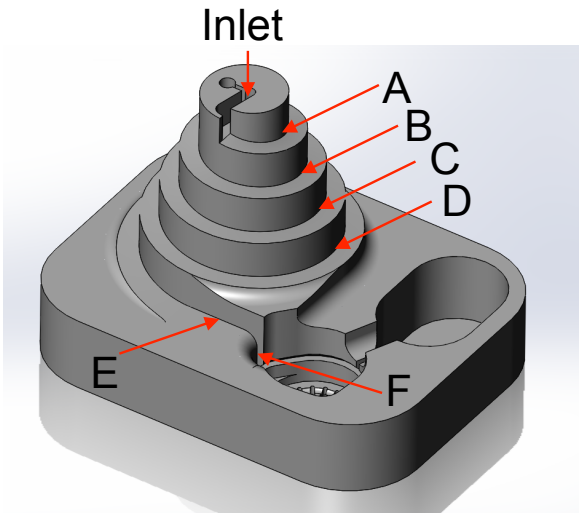

Figure 2-27: To assess the oxygenation potential at different oxygenator lengths, the downstream probe was sequentially placed at the locations shown. Lengths from inlet: A = 5.5 mm; B = 34.5; C = 75.2; D = 127.6; E = 177.5.

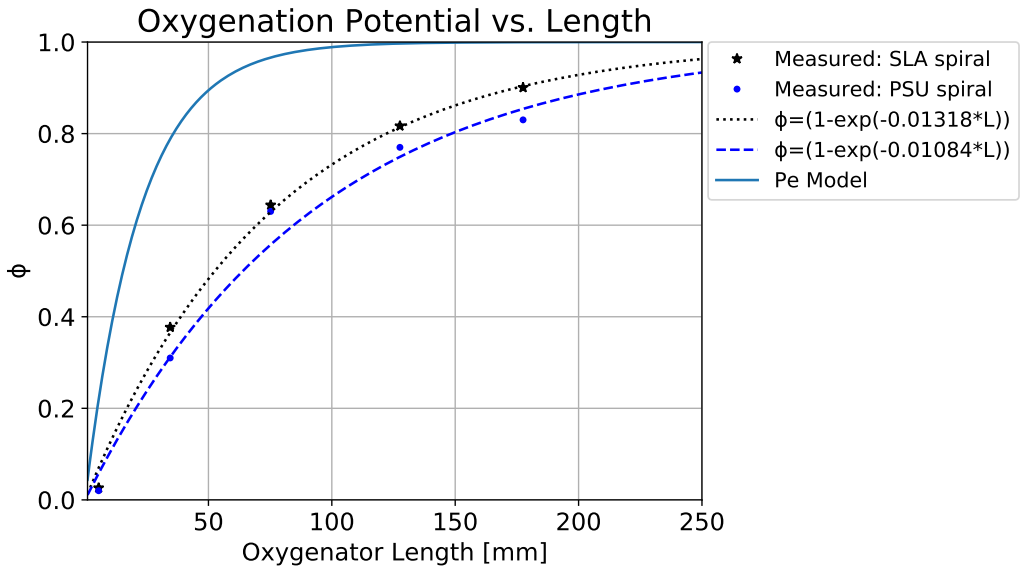

Figure 2-28: Oxygenation potential measured at various distances from the oxygenator inlet of the SLA and PSU spiral breadboards, as shown in Figure 2-27. Flow rate is 1 μL/s. Exponential fit parameters k are from a linear fit of $\ln(1-\phi) = -kL$. The Peclet Model (2.21) uses the values of $w = 1.5$ and $h = 0.2$ measured for position C at 1 μL/s as described in figure 2-22.

The resulting data do show a decaying exponential approach to full oxygenation as the length increases. Between the polysulfone and SLA materials, the difference is minor. The Peclet model uses $w = 1.5$ and $h = 0.2$ measured for position C (see figure 2-22). Substituting these values into equation 2.21 yields

$$\phi \approx 1 - e^{-0.045L} \tag{2.30}$$

The model over-predicts the oxygenation potential as described in Section 2.5.

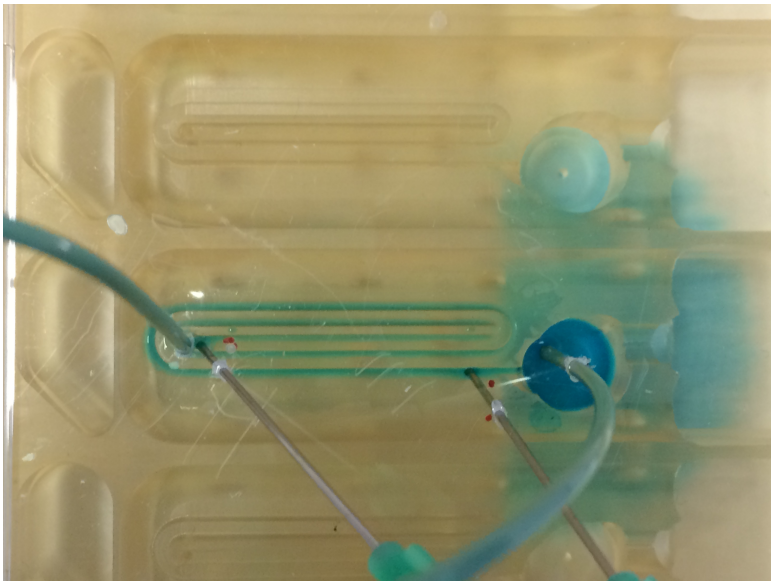

Figure 2-29: The revision 2 spiral being fed externally through a PEEK inlet tube. The inlet source was subsequently changed to a cannula entering from the bottom, but the probe position remained the same. The probes and tubes pass through holes drilled in the clear polystyrene lid.

To test the oxygenation potential of the revision 2 oxygenator, deoxygenated media is first fed from above through PEEK tubing. This setup resulted in dramatic fluctuations in the probe readings due to bubbles at the top of the oxygenator. To resolve this issue, a 1 mm OD stainless steel canula is inserted in the oxygenator inlet hole from the bottom and fixed in place with a cyanoacrylate adhesive that loosens with isopropyl alcohol (Loctite 4851, Henkel, DEU). Deoxygenated media is flowed through the oxygenator using a syringe pump (Pump 11 Pico Plus Elite, Harvard Apparatus, Holliston, MA). The dissolved oxygen concentration is measured at inlet

and outlet (Figure 2-29). The oxygenation potential data are presented in Figure 2-21. The revision 2 shows an oxygenation potential similar to the LiverChip at low flow rates, but considerably lower than the earlier breadboards. This may be due to the smaller Δh (4 mm for revision 2, 8 mm for revision 1, and 16 mm for earlier breadboards). Integration of the breadboards with the other components of the platform is discussed in Chapter 3.

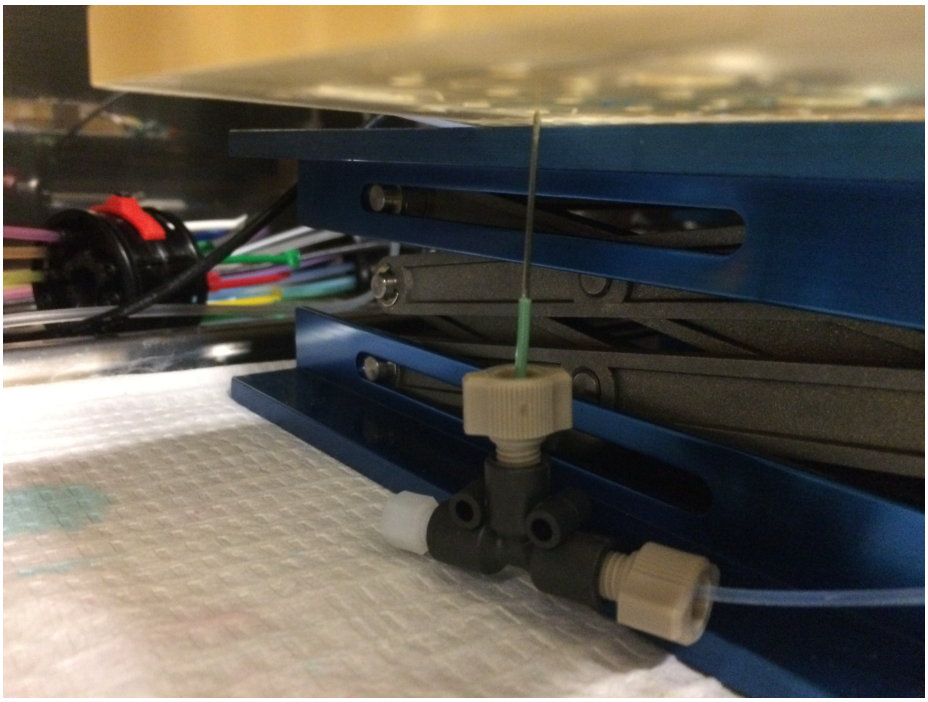

Figure 2-30: A 1 mm OD stainless steel cannula is inserted into the oxygenator inlet from the bottom. The cannula is adhered to a segment of PEEK tubing which is connected to flexible 0.01 in. ID PTFE tubing to prevent stress on the cannula.

The volume captured during flow is challenging to measure directly. 50 μL pipetted onto a spiral that had been primed with BSA and then dried appeared qualitatively to produce a profile similar to that seen at 2 μL/s, but this is a rough estimate. When flow at 2 μL/s was suddenly stopped and the fluid immediately aspirated with a pipette tip and massed, a maximum of 12 mg were recovered (12 μL). Neither of these values are difinitive, but lacking a better way of measuring the oxygenator volume while it is pumping, they serve as an estimated range. The LiverChip, for comparison, has an estimated oxygenator volume of 400 μL (1.2 mL total volume, less 50 μL for the retaining ring and scaffold, less 750 μL in the MPS and channels,

shown in Figure 2-31).

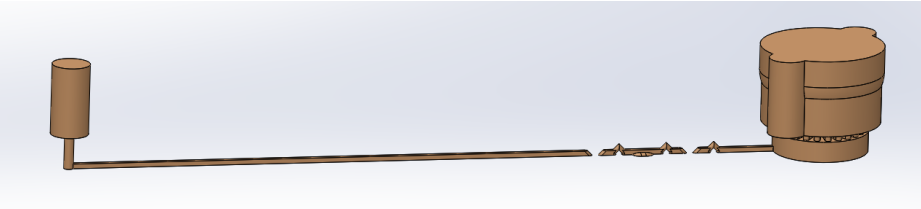

Figure 2-31: The volume shown, 750 μL, was used as part of the estimate of the LiverChip oxygenator volume.

2.7 Summary

In this chapter, we present a wide array of free-surface oxygenator concepts, in addition to a standard membrane approach. Of these, the spiral corner flow oxygenator has the advantages of being robust to disturbances, self clearing, and simple to fabricate as part of the platform itself, improving ease and quality of sterilization. We validated SLA breadboards to develop this concept into an elongated spiral oxygenator that performs equivalently to the oxygenation channel on the CN Bio LiverChip.

A tighter radius on the fluid free surface yields better oxygenation. How tightly the fluid clings to corner depends on surface and fluid wetting properties, path curvature (spiral versus straight path), and pressure drop from top to bottom which is height dependent. The taller spirals show better oxygenator performance, but we have not developed analytically the relationship between the fluid surface radius and the oxygenation. This modeling, in concert with testing, might provide guidance as to how sensitive the configuration is to changes in height, and what the right balance is between performance and additional material cost.

Chapter 3

Media Circulation Layout

This chapter addresses the circulation system of the platform, which integrates the oxygenator discussed in Chapter 2 with the microphysiological system (MPS) that contains the cells. First, the requirements are described in Section 3.1. Concepts are described in Sections 3.2 and 3.3. Analytic models of inline and mixed flow are discussed and compared in Sections 3.4 through 3.6. Finally, data presented in Section 3.7 suggest that the chosen configuration behaves like an inline system at low flowrates, and will meet all requirements when flowing up through the scaffold, but may not meet the 150 μM concentration requirement when flowing down. Experiments with the revision 2 platforms are still required to determine if this prediction is accurate, and if so, the significance of not reaching 150 μM before flow reversal.

3.1 Circulation Requirements

The fluid channel and pump arrangement will ultimately determine the oxygen concentration of the media that is delivered to the cells. The following requirements guided the concept selection and design process.

1. ***Re-circulation flow through scaffold must be reversible***

   When grown on the standard polystyrene scaffold, cells are "seeded" during the first 8 hours, in which media flows down through the scaffold.

In this flow direction, the filter prevents cells from passing through, and they bind to the scaffold. After 8 hours, the flow is reversed and flows up to prevent further accumulation of cells from clogging the scaffold channels, and this upward flow continues for the duration of the experiment.

2. ***Device must circulate media at 150 μM O_2 or greater, with flow through the scaffold at 1 $\mu L/s$*** **(MPS flow rate)**

   This requirement assumes 250k rat hepatocytes or 600k human hepatocytes, with an expected oxygen consumption rate of approximately 100 pmol/s. 150 μM is a target minimum, but the range of acceptable values is not clearly defined. Blood oxygen concentration is approximately 150 μM in the arteries and closer to 65 μM in the portal vein, which feeds into the liver [28]. However, because hemoglobin is storing additional oxygen in the blood, cell culture medium must be at higher concentrations than these to deliver the same total amount of oxygen. The flow rate through the scaffold, 1 μL/s, is chosen to match that used on the LiverChip.

3. ***Each pump should be coupled across replicates***

   The existing pneumatic architecture controls one pumping degree of freedom (DOF) with three pressure/vacuum tubes (controlling one pump chamber and two valves). To reduce complexity of the set-up, each pump function (e.g. re-circulation, oxygenation, or media exchange) that is consistent across replicates should be controlled by a single pneumatic DOF, which consists of one three-tube cluster. For experiments to compare different flow rates, the flow rate can be varied over time, or multiple platforms can be used; in any case a minimum of 6 replicates would be desired for a single experimental case, justifying parallel flow rates across replicates in a single chip.

3.2 Circulation Concepts

The flow circulation configuration should meet the above requirements without increasing the circulating volume beyond 500 μL, and should allow relatively simple fabrication and assembly.

3.2.1 In-line

The inline configuration (Figure 3-1) is the simplest, and is used on the existing LiverChip platform (Figure 3-2). The media flows in a single loop, with the cells consuming oxygen and the oxyenator replenishing it. The oxygenator flow rate is therefore the same as the cell perfusion flow rate. Because the cell culture protocol requires reversing flow after the first 8 hours, the oxygenator needs to function in both directions, which precludes the use of of a down-hill self-clearing oxygenator. An active flow path switching mechanism could allow use of a one-direction oxygenator, but introduces additional complexity and circulating volume.

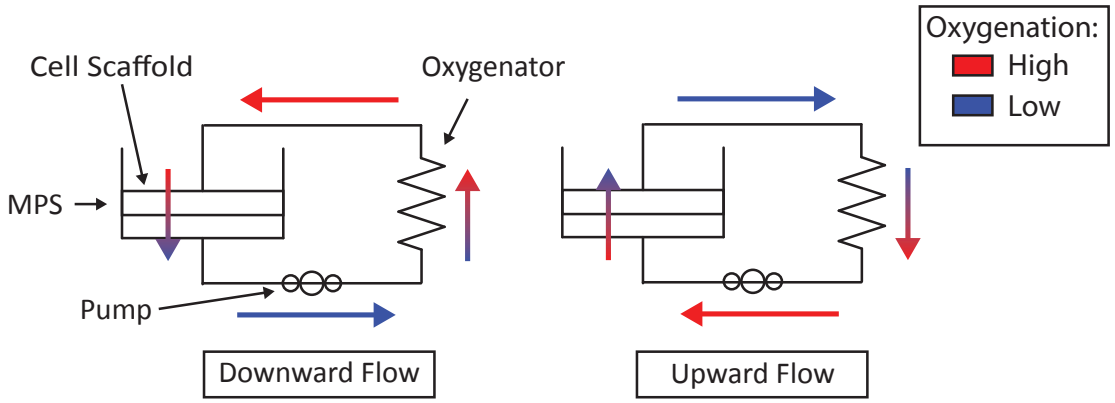

Figure 3-1: Inline Configuration: the oxygenator is on the same flow circuit as the MPS and cell scaffold. The flow is downward (left) for the first 8 hours to help the cells seed on the scaffold. After 8 hours, the flow reverses (right). This configuration requires a reversible oxygenator.

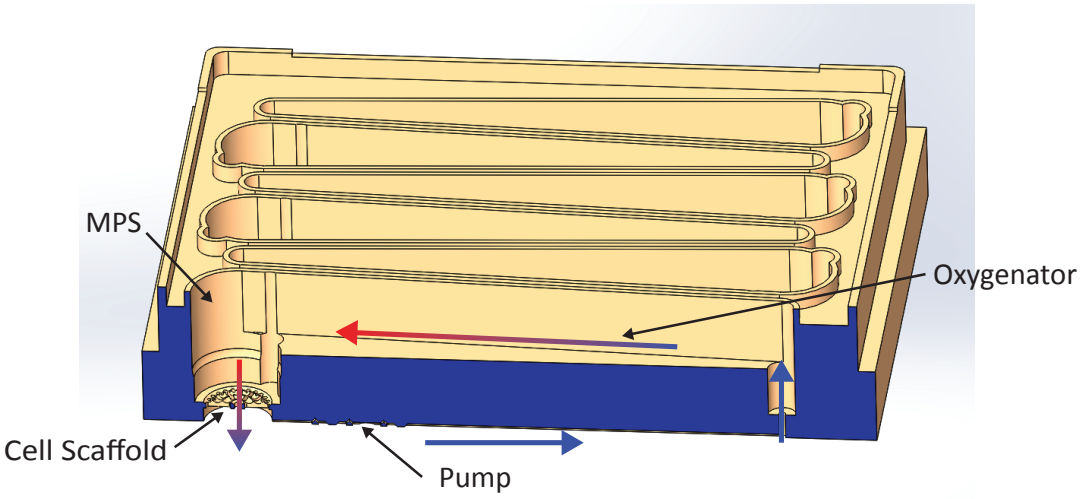

Figure 3-2: Inline Circulation on the CN Bio LiverChip during downward flow. The oxygenator consists of a wide channel with enough exposed surface area to oxygenate the media as it travels back to the MPS.

3.2.2 Co-flow

The co-flow configuration (Figure 3-3) decouples the oxygenator from the MPS recirculation flow circuit. This allows a uni-directional oxygenator. When flowing downward, if the flow rates are equal, the system behaves like an inline system, and the cells are exposed to the highest saturation media in the system. However, when flow is upward, the cells are exposed to a mix of oxygenated media from the oxygenator and deoxygenated media from the MPS outlet. This results in the cells being exposed to a lower oxygen concentration for a given oxygenator efficiency than in an inline system.

3.2.3 Counter-flow

The counter-flow configuration (Figure 3-4) is similar to co-flow, but the cells are exposed to the high-concentration media during upward flow, rather than downward flow. This is advantageous, since exposure to the lower concentration mixed media is limited to the first 8 hours of a multi-day experiment. Like co-flow, counter-flow allows a unidirectional oxygenator. However, if the oxygenator flows downhill and is not a closed system capable of suction, the pump must come before the oxygenator.

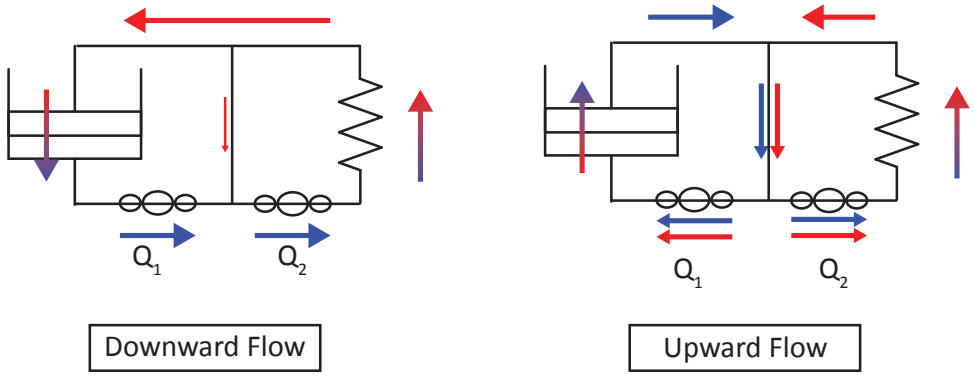

Figure 3-3: Co-Flow: *Left:* During seeding, mixed oxygen concentration media enters the oxygenator, and high oxygenconcentration media is fed to the cells. The small flow down the central channel assumes Q_2 is only slightly greater than Q_1. *Right:* After seeding, mixed media is fed to cells and to the oxygenator. Q_2 is in the same direction in both flow conditions, so a unidirectional oxygenator can be used.

This makes fabrication more challenging than for the Co-Flow configuration, and multiple vertical channels are needed to bring the pumps into the same plane. If these channels are open, very slight differences in pump flow rates can lead to fluid accumulation or depletion over time.

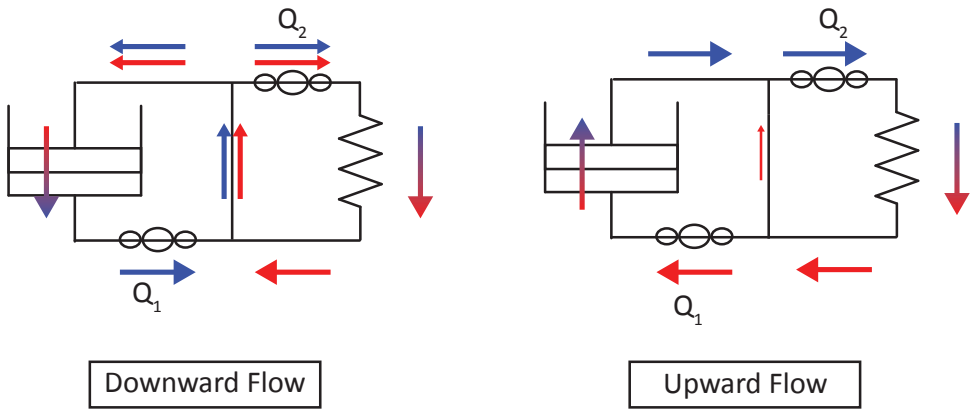

Figure 3-4: Counter-Flow: *Left:* During seeding, mixed concentration media enters the cells and oxygenator *Right:* After seeding, high concentration media is fed to cells

3.2.4 Laminar Figure-8

What we call the figure-8 configuration (Figure 3-5) attempts to combine the strengths of the co- and counter-flow concepts, so that the cells are exposed to high-concentration media, but the oxygenator does not need to be reversible. During downward flow, the system behaves like an inline system if the oxygenator and re-circulation flow rates are the same, feeding high concentration media to the cells. During upward flow, the short laminar section attempts to limit mixing, separating the flow paths into a high concentration stream for the cells and a low concentration stream for the oxygenator. The main drawback of this concept is its difficulty to manufacture, and the potential requirement for additional volume compared to the other systems.

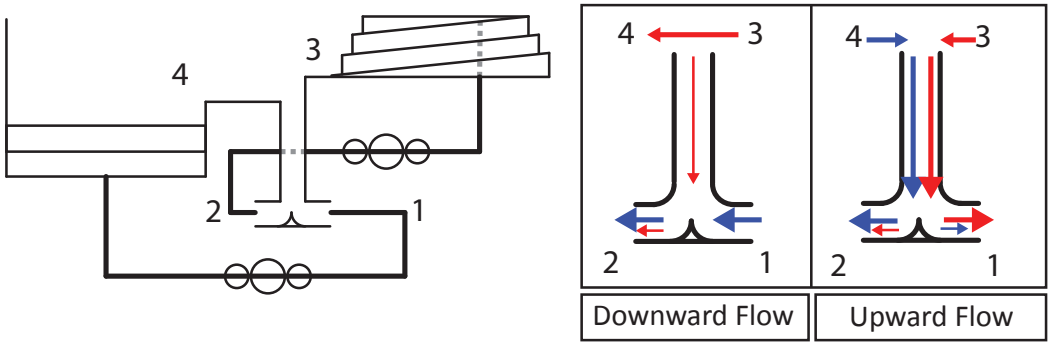

Figure 3-5: Laminar Figure-8: A laminar flow channel allows fluid paths of high and low concentration to flow side-by-side only mixing by diffusion. At the bottom of the channel, a wedge splits the flow, allowing the high and low concentrations to be directed to the cells and the oxygenator, respectively. During downward flow, the flow coming from the cells flows primarily around the flow splitter (1 to 2), through the oxygenator (2 to 3), and into the cells (3 to 4), with flow from 3 to 2 if the oxygenator flow rate is higher than the cell perfusion flow rate. During upward flow, media comes up through the cells (1 to 4), primarily down the left side of the laminar channel (4 to 2), through the oxygenator (2 to 3), and primarily down the right side of they laminar channel (3 to 1).

3.2.5 Selective Sourcing

The selective sourcing configuration (Figures 3-6 and 3-7) attempts to feed the cells high concentration media during upward flow by placing the recirculation intake directly under the oxygenator output. During downward flow, the cells see a mixed concentration, but the oxygenator flowrate can be increased to increase oxygen transfer to the system. Both pumps can be on the same plane below the MPS, and the oxygenator can flow downhill to empty passively without reversing. Further, no extra reservoirs are required, making this configuration nearly as compact as the inline system.

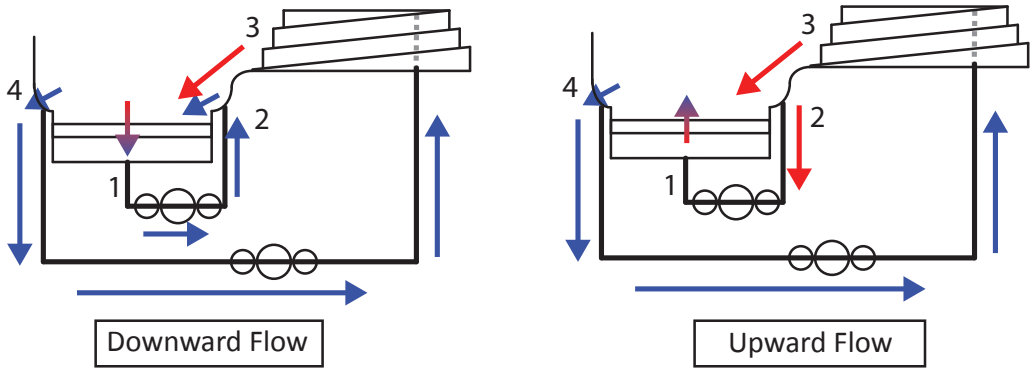

Figure 3-6: Selective sourcing. During seeding (left), media flows down through the cells, where oxygen is consumed, then from 1 to 2. A mixture of media from 3 (high oxygen concentration) and 2 (low concentration) then flow both back through the cells, and also to 4, which feeds the oxygenator. During upward flow (right), the cells are fed by media sourced from 2, which is a mix of high concentration from 3 and low concentration from the cells. The position of 2 directly under the oxygenator output 3 increases the ratio of high to low concentration media, so the cells see an oxygen concentration above the bulk average in the well. At the input to the oxygenator (4), the opposite occurs, pulling media that is below average oxygen concentration.

3.3 Circulation Concept Selection

The selective sourcing configuration was chosen as the best compromise between feeding the cells high oxygen concentration and keeping fluid volume low and manu-

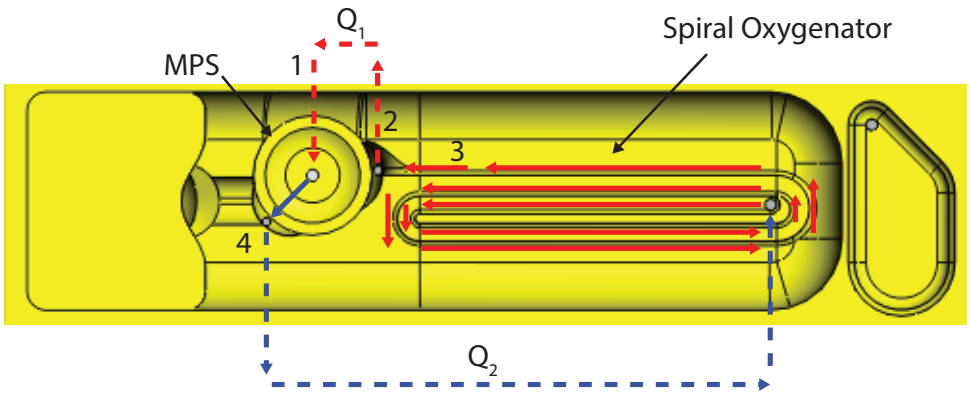

Figure 3-7: Selective sourcing shown on the Rev2 platform during upward flow. Q_1 is the flow through the scaffold, and Q_2 is the oxygenator flow.

facturing straightforward. The inline concept feeds the cells the highest concentration, but precluded the self-clearing oxygenators considered. The figure-8 configuration is promising, but was deemed too complex a development effort for the scope of this project.

3.4 In-Line Reactor Model

In the existing LiverChip platform, media flows in a single circuit through the cell scaffold and along a long open well where the media is reoxygenated by passive diffusion [3]. This can be understood with the simple model shown in Figure 3-8 (A). In steady state, $(C_{high} - C_{low}) = \frac{r}{Q}$. Using the definition of the oxygenation potential (eqn. 2.21), the steady-state concentrations in the system (where the subscript i indicates the inline model) are

$$C_{low,i} = C_{sat} - \frac{r}{Q_i \phi_i} \tag{3.1}$$

$$C_{high,i} = C_{sat} - \frac{r}{Q_i \phi_i}(1 - \phi_i) \tag{3.2}$$

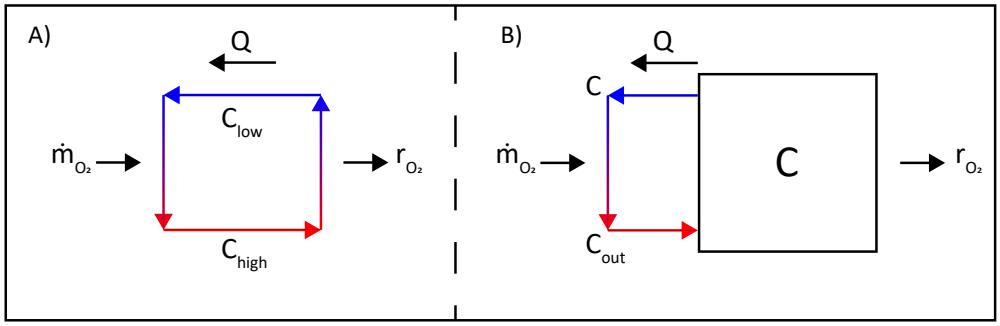

Figure 3-8: Schematic of *(A)* the inline and *(B)* the mixed reactor models. In *A)*, media leaving the oxygenator at C_{high} feeds directly into the cells and re-enters the oxygenator at $C_{low} = C_{high} - \frac{r}{Q}$. In *(B)* Media exits the oxygenator at a high oxygen concentration C_{out}, mixes with bulk fluid volume to reach a mixed concentration C and media at concentration C then re-enters the oxygenator.

3.5 Mixed Reactor Model

During downward flow, and for sufficiently high oxygenator flow rates during upward flow, we assume that the oxygenator is in a closed loop with a fully mixed chamber at concentration C, which is steadily consuming oxygen at rate r. The input to the oxygenator is therefore C, and the mass transfer into the oxygenator is $\dot{m}_{O_2} = Q(C_{out} - C_{in})$, or $\dot{m}_{O_2} = Q\phi(C_{sat} - C)$, where ϕ is the oxygenation potential.

The rate of change of mass in the fully mixed system of volume V is balanced by the mass transfer into the oxygenator and the oxygen consumption by the cells:

$$V\frac{dC_m}{dt} = \dot{m}_{O_2} - r = Q_m\phi_m(C_{sat} - C_m) - r. \tag{3.3}$$

Substituting for $\dot{m}_{O_2}$ and solving for concentration C:

$$C_m = \left(C_{sat} - \frac{r}{Q_m\phi_m}\right)(1 - e^{-\frac{Q_m\phi_m}{V}t}). \tag{3.4}$$

The steady-state ($t \to \infty$) bulk concentration is therefore

$$C_m(t \to \infty) = \left(C_{sat} - \frac{r}{Q_m\phi_m}\right) \tag{3.5}$$

and the transient response time constant is $\frac{V}{Q_m \phi_m}$. Note that because this model assumes a fixed oxygen consumption rate r, $\left(C_{sat} - \frac{r}{Q\phi}\right)$ can be less than zero; this is clearly non-physical. This error could be mitigated using better model of oxygen consumption kinetics, such as the first-order Michaelis-Menten model (Inman develops this model for the scaffolds used [3]). However, as a hardware design tool to develop a platform that can oxygenate equivalently to the LiverChip performance, this simplified model is sufficient.

Equation 3.4 allows us to see the bulk concentration (and in this model, the concentration entering the oxygenator) in terms of oxygenator flowrate Q_m and oxygenation potential ϕ. We can then estimate ϕ for a given geometry by using equation 2.21.

The steady-state bulk concentration is $C = C_{sat} - \frac{r}{Q_m \phi_m}$. Plotting (Figure 3-9) this concentration against flowrate for different geometries (represented by $\frac{h}{A}$), we find a range of acceptable flow rate (Q_m) and geometry ($\frac{h}{A}$) combinations that will provide adequate mass transfer (r) without requiring a bulk concentration C below a minimum acceptable lower limit (no less than zero). The solid lines are the mixed model predictions for varying geometries, and indicate that a ratio $\frac{h}{A}$ of below .001 would be required at a minimum of 5 μL/s oxygenator flow rate to meet the requirement of 150 μM oxygen concentration flowing to the cells. The dashed lines are model predictions using the measured oxygenation potential values shown in Figure 2-21. The mixed model predicts that while the revision 1 prototype at 4 μL/s will meet the functional requirement of 150 μM steady state concentration, the revision 2 prototype will not. However, this may only be the case for the first eight hours of downward flow. An experiment discussed in Section 3.7 suggests that during upward flow, the system behaves more like an inline system for oxygenator flow rates near 2 μL/s.

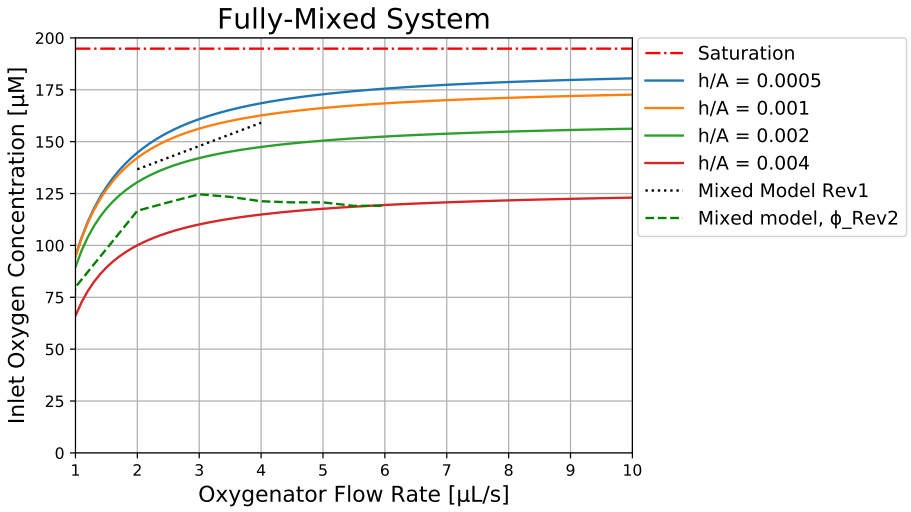

Figure 3-9: Predicted steady-state bulk concentration for the mixed model, where cell consumption rate $r = 100$ [pmol/s]. The saturated concentration is 195 μM (see Appendix A). Predicted values for the revision 1 and 2 prototypes represent the measured values for the oxygenation potentials ϕ substituted into equation 3.5 (dashed lines). Note that because the consumption rate r is assumed to be fixed, this model can include non-physical negative concentrations.

3.6 Inline vs. Mixed Equivalence

Comparing equations 3.2 and 3.5 shows the parameters required of the two systems to achieve equivalent oxygen concentration in the cell environment. In the inline system, the cells experience the high concentration media directly from the oxygenator. In the mixed system, the cells experience a mixed concentration because the freshly oxygenated media is diluted by the bulk concentration in the MPS. Equating the concentration going to the cells in these two scenarios,

$$C_{cells,i} = C_{high,i} = C_{sat} - \frac{r}{Q_i \phi_i}(1 - \phi_i) \tag{3.6}$$

$$C_{cells,m} = C_m = C_{sat} - \frac{r}{Q_m \phi_m} \tag{3.7}$$

$$Q_m \phi_m = \frac{Q_i \phi_i}{(1 - \phi_i)}. \tag{3.8}$$

Equation 3.8 gives a simple criterion for the desired Q_m and ϕ_m of a mixed system required to match the steady-state concentration of a given inline system. Based on

the oxygenation potential of 0.8 measured on the LiverChip at a flow rate of 1 μL/s (the scaffold perfusion flow rate recommended by CN Bio), equation 3.8 predicts that $Q_m\phi_m = 4$ μL/s is required to match the steady-state concentration observed on the LiverChip (shown as a dashed line in Figure 3-10). Predicted and measured $Q_m\phi_m$ values are shown in Figure 3-10. This figure suggests that $\frac{h}{A}$ four times smaller than that of the revision 2 prototype would be required to reach LiverChip equivalency. This can also be seen by comparing the predicted concentrations in Figure 3-9 to the steady state concentration of 170 μM at 1 μL/s shown in Figure C-2.

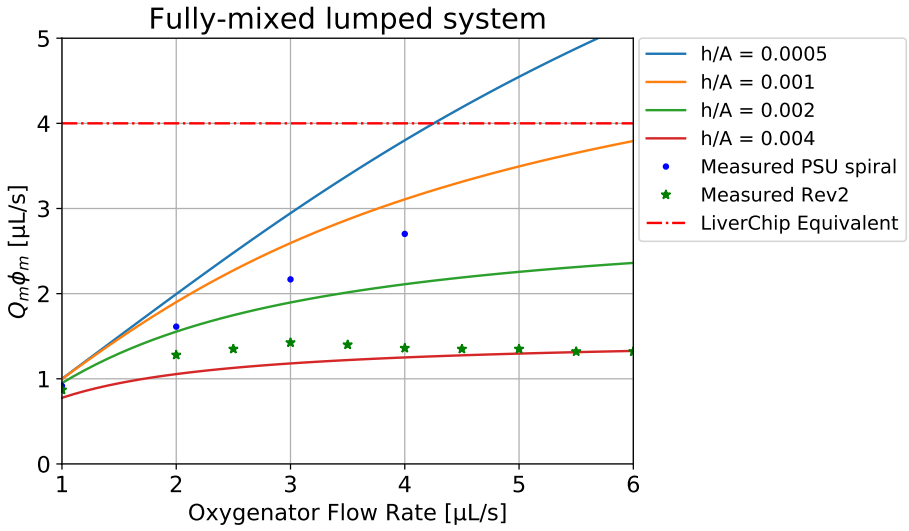

Figure 3-10: Based on the mixed reactor model approximation (Section 3.5), the Rev2 oxygenator will not achieve the same steady state concentration going to the cells as the LiverChip. To do so, the mixed reactor model predicts a flow rate of 4 μL/s and $\frac{h}{A} < .0005$ would come close to equivalency.

This reduced $\frac{h}{A}$ could likely be achieved by making the oxygenator four times longer, 2 times taller, or some combination of longer and taller (see Section 2.5).

3.7 Selective Sourcing Validation Experiment

The selective sourcing concept aims to pull media for feeding the cells from under the oxygenator (potentially a high concentration zone), while feeding the oxygenator from the opposite side of the MPS well (potentially low concentration). At very high

oxygenator flow rates, we expect the MPS to be fully mixed, but it is difficult to predict at what flow rate that mixing begins to dominate.

To assess the selective sourcing effect, the revision 1 prototype was used. Feeding deoxygenated Bovine Serum Albumin (BSA) solution into the MPS and removing partially oxygenated fluid created a net oxygen mass transfer out of the system, simulating oxygen consumption by the cells (Figure 3-11).

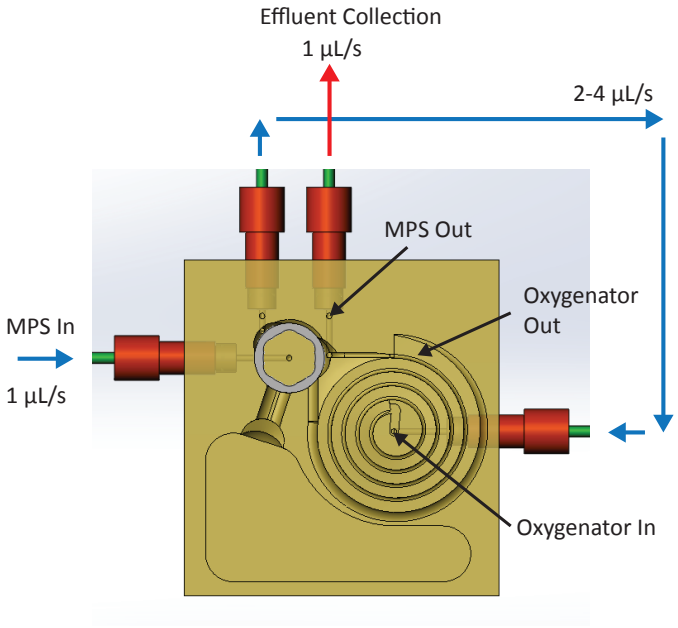

Figure 3-11: To simulate oxygen consumption, fluid is pumped out of the MPS (MPS out) and replenished with deoxygenated media (MPS In). In parallel, fluid is pumped from the MPS into the spiral oxygenator, where it flows into the MPS after the oxygen concentration is measured.

The experimental setup is shown in Figure 3-12. A 1% BSA solution in saline (PBS) was deoxygenated by bubbling nitrogen in a glass jar which was vented outside the incubator. A piece of 1/16 in. OD PEEK tubing withdrew fluid from the bottom of the jar, below the bubbling tube to prevent bubbles from being pumped into the oxygenator. A pneumatic diaphragm pump block pumped this deoxygenated fluid into the bottom of the MPS, and withdrew partially oxygenated fluid from the recirculation intake directly under the oxygenator output. Separately, two channels on a second pump block were combined in parallel to flow fluid at 2 to 4 μL/s into

the oxygenator, drawing from the side of the MPS opposite the recirculation intake. Fiber-optic oxygen probes (Lucid Scientific, Atlanta, GA) measured dissolved oxygen concentration at the three locations marked by black arrows in Figure 3-11 and also in the deoxygenation jar.

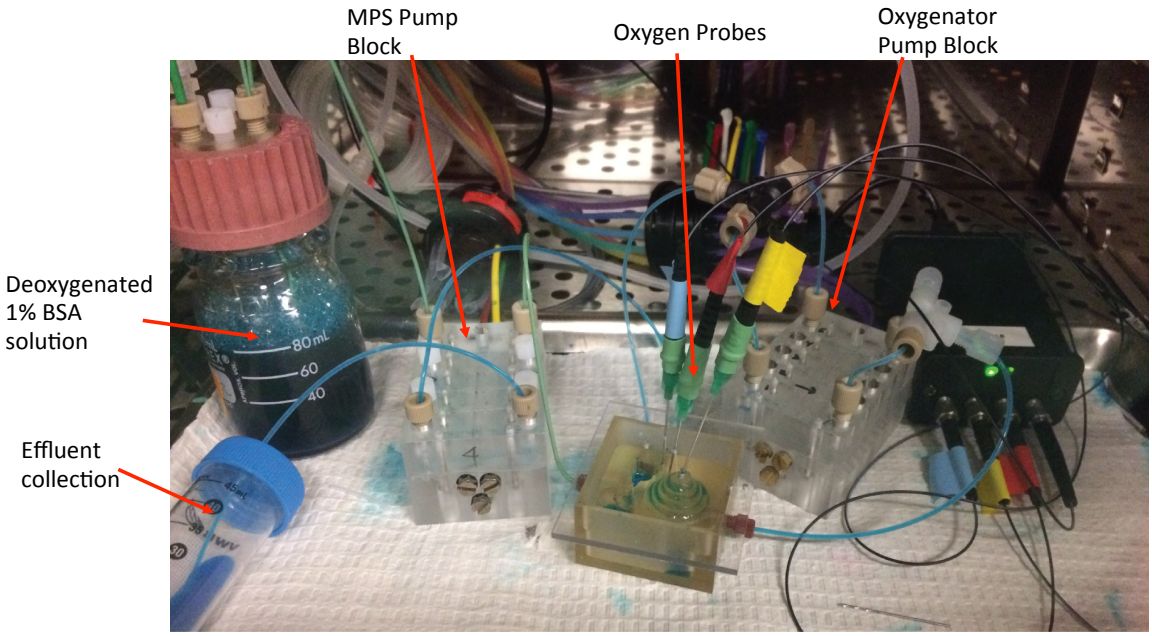

Figure 3-12: The setup used to test the Rev1 prototype. The MPS pump block both pumps deoxygenated BSA solution into the MPS, and also withdraws mixed concentration BSA into the effluent collection at the same flow rate. Only three oxygen probes are visible; "MPS In" is measured with a hidden probe in the bubbler shown at left. Previous experiments showed that at 1 μL/s, oxygen permeation through the short length of PEEK tubing is negligible. The oxygenator pump block circulates fluid through the oxygenator using two channels in parallel.

The concentration values measured at these locations are shown in Figure 3-13. The recirculation was flowing upward at 1 μL/s, as it does after the flow reversal at eight hours. Before timepoint A, the oxygenator pump block was flowing at 2 μL/s. Shortly after timepoint A, it began pumping at 4 μL/s. After some initial effects (likely from clearing dead volume), the probes show an exponential rise to a new steady-state value. The cause of an apparent steady increase at the oxygenator inlet around timepoint B is unknown, but the observed effect is small.

If the system behaves more like an inline system, then the "MPS Out" reading (point 2 in Figure 3-6), which the cells would be exposed to during upward flow,

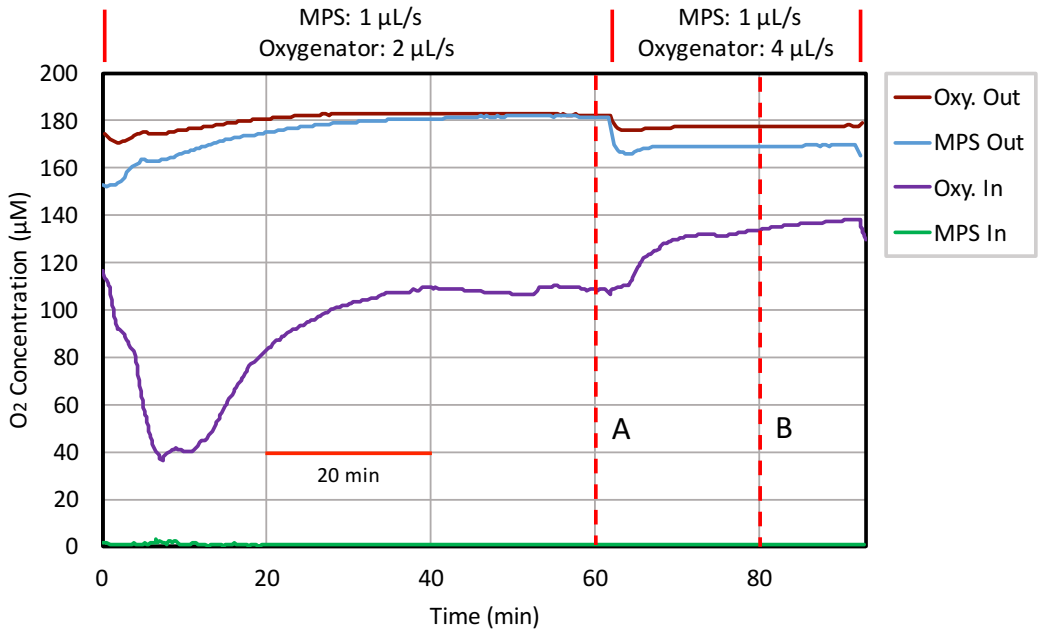

Figure 3-13: Oxygen probe data from the setup shown in Figure 3-12. Shortly after time point A, the oxygenator flow rate was changed from 2 to 4 μL/s. In the incubator environment, oxygen saturation is at 195 μM (see Appendix A).

should be the same as the oxygenator output, "Oxy. Out" (point 3 in Figue 3-6). If, on the other hand, the system behaves like a lumped fully mixed system, "MPS Out" should match the predicted steady state concentration value given by equation 3.5. Figure 3-14 shows this comparison at two different flow rates. At timepoint A (2 μL/s), the simulated consumption rate $r' = 1\ [\mu\text{L/s}] \times (C_{\text{MPS out}} - C_{\text{MPS in}})\ [\mu\text{M}] = 178$ pmol/s and $\phi = 0.86$. At timepoint B (4 μL/s), $r' = 165$ pmol/s and $\phi = 0.73$. It appears that in both cases, the system behaves closer to an inline system at 2 and 4 μL/s, though less so at 4 μL/s. This suggests that the model developed in Section 3.5 is a very conservative lower bound that is more applicable at higher flow rates than at lower ones. Further, while the mixed model assumed in Figure 3-10 suggests that higher flowrates yield better performance, these data suggest the opposite occurs at lower flow rates, and an inline model is more appropriate. Because the inline system is more effective, keeping the system in this unmixed regime can yield higher oxygen concentration delivered to the cells. Note that the simulated oxygen consumption

rate r' is a function of the "MPS Out" concentration, and therefore different between timepoints.

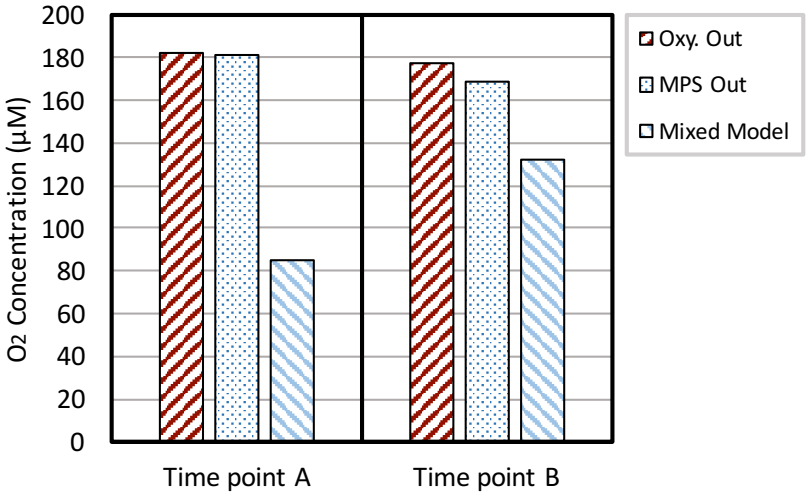

Figure 3-14: Concentration readings at time points A and B in Figure 3-13. Oxy. Out is the oxygenator output, which would go to the cells in an inline configuration. MPS Out is what goes to the cells in the selective sourcing configuration described. Concentration going to the cells in the mixed model is predicted from equation 3.5, where ϕ is calculated from the probe readings at the specified time point, and the simulated consumption rate r' is calculated from measured concentrations as $r' = Q_{\text{MPS}}(C_{\text{MPS out}} - C_{\text{MPS in}})$ in [pmol/s], where Q_{MPS} is 1 [μL/s] and the concentrations are in [μM]. The mixed model underestimates the oxygen concentration relative to the experimental results.

This simulated oxygen consumption experiment is challenging to perform with the revision 2 platforms because the pumping is on-board and difficult to interrupt. However, because the MPS well geometry is the same between revisions 1 and 2, we expect that the trend shown in Figure 3-14 will hold for revision 2 as well, and at an oxygenator flow rate of 1-2 μL/s, the inline model will give a better prediction of the steady state oxygen concentration of media going to the cells. While using the mixed model would lead to selecting an oxygenator flow rate of 3 μL/s or above, Figure 3-15 suggests that if the selective sourcing behaves like an inline system at low flow rates, a flow rate of 1-2 μL/s would in fact give a higher cell feed concentration.

This selective sourcing effect is only expected to occur after during upward flow, when the cell feed pulls from under the oxygenator output. In the first eight hours

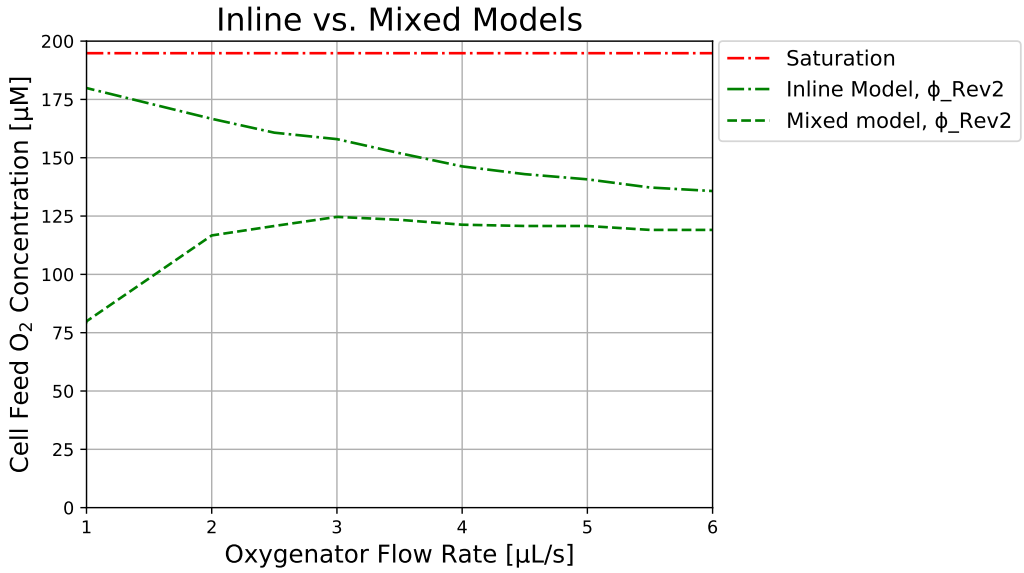

Figure 3-15: The oxygen concentration of media going to the cells for a fixed cell oxygen consumption rate $r = 100$ pmol/s, predicted from measured revision 2 oxygenation potential data using the inline and mixed models (eqns. 3.6 and 3.7, respectively).

flowing down through the scaffold, the oxygenator output and deoxygenated media from the cells will flow into the MPS above the scaffold in the same location (as shown at left in Figure 3-6). The system is therefore likely to behave more like the mixed system, and should be operated at a higher oxygenator flow rate. Figure 3-15 suggests 3 μL/s would offer the highest cell feed concentration at 125 μM for the mixed model; this is below the 150 μM requirement, but may be acceptable for a short duration.

3.8 Summary

The selective sourcing concept was chosen as a compromise to balance the fabrication considerations that favored the mixed co-flow concept against the higher concentration achieved in an in-line system for a given consumption rate and oxygenator efficiency. The mathematical models developed to describe the in-line and mixed systems serve to bound the expected steady state concentration going to the cells. Empirical testing with the revision 1 prototype simulating oxygen consumption

indicate that for upward flow, the system behaves like an inline system at low oxygenator flow rates. This indicates that the revision 2 system will achieve 150 μM cell feed concentration (requirement 2) after eight hours, while not meeting the requirement during the initial downward flow. Whether this is the case in practice, and the impact that it might have on the cells, are questions needing further investigation.

Reversible recirculation (requirement 1) is allowed by decoupling the oxygenator and recirculation loops, and the degrees of freedom are coupled across replicates as described in Section 1.4.1 (requirement 3).

Chapter 4

Scaffold Attachment

This chapter explores several methods for securing the cell culture scaffold and preventing media from bypassing the cells. This design effort was secondary to the oxygenator and flow circuit designs, and the prototyping occurred primarily in the time that the revision 2 platforms were out for fabrication. Due to this constrained time-line, a low-risk elastomeric sealing method was used for the revision 2 platforms despite the potential drug and biomarker adsorption limitations of elastomers. In addition to documenting the attachment method used, this chapter aims to provide ideas to speed the development of a non-elastomeric solution in future efforts.

Section 4.1 describes the method used in the LiverChip and its limitations. Section 4.2 establishes the requirements for a new design. Sections 4.3 and 4.4 describe the concepts explored and which concepts were chosen to prototype. The design and prototyping process is described in Section 4.5.

4.1 Current Approach and Limitations

On both the LiverChip platform and the platform developed for this thesis, the cells are grown on a perforated polystyrene scaffold (CN Bio Innovations, Welwyn Garden City, UK). On the LiverChip, as shown on the left in figure 4-1, a polypropylene retaining ring secures the scaffold by means of an interference fit with the wall of the culture well. A user installs the ring by pressing down on it with a 10 mm

outer diameter tube. Under the scaffold is a filter and a scaffold support. The filter serves to diffuse the flow and, in combination with a membrane capacitor, reduce the pulsatility of the diaphragm pumps [1, 19]. During the initial downward flow that seeds the cells on the scaffold, the scaffold support prevents the filter from separating from the scaffold. Separation of scaffold and filter would allow cells to leak between the two and not bind to the scaffold openings.

The LiverChip retaining ring does not apply a consistent downward force, and thus relies on the deformation of the thin filter during installation, and its subsequent elastic response, to provide sealing, as illustrated in Figure 4-2. Because the filter is so thin, any force generated is negligible, and the leak path around the scaffold is not sealed in a strict sense. In a looser sense of sealing, the majority of the media does in fact flow through the scaffold rather than taking the higher-resistance path through the filter edge-wise and around the scaffold, because the flow resistance through the LiverChip scaffold is comparatively low. However, when using higher resistance scaffolds, leaking around the scaffolds has been observed. This can result in uncertainty about local shear stresses and the transport rate of oxygen and nutrients to the cells, confounding interpretation of experimental data.

A design pre-dating the LiverChip, described by Domansky et al. [2], used a silicone o-ring to provide the elastic deformation and conformal contact required to maintain a seal. Silicone, however, can absorb lipophillic drugs and biomarkers, confounding an experiment that measures such compounds. Viton, a fluoroelastomer used for the revision 2 platform, does not appreciably absorb these compounds, and its adsorption of many relevant biological compounds is negligible (absorption describes incorporation of compounds into the bulk of material, while adsorption refers to binding only at the surface). Even so, other compounds such as some steroids [29] can be adsorbed in significant amounts, so a non-elastomeric solution is preferable long-term to avoid unwanted adsorption.

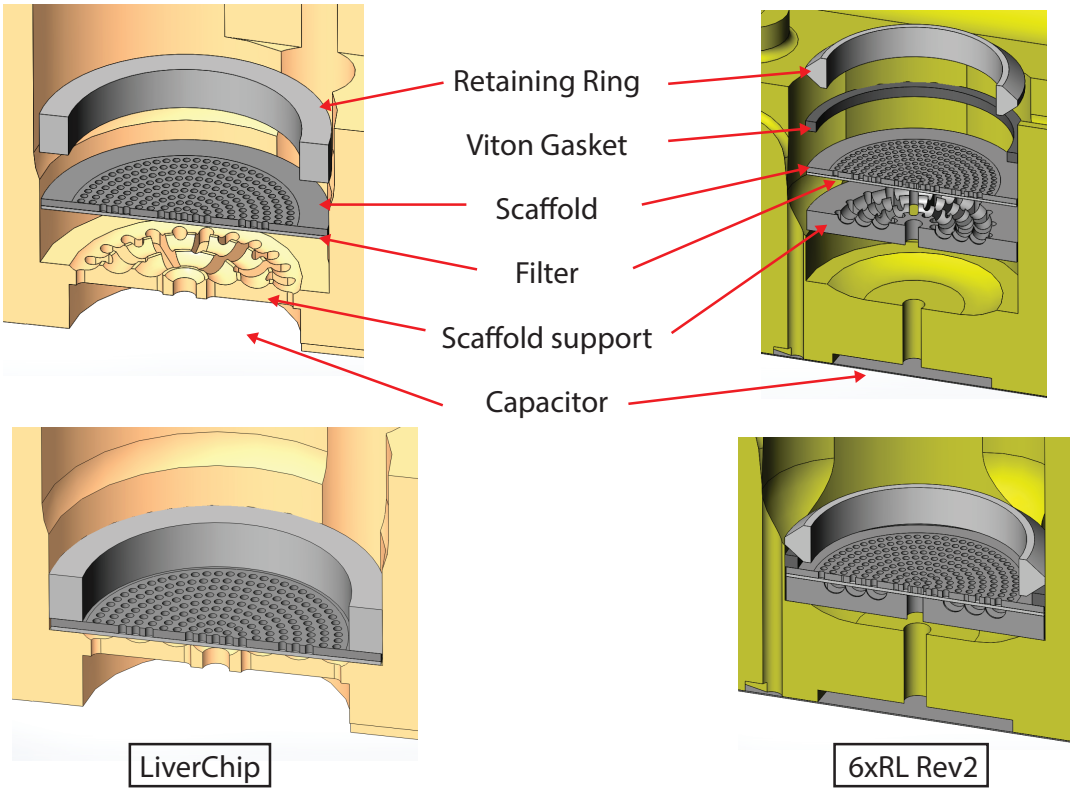

Figure 4-1: The scaffold assembly for the LiverChip (left) and reduced volume Rev2 platform (right). Both platforms use the same polystyrene scaffold (CN Bio Innovations, Welwyn Garden City, UK) and filter (Durapore 5 μm SVPP membrane filter, MilliporeSigma). Cells are initially seeded above the scaffold while the fluid is flowing downward and collect in the scaffold pores where the filter prevents them from passing through. The scaffold support prevents the filter from deflecting, which would allow the cells to move in between the filter and scaffold. After eight hours, the cells have attached to the scaffold walls and the flow is reversed to prevent cell growth from clogging the pores. The retaining ring holds the assembly in place and aims to prevent fluid from flowing around the scaffold and bypassing the cells. The Rev2 assembly improves this sealing function with a Viton gasket. The membrane capacitor, in combination with the filter and scaffold resistance, reduces the pulsatility of the flow, reducing the peak pressure below the scaffold (the membrane is not shown for the LiverChip on the left).

4.2 Scaffold Attachment Requirements

The following requirements were used to guide the design of the scaffold attachment feature.

1. ***Attachment method must withstand at least 5 N of upward force***

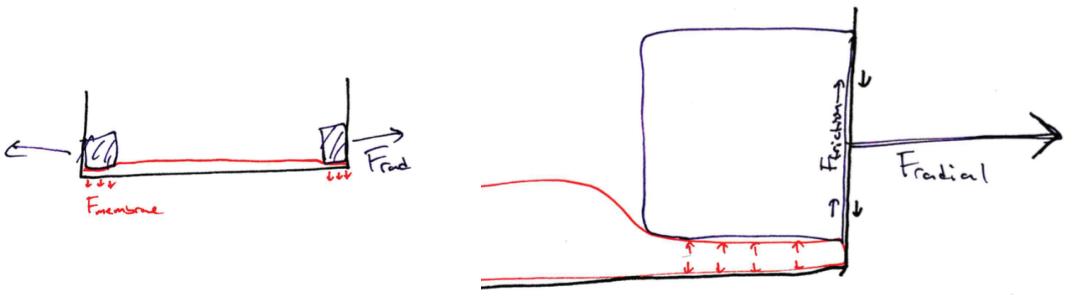

Figure 4-2: During installation of the LiverChip scaffold, the user presses down on the retaining ring, compressing the filter against the scaffold support. After installation, the thin filter provides minimal reaction force, and the system functions primarily by relying on the flow resistance of the filter and scaffold in the vertical direction being much lower than the resistance through the edge-wise filter.

To maintain the scaffold in position and prevent fluid from bypassing it, the device that applies downward pressure on the scaffold must not become dislodged. The maximum fluid pressure multiplied by the area of the scaffold gives an upper bound on the upward force exerted on the scaffold assembly. The driving air pressure of the pneumatic pumps is typically 40-60 kPa, so the maximum fluid pressure can be no greater than 60 kPa. The scaffold diameter is 10 mm, so the required force is 4.7 N. This is a highly conservative upper bound on force; the membrane capacitor under the scaffold, combined with the fluid resistance across the scaffold assembly, will limit the peak pressure at the scaffold to below the pump driving pressure. For the existing scaffold, the very low flow resistance means that the upward force is minimal. However, alternative scaffold designs are under development at MIT in the Griffith Lab that may have a greater flow resistance, and a design that accommodates this higher pressure drop would be useful in this and other applications.

2. ***Scaffold should leak no more than 0.1 $\mu L/s$ at a pressure differential of 40 kPa***

It is important to know the flow rate of fluid past the cells to calculate shear stresses and oxygen consumption; leaking around the side of the scaffold, rather than passing through it, will introduce error in these measurements. Ideally, the scaffold would be fully sealed and no leaking would occur. However, a leak rate of 0.1 μL/s is only 10% of the overall flowrate (1 μL/s), and the high pressure peaks would be both short in duration and likely lower than 40 kPa, due to the membrane capacitor. This limited leaking was agreed upon by the biology team as acceptable, understanding that full sealing is desirable.

3. ***Insertion force should be less than 50N***

   The mean maximum strength of subjects ages 21-60 pushing down with fingers on an object at seat height has been measured to be above 100 N for female subjects and 200N for male subjects [30]. 50% of the lower value provides a reasonable upper limit for insertion.

4. ***Attachment method must not damage scaffold or other components***

   Insertion and removal should damage neither the scaffold nor the platform itself. Because the platform is reusable, it must withstand many insertion/removal cycles, but a specific lifetime requirement was not determined within the scope of this project.

5. ***Attachment method must not occlude holes on cell scaffold***

   For flow to pass evenly through each hole in the scaffold, the attachment device must not cover the holes. This confines the sealing footprint area available on the scaffold to a band from 8 mm inner to 10 mm outer diameter.

6. ***Material must be cell- and drug-compatible***

   This requirement is explained in the general system requirements described in Chapter 1, but is included here for further clarification. Incorporating a fluoroelastomer such as Viton will allow more reliable sealing, but the biology team was uncertain about its tendency to bind certain drugs. While non-elastomeric materials such as polysulfone, polystyrene, or polypropylene are preferred, the team agreed that for the pilot experiments planned, Viton would be an acceptable material.

7. ***Design should allow a path to mass-manufacture, or be reusable***

   If the retaining ring is disposable, there must be a feasible method of mass-manufacture, such as injection molding. Alternatively, reusable devices could allow slower and more expensive processes. While the devices made within the scope of this project need not be mass-manufacturable, the design should be chosen and pursued with this end in mind.

4.3 Scaffold Attachment Concepts

This section presents concepts developed for sealing. The aim of these designs was a more deterministic method of applying a downward force to prevent flow around the scaffold that met the requirements described above.

4.3.1 Sealing Lands

If the contact area between the filter and scaffold support is reduced to a narrow band, a given downward force will produce a higher sealing pressure (Figure 4-3). This can be used with any of the other concepts, although it is unnecessary if an elastomer is used for sealing.

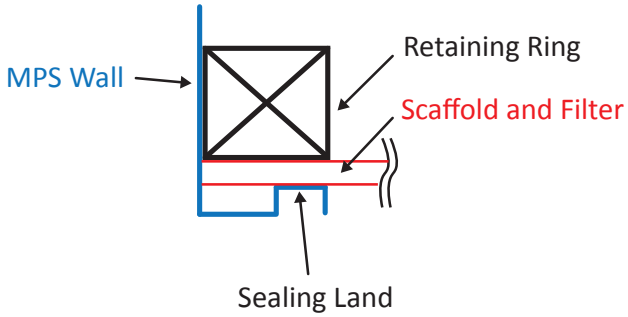

Figure 4-3: Sealing land: Reducing the contact area on the scaffold support to a narrow band increases sealing pressure for a given downward force.

4.3.2 Bi-Stable Spring

A bi-stable belleville washer, shown in Figure 4-4, could provide a strong downward force by engaging with features on the MPS wall. If a conical washer is sufficiently thin and elastic, it can be stable in the two positions shown, and will resist being flattened. Using a stainless steel washer, this may deliver the required forces in a compact mechanism. The primary challenges are ensuring that the outer edge reliably catches the MPS wall, and providing a means of easy removal. The latter might be accomplished by providing a hole or a tab punched through the middle portion of the ring, which a custom tool could use to flip the spring to the original upward position. Once in this position, it could be easily removed with tweezers.

4.3.3 Angled Ring and Lip

One simple improvement over the LiverChip retaining ring is to use an angled face to direct some of the radial force exerted by the ring downward to provide sealing force on the scaffold (Figure 4-5). The angled face can be on the retaining ring, or on the MPS wall. The main challenges with this concept are 1) achieving adequate radial expansion while staying within the elastic limit of the material, and 2) providing a convenient removal method.

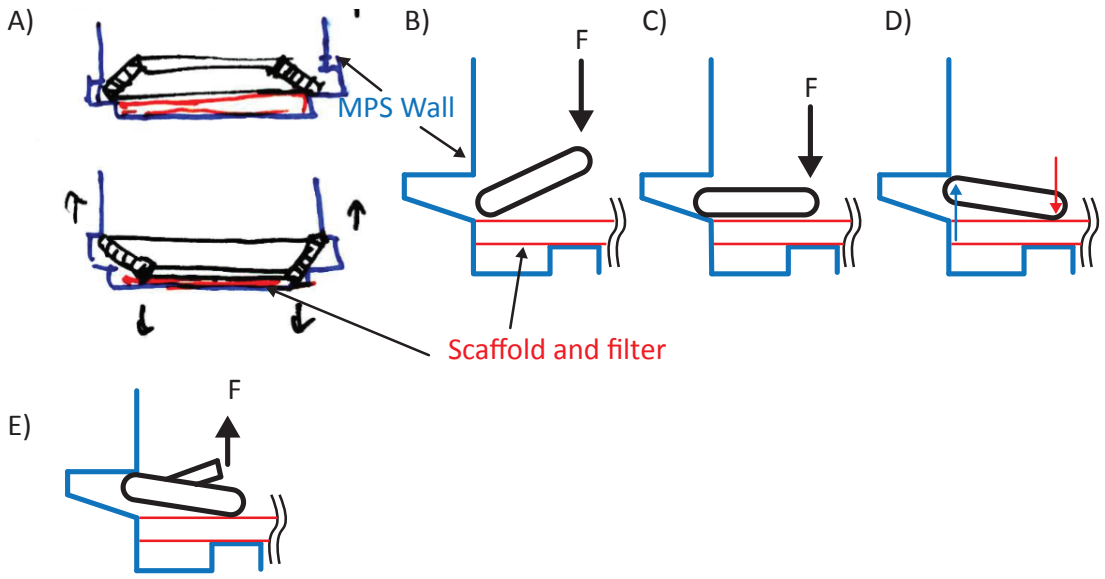

Figure 4-4: Bi-stable spring: *A)* A bistable spring, such as a belleville washer, can engage with features on the MPS wall to provide a downward force on the scaffold. *B)* In its relaxed state, the outer diameter of the washer can fit within the MPS wall. A downward force initiates deflection. *C)* As the washer deflects past the equilibrium point, the outer edge expands, and a ramp on the MPS wall pushes this edge upward. This creates a small gap under the washer required to push it past equilibrium. *D)* The pocket in the MPS wall is short enough that it catches the edge of the washer before the washer can relax to the full height. *E)* The washer may require tabs or some feature for removal.

4.3.4 External Screw Mount with Spring

The above concepts attempt to solve the challenge of providing adequate sealing force in a small, fully submerged mechanism. The concept presented here is to attach to the platform outside of or further up the MPS well, outside of the fluid, as shown in Figure 4-6. This provides more options for attachment, such as a screw or bayonet mount. This fixes the position of the retaining device, and a predictable downward force is provided by an elastic element, whether a solid tube with a low Young's Modulus, a spiral or wave spring, or a custom flexure. The main development challenge with this concept is ensuring that fluid does not wick up between the spring and the MPS wall, depleting the fluid at the bottom of the MPS and increasing the total volume required to keep the cells covered. This might be mitigated by keeping the gap small enough that the fluid volume is acceptable, or by use of a hydrophobic

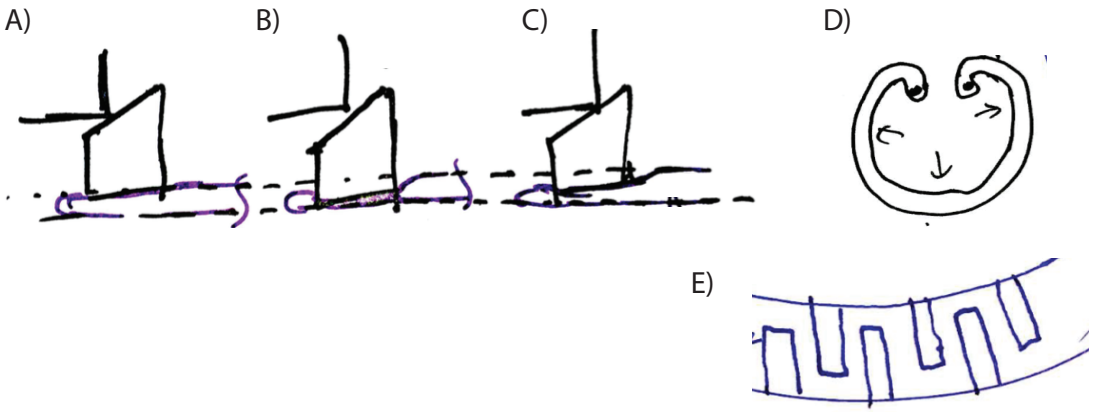

Figure 4-5: Ring and lip: *A)* An elastic chamfered ring with an outer diameter slightly larger than the MPS wall diameter relaxes into a groove in the MPS wall. *B)* A downward force on the ring compresses the filter material and allows the ring to relax further into the groove. *C)* when the downward force is released, the radial outward force of the ring results in a force downward on the filter and scaffold assembly due to the chamfered edge. *D)* Various existing expanding ring designs could increase the allowable deflection over a solid ring. *E)* One such design involves a zig-zag pattern cut into a ring to convert hoop compression into bending of many small beams in series, thus allowing greater deflection while remaining within the material elastic limit.

material or coating.

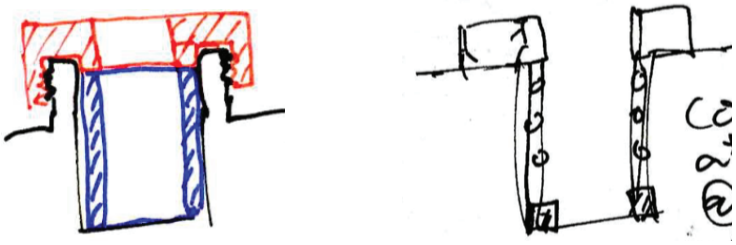

Figure 4-6: External screw mount: A screw or bayonet mount to the top of the MPS compresses an elastic tube (left) or a spring (right) to provide a downward sealing force on the scaffold assembly.

4.3.5 Snap Fit with Flexure

Similar to the external screw mount, the concept shown in Figure 4-7 uses a point of attachment outside of the fluid. A simple snap fit can engage with a pocket in the MPS wall and provide a downward force by elastic energy stored in the snap feature itself, or in a separated dedicated spring element. This concept, like the external screw mount concept, faces the challenge of wicking fluid away from the bottom of the MPS, with similar mitigation strategies.

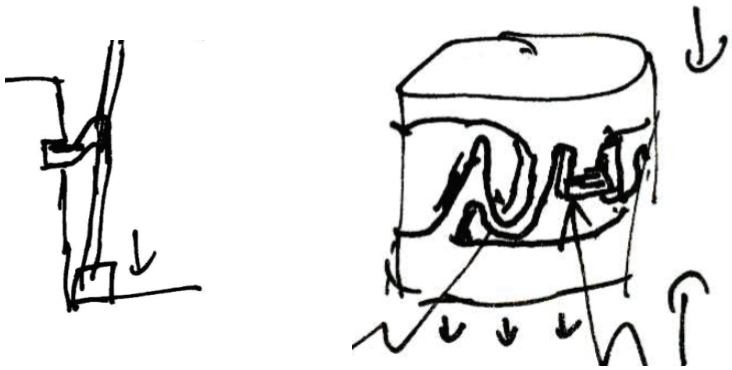

Figure 4-7: Snap fit: A cantilever snap feature engages with a pocket in the MPS wall. The downward sealing force can come from deflection of a beam at on the snap feature (left), or from a separate spring element, such as a flexure cut from a single tube (right).

4.3.6 Deflecting Beam

As a means of storing elastic energy and providing a downward sealing force, a deflecting beam could be integrated with an interference-fit ring (Figure 4-8). If the beam deflection remains elastic, this can provide a repeatable sealing force. The compact size and simplicity of the design may be outweighed by the challenge of achieving high enough forces without exceeding the elastic limit of such a small beam, as well as manufacturing and integrating a convenient means of removal.

Another variation of this concept was explored during development, where a beam element compresses both radially and axially. An example of is shown in Figure 4-9

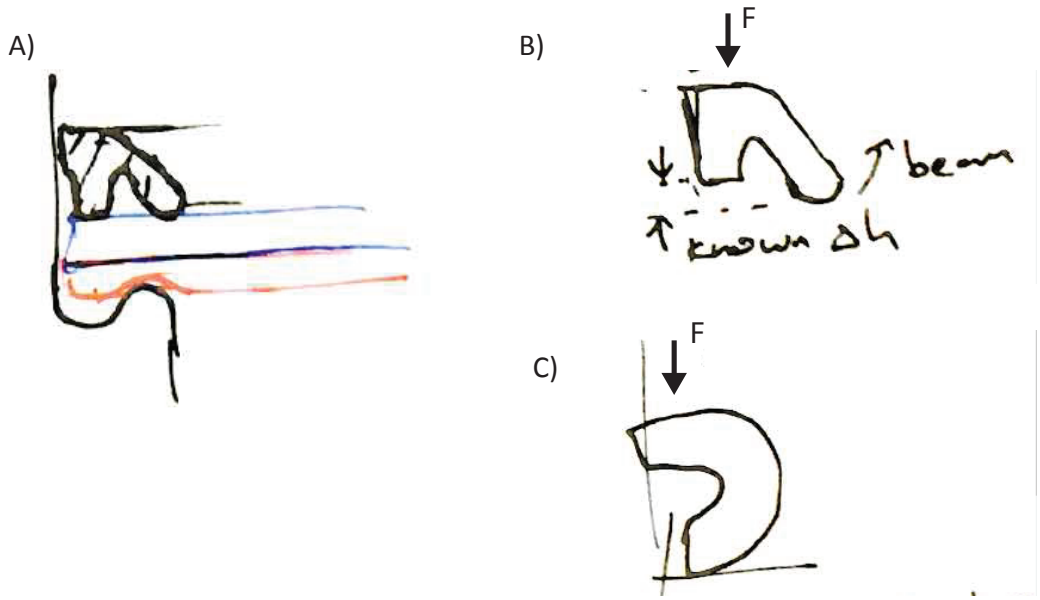

Figure 4-8: Deflecting Beam: Examples of ring cross-sections that use a deflecting beam to provide a downward sealing force. *A)* An outer ring interferes with the MPS wall, and this radial force results in a frictional force that keeps the ring in place. When the user presses the ring downward, a thin section of the ring deflects elastically in bending, providing a consistent downward sealing force that is less than the friction force against the wall. *B)* By incorporating a height difference between the beam and the base of the ring, a repeatable deflection (and therefore force) can be achieved, regardless of the insertion force F. *C)* A rotated configuration reduces the footprint of the ring, potentially providing a greater force without occluding the scaffold.

The advantage of such a method is that the radial stiffness can be lower than that of a ring, meaning that the holding force is less sensitive to small variations in well diameter. However, to achieve the high forces specified in the requirements at such a small size, the elastic stress limit of the ring must be significantly higher than polymers allow. Stainless steel may perform adequately, but gouging the polysulfone MPS walls becomes a significant risk, and the spring must have a large contact radius to avoid excessive contact stresses in the polysulfone. While exploration of this concept was cut short by schedule constraints, the challenge appeared to be in finding a beam geometry that was appropriately stiff in both directions at reasonable deflections, but that did not exceed the material yield stress. Making a beam wider will increase its stifness linearly without increasing the maximum material stress, but this makes the

beam stiffer in the perpendicular direction as the width to the third power. If the stiffness requirements in each direction are similar, this results in a roughly square cross section and the limiting factor becomes material yield stress. A material such as a superelastic nickel titanium alloy could resolve this, potentially being cut from a tube as many stents are, but the cost seems to quickly outweigh any benefit of a purely friction-based approach. This approach is worth considering, however in a configuration where the beams catch on pocket features in the MPS well, and the holding force is not from friction alone.

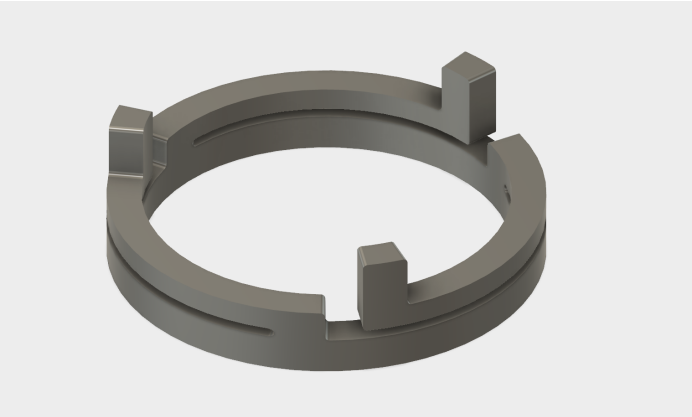

Figure 4-9: An alternate deflecting beam concept: the beams act as both the radial spring element that generates friction force, and also the vertical spring that is loaded during installation to provide a downward sealing force.

4.3.7 Tilting Ring

With an interfering ring of a triangular cross-section, as shown in Figure 4-10, if the outer top edge is pressed below the inner top edge, the hoop compression of the inner bottom edge results in reaction forces which create a moment on the ring. When installed, this moment is balanced by the frictional force from the wall and the compressive sealing force on the scaffold assembly.

The primary challenge to developing this concept is manufacturing to tight tolerances. While the existing ring can plastically deform without much consequence, the tilting ring concept would require elastic deformation to produce a reliable sealing force. The high stiffness of rings in radial compression results in a narrow window of

radial deflections that provide adequate friction force but avoid plastic deformation.

One embodiment of the tilting ring concept uses deflection of multiple projections to provide the required twisting of the ring, rather than pushing on the outer edge (Figure 4-11). These projections could then be used for removal. The projections must be stiff enough to twist the ring outward against its own elastic force as well as the friction force on the wall. In practice, it is challenging to make these beams stiff enough to cause adequate torsion at this small scale.

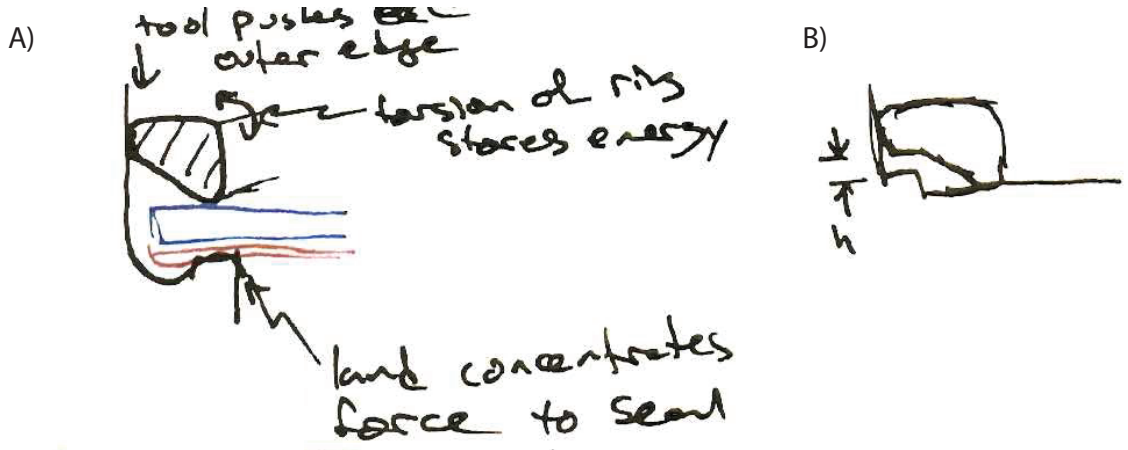

Figure 4-10: Tilting Ring: *A)* A downward force on the outside top edge results in a stored moment from the compression of the inside bottom edge. Because the outside top edge is constrained by friction against the MPS wall, this results in a downward sealing force on the scaffold. *B)* The deformation, and therefore reaction force, can be made more repeatable by a feature that limits the deflection distance h.

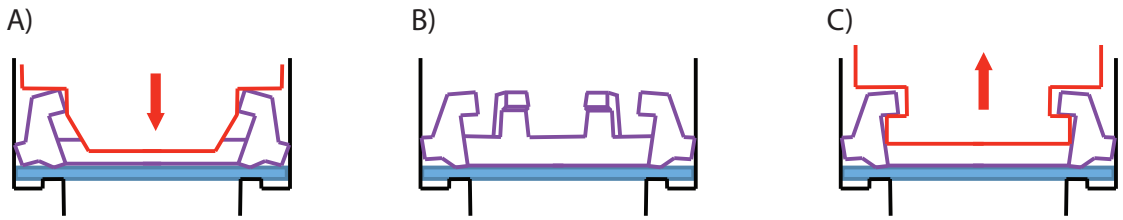

Figure 4-11: Tilting ring with deflecting clips: *A)* An insertion tool displaces multiple protruding clips radially outward and down, causing the outer edge of the ring to slide downward on the MPS wall. *B)* When the tool is removed, the ring partially untwists, exerting a downward force on the scaffold. *C)* To remove, a tool with fine teeth engages with the protrusions to remove them.

4.3.8 Wave Spring

The wave spring, shown in figure 4-12, is a variation on the tilting ring concept, using a waved piece of stainless steel wire bent into a shallow cone shape. The smaller diameter is placed down, and the larger diameter, which is slightly larger than the well, is pushed down. The crests at the top are held by friction against the well wall, and as they are pushed downward the bottom crests of the spring make contact with the scaffold, twisting the ring inward and causing reaction forces that push down on the scaffold to seal. The wire must be stiff enough to resist this twisting. The primary advantage that this method has over the retaining ring is that the waves introduce more compliance to the ring, allowing looser tolerances in the diameters of the ring and the well.

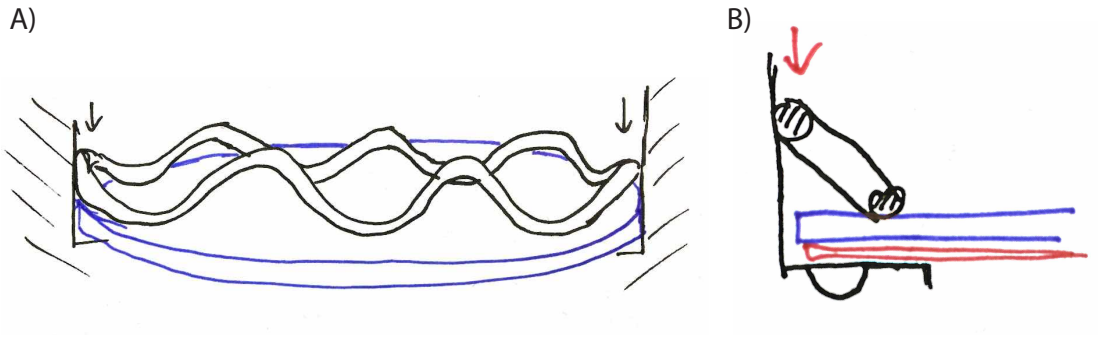

Figure 4-12: Wave spring: *A)* The ring consists of a ring of stainless steel wire that has waves that have been formed into a shallow cone. *B)* Similar to the tilting ring, when the top crests are pushed down by the installation tool, this induces reaction forces that provide a downward sealing force against the scaffold.

4.3.9 Ring with Elastomer

If an elastomer such as Viton can be used for the particular experiment performed, their high yield strains and low Young's moduli offer reliable sealing at a small size. Possible configurations are shown in Figure 4-13. The low yield strain of non-elastomeric materials such as polystyrene or stainless steel requires long beam lengths to reach high forces while remaining elastic, and when directly compressed, their high Young's moduli result in high forces at deflections below machining tol-

erances. Elastomers, by contrast, can deform under low forces to make conformal contact with mating surfaces, which improves sealing, and can store elastic compressive forces at reasonable deflections without plastically deforming. An elastomeric seal is therefore desirable when there is no risk of adsorbing lipophillic compounds. Due to these sealing advantages, it is worth further assessment of the sorption potential of the small surface area exposed to circulating media, or of materials other than Viton that might be acceptable.

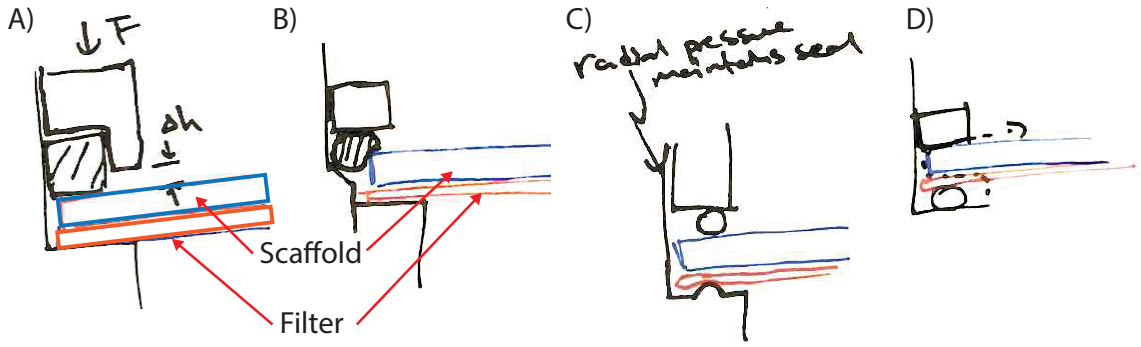

Figure 4-13: Elastomeric sealing: *A)* A constrained volume causes a downward force to provide sealing against both the MPS wall and the scaffold. *B)* This same effect could be achieved by a round gasket pressed into a gap between the MPS wall and the scaffold. *C)* If a ring with a smooth interference fit against the wall is used, the radial force may provide adequate sealing against the wall, and only a seal against the scaffold is necessary. *D)* If the gasket is under the filter, as described by Domansky [2], there is a potential leak path through the filter. The scaffold support is not shown.

4.4 Scaffold Attachment Concept Selection

Many of the concepts described above appear promising, but were excluded due to scheduling constraints. To provide adequate time for manufacturing, the revision 2 platform was released before much of the design effort on the scaffold attachment occurred. The Rev2 platform was designed to accommodate the existing retaining ring with a removable scaffold support to mitigate risk, with the goal of developing improved sealing method while the platform was out for production.

The design was therefore limited to friction-based approaches, such as the de-

flecting beam, the tilting ring, and a ring with a Viton gasket. The tilting ring was pursued as the easier to manufacture non-elastomeric strategy, while the ring and gasket approach was developed in parallel to ensure having a functional sealing option on schedule.

4.5 Scaffold Attachment Design and Prototyping

4.5.1 Testing Apparatus

The test fixture shown in Figure 4-14 was built to test the sealing of retaining ring prototypes. The machined pockets simulate the MPS well. The pockets were filled with water until an air-water interface was visible in the connected tube, and the retaining ring prototypes were assembled with the usual filter and a solid polyester disc replacing the scaffold to simulate full occlusion. The tube was then lightly pressurized, starting at <1 kPa, and slowly increased to 40 kPa (measured with Fluke 717 300G Pressure Calibrator). The air-water interface in the tube was observed to move in two cases: 1) while pressure increased, due to deflection of the polyester disk, and 2) when fluid was leaking. To avoid confounding these two effects, the pressure was therefore maintained static for 60 seconds at discrete pressure intervals to observe movement of the interface due to leaking alone. The inner diameter of the tube is approximately 1/16 in., allowing an estimate of leak rate by measuring the time over which the interface moved a known distance. Interface movements of less than 1 mm were observable, allowing detection of leaking lower than 0.2 μL/s. A hold time longer than 60 sec can be used to detect slower leaks. With this setup, the existing retaining ring was observed to leak in excess of 1 μL/s at pressures below 1 kPa, which was the lower detection limit. Because of possible differences in diameters, it is difficult to predict from this test the ring's performance in the actual LiverChip platform, but the presence of removal pockets cut into the wall of the well where the LiverChip retaining ring seals will likely limit any improvement that could be obtained from a smaller diameter well.

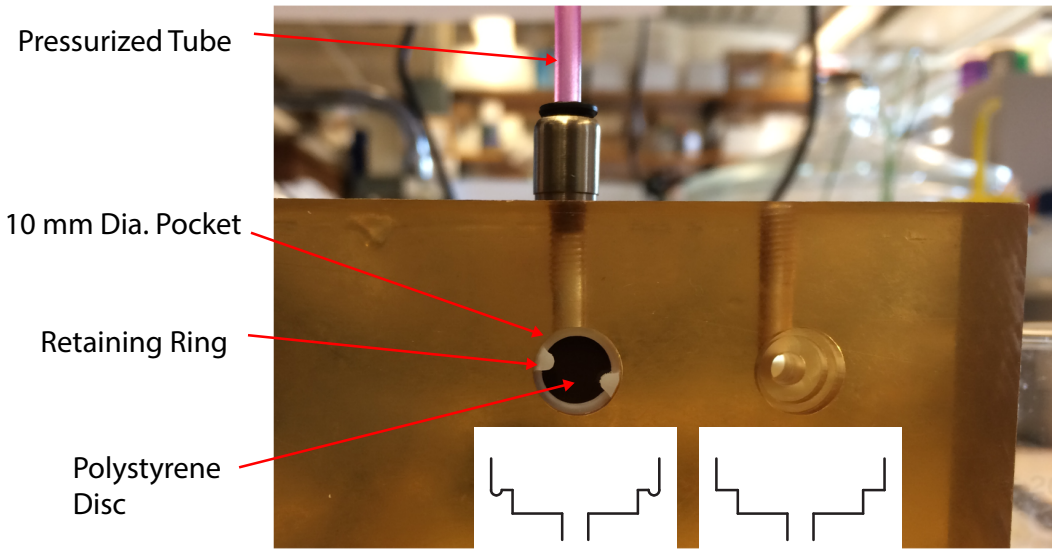

Figure 4-14: A fixture for leak testing retaining ring prototypes. Two pockets 10 mm in diameter, one with the sealing land (left) and one without (right), were CNC machined into polysulfone. Sections of these profiles are shown. A pneumatic connector (LEGRIS 3171-53-20, Parker Hannefin, FR) sealed to the polysulfone with an o-ring (hidden) and connected to 1/8 in. outer diameter (1/16 in. ID) tubing. Retaining rings were tested with a 9.8 mm diameter polyester shim the same thickness as the scaffold (0.10 in.) to simulate a fully occluded scaffold.

The diameter of the pocket is critical to the retaining ring performance, as it determines, for a given ring geometry and friction coefficient, the holding force achievable. To measure the internal diameter, a metrology grade rubber was cast into each pocket (see Figure 4-15), and measured with a micrometer (293-340, Mitutoyo, JP). To avoid compressing the rubber, the diameter was taken when it could no longer slide easily through the micrometer jaws. The pockets with and without the sealing land measured 10.02 ± 0.01 mm and 9.98 ± 0.01 mm, respectively. For machining the pockets, the toolpaths were identical before the final cut to form the sealing land. This final cut put the outer cutting edge of a smaller end mill at the same outer diameter, making a second cutting pass on the same surface, which may be responsible for the small difference in diameters.

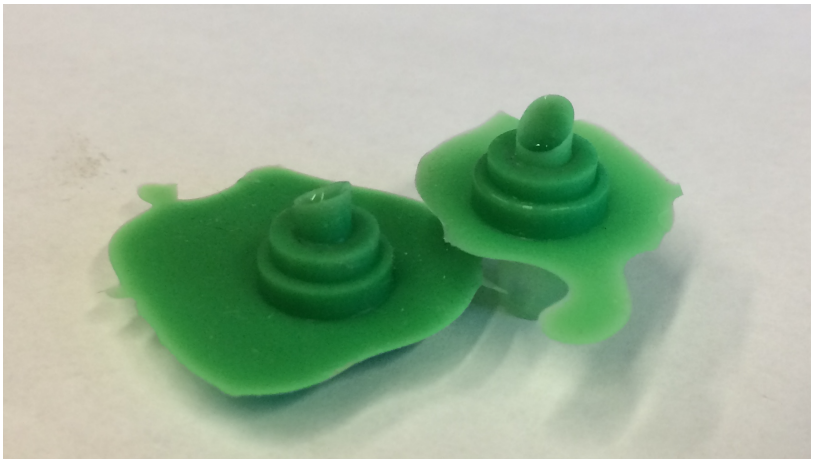

Figure 4-15: Casts for measuring pocket diameter. The casts are made from a low-shrinkage metrology grade rubber (Reprorubber Thin Pour, Flexbar, Long Island, NY).

4.5.2 Tilting Ring

The tilting ring concept described in Section 4.3.7 is installed by pushing the outer edge of the top surface downward, where it stays due to friction with the MPS wall. The elastic compression of the inside edge acts as a spring, applying a downward sealing force on the scaffold assembly. Several prototypes were machined to test the efficacy of this approach; the three main profiles explored for the tilting ring concept are shown in Figure 4-16. For profiles B and C, the removal clips were omitted for testing purposes.

The tilting ring prototypes were fabricated from high impact polystyrene on a desktop CNC mill (Othermill Pro, Bantam Tools, Berkeley, CA). CAD and toolpaths were generated in Autodesk Fusion 360. The primary fabrication challenge was indexing the part between milling operations on opposite faces. The most effective method used for these prototypes, illustrated in Figure 4-17, was to mill the bottom features on a cylindrical blank from the flat stock (Figure 4-18-A), then to press-fit this blank onto a machined post before machining the removal clips on the top. Because the locating post remained fixed after milling, its center was known, and the top features could be machined concentric to the bottom features.

While the LiverChip retaining ring is inserted using a tubular punch with a flat

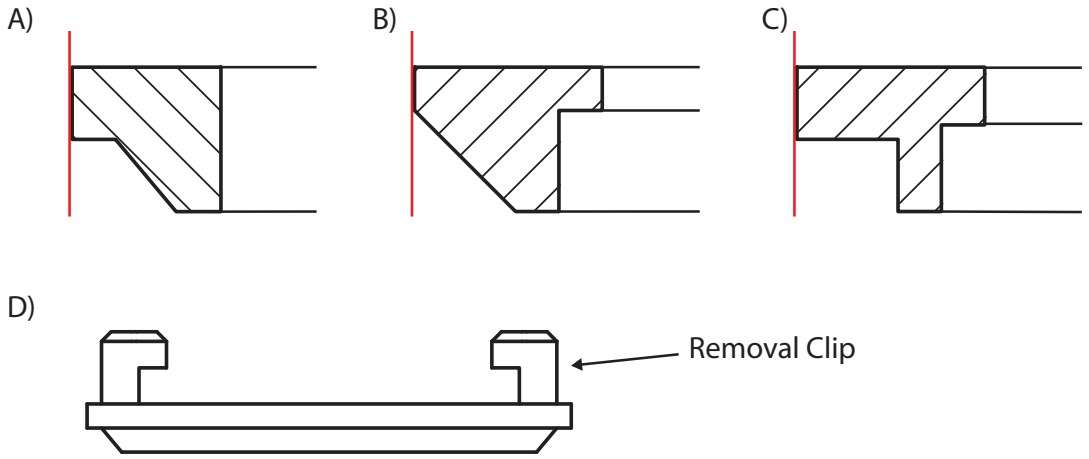

Figure 4-16: Cross-sections of the three main tilting-ring prototype. The MPS wall is to the left of the profile, and the ring center is to the right. *A)* The first profile sealed up to 25 kPa. *B)* This triangular profile sealed up to only 5 kPa. *C)* A T-shaped profile sealed up to 25 kPa. *D)* Removal clips were included on prototype A, but not on B or C. All prototypes were nominally 10.06 mm outer diameter and 1 mm tall.

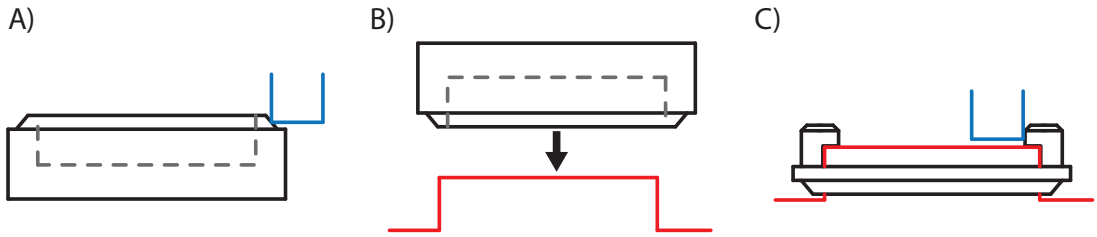

Figure 4-17: The fabrication process used for retaining ring prototypes with removal clips. *A)* First, the bottom features were machined into a cylindrical blank (endmill shown in blue). *B)* A locating post (red) was machined into sacrificial material, and the cylindrical blank was press-fit onto the post. *C)* With the center of the post known, the removal clips and other top features of the ring could be machined.

bottom, the tilting ring concept requires an insertion tool with a beveled edge to apply force only at the outer edge (Figure 4-19). For the ring with removal clips, the insertion tool requires clearance pockets, and therefore does not press down on the outer edge in the two locations behind each clip.

On first installation of the tilting ring with profile A (Figure 4-16-A), fluid accumulated behind each clip where the insertion tool had not pressed down the outer edge. After pressing the clips radially outward by hand, the ring sealed up to 25 kPa

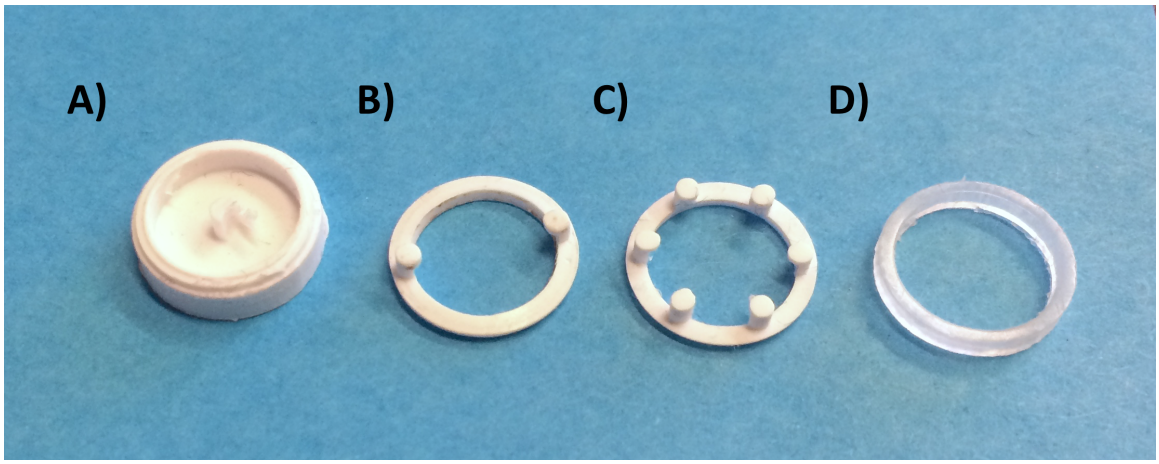

Figure 4-18: Scaffold Retaining Rings: *A)* The first machining operation resulted in the blank shown, which was then inverted on the locating post before the removal clips were machined from the other direction. *B)* Two clips allow removal; their section is shown in Figure 4-16-D. The presence of these clips required an insertion tool with clearance notches, shown in Figure 4-19-B. *C)* A prototype with six clips was fabricated to evaluate the tilting ring variant shown in Figure 4-11. *D)* The existing LiverChip retaining ring consists of a polypropylene annulus with a rectangular cross section.

in the test block pocket that included a sealing land, using a standard filter and the polyester scaffold simulator disc. A ring with profile B, without removal clips, leaked at 5 kPa. This was thought to be caused by the increased bulk and therefore stiffness of the profile. Profile C, which is less stiff to twisting, sealed up to 25 kPa.

These results are promising: while below the target 40 kPa, this is far better performance than the existing retaining ring exhibits. However, the performance is critically dependent on the extent of interference between the ring and the pocket. The actual interference in these tests was below our ability to measure, partly because the rubber cast and retaining rings both deflect when measured with physical means. An optical comparator did not offer the precision needed. To emphasize the risk of these tight tolerances: when the tool was changed from a 1/8 in. end mill to 1/16 in., and the tolerance of linear interpolation was adjusted slightly, rings of the same profile no longer sealed beyond 1 kPa or so. Given our time constraints, this supported the decision to use elastomeric gaskets for near-term experiments.

The six-clip prototype was built to evaluate whether the twisting of the ring could

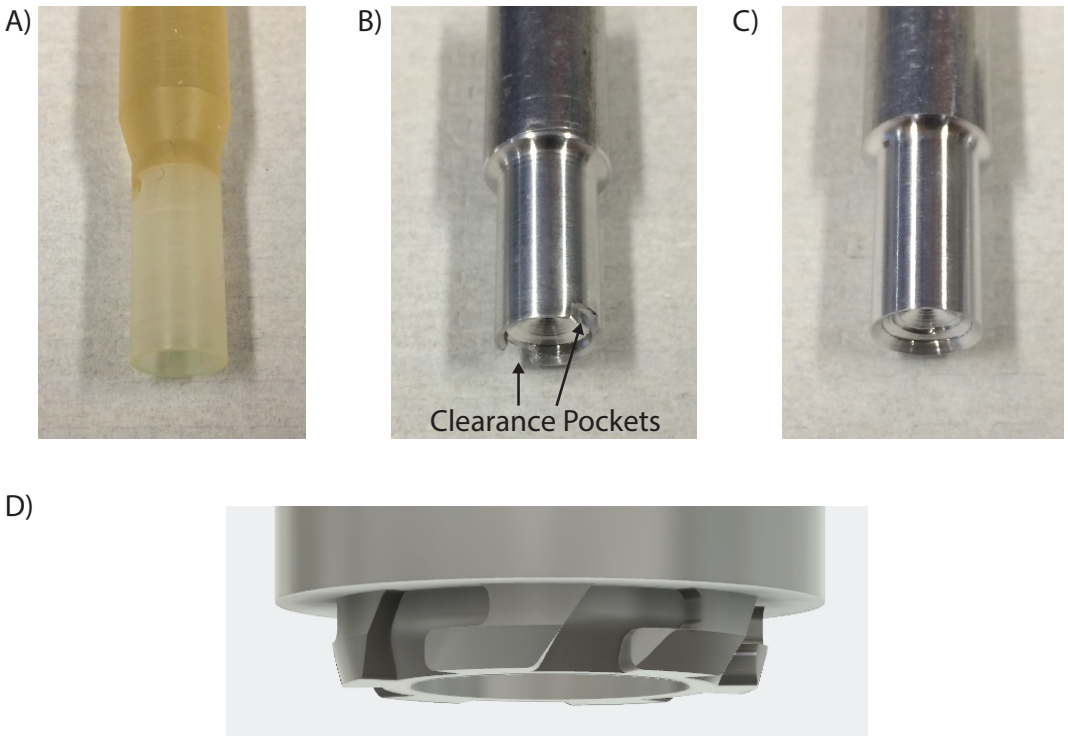

Figure 4-19: *A)* The retaining ring insertion tool for the liverchip is a polysulfone tube with a flat rectangular edge on the bottom. *B)* The tilting ring concept require a beveled edge, and clearance slots to accommodate the removal clips. The material is aluminum for prototyping only. *C)* A beveled insertion tool was fabricated for tilted ring prototypes without removal clips. *D)* An insertion/removal tool was designed and 3D printed to test the prototype with six removal clips, but the design applies as a removal tool for the two-clip design as well.

be accomplished by deflecting the removal clips alone, rather than pushing on the outer edge. This prototype did not seal, likely because the clips were too weak to overcome both the ring stiffness and the wall friction to twist the ring enough that in provided a downward force after the clips were relaxed. While further development might yield a working prototype, it seems challenging to achieve the required clip stiffness if the ring is to be a uniform material.

4.5.3 Beveled Ring with Viton Gasket

An elastomeric sealing solution was developed as a short-term solution for experiments where Viton is an acceptable material but which require better sealing than

the LiverChip retaining ring can provide. It offers several advantages over the tilting ring described above. First, the tolerances are looser than for the tilting ring concept because plastic deformation is allowable in this case. Second, an axially symmetric design allows fabrication on a lathe, where tight diametric tolerances are easier to maintain. Third, the increased deflection and conformal contact of the elastomer will provide a more reliable seal. The gaskets and ring described below sealed to 40 kPa in the test fixture described above.

The assembly, shown at right in Figure 4-1, consists of a chamfered retaining ring and a rectangular cross-section Viton gasket. The chamfered retaining ring design was chosen to direct force on the gasket both downward and radially outward, sealing both possible leak paths around the gasket, while being easier to fabricate than the stepped design shown in Figure 4-13-A. The ring is chamfered on the top and bottom and can be inserted in either orientation, so the user does not risk inserting it upside-down. The gasket was punched from a 1/64 in. thick Viton sheet using the custom punch shown in Figure 4-20 and a 1-ton arbor press.

Figure 4-20: This two-part punch machined from 4140 Alloy steel was used to produce the Viton gaskets. The shorter punch is used first, then the longer punch is inserted inside the shorter one to form the internal diameter of the gasket.

The chamfered retaining ring was fabricated from polystyrene on a lathe with a custom-ground cutoff tool, to an outer diameter of 10.10± .01 mm. This method was aimed at quickly fabricating the 20 rings needed for pilot experiments; for larger quantities, a Swiss screw machine shop could fabricate these rings to high precision on a six to eight week time-line. The fabrication process is shown in Figure 4-21.

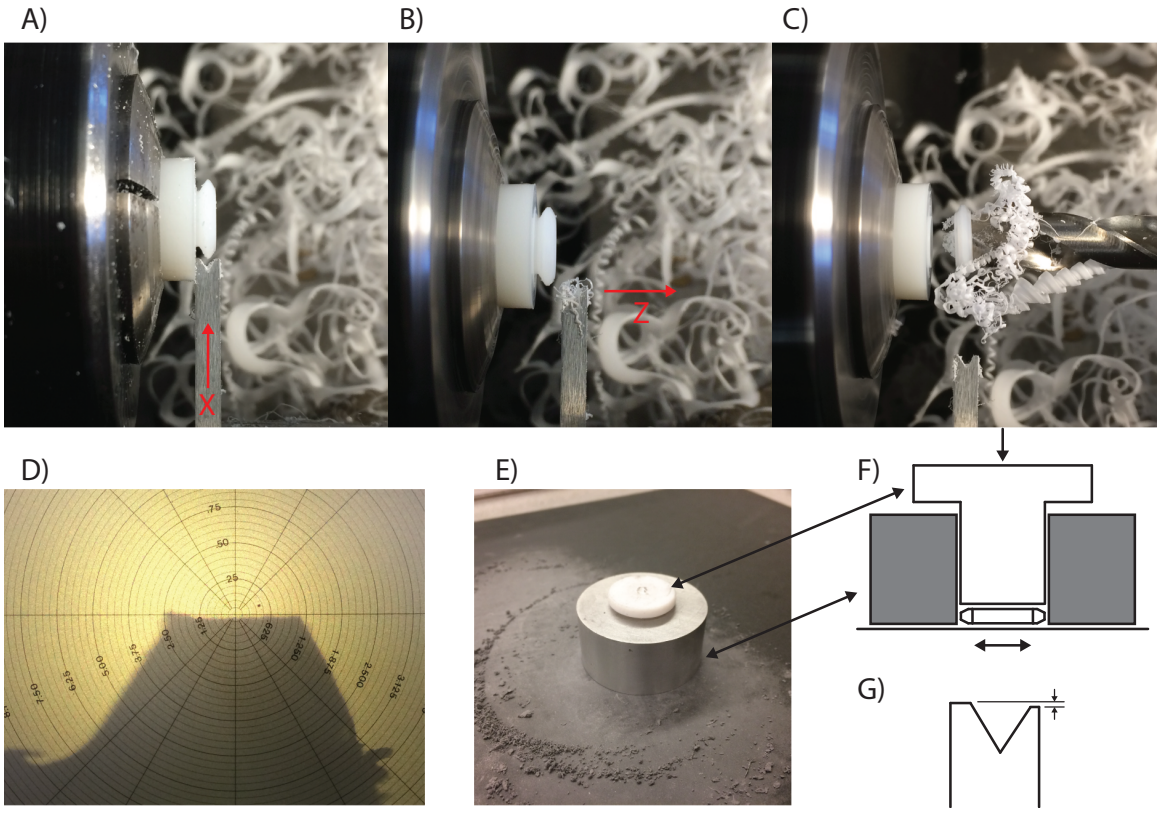

Figure 4-21: Fabrication of the chamfered retaining ring. *A)* First, a custom-ground cutoff tool is advanced in the x direction to shape the two chamfers. *B)* The cutoff tool is then retracted to a second position and moved in z while the left edge of the cutoff tool cuts the required outer diameter. *C)* A final drilling operation both machines the inner diameter and separates the ring from the stock. *D)* The ring profile is checked with an optical comparator. The outside edge (at center of cross-hairs) is 0.5 mm wide. *E)* The top and bottom of the ring are sanded flat using an aluminum and Delrin fixture. *F)* A section of the sanding fixture shows how the Delrin plunger pushes the retaining ring flat while the aluminum cylinder constrains it. *G)* A diagram of the cutoff tool shows the v-groove that defines the chamfers, and the left side edge of the tool that extends further than the right and defines the outer diameter of the ring.

To remove the ring, a tool was fabricated from 316 stainless steel rod (Figure 4-22). While this is a simple and effective solution, it does require user care to avoid damaging the platform itself.

The scaffold support (Figure 4-23) is similar to the LiverChip support, except that it is a separate component from the platform itself. This served two purposes: first, the scaffold sealing method was not determined when revision 2 parts needed to be

Figure 4-22: A tool for removing retaining rings from platforms without tweezer pockets. *Top:* The point can either pry under the retaining ring or dig into its inside bore. In the former case, the user must be careful not to gouge the MPS wall. The length of the point and curvature of the heel are such that the point is pushed into the retaining ring, but the heel does not touch the scaffold. *Bottom:* A simple stainless steel guard ensures that the point does not injure the user during storage and handling, nor perforate the sterilization pouch.

released, and second, separating the scaffold support allowed the bottom of the MPS to be much higher than it is in the LiverChip. Raising the MPS well is necessary to ensure passive draining of excess volume—introduced by the media exchange pump—from the MPS into the effluent collection. The LiverChip does not have automated media exchange, and thus has no spillway, so the MPS height is not a concern on that platform.

The scaffold support was machined from a 1 mm thick polystyrene tissue culture lid (Costal universal lid #3099, Corning Incorporated, Corning, NY) using the Othermill Pro desktop mill. Each face was sanded with 1000 grit sandpaper, and additional deburring was performed with a toothbrush under a stereo microscope. For larger batches, a cryogenic deburring method such as dry ice blasting could be employed.

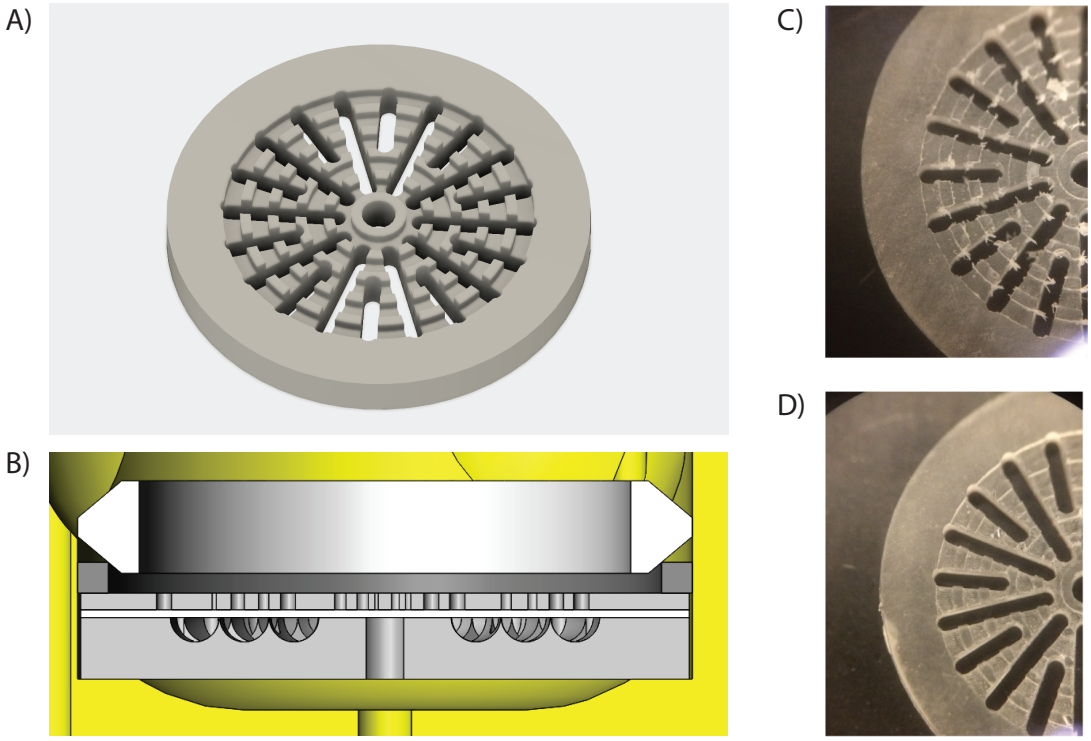

Figure 4-23: The scaffold support for the Rev2 prototype. *A)* The design is similar to the LiverChip scaffold support, but is removable from the platform. *B)* A cross-section of an older version of the scaffold support, with the filter, scaffold, Viton gasket, and chamfered retaining ring, from bottom to top. The scaffold, filter, and scaffold support are slightly under 10 mm so that they drop into the well. *C)* The support was machined from polystyrene on a desktop mill. Many burrs are visible. *D)* Lapping both sides with 1000 grit sandpaper and scrubbing with a toothbrush removed the burrs, which was confirmed with a stereo microscope.

4.6 Summary

This chapter describes many potential solutions to the problem of fluid bypassing the cell scaffold. The retaining ring with a Viton gasket presented above was developed as a short-term solution to provide significantly better sealing (>40 kPa vs <1kPa for the LiverChip retaining ring). The tilting-ring approach showed promise, sealing to 25 kPa, but is fundamentally limited by the narrow machining tolerances required to prevent plastic deformation. In future development, we suggest designing the scaffold retaining device in tandem with the well geometry, rather than confining oneself to a friction based approach in the existing well.

Chapter 5

Platform Design, Manufacturing, and Testing

5.1 Design

The Six replicate Reduced volume Liver culture platform (6xRL) integrates the oxygenator, media circulation, and scaffold attachment designs discussed in Chapters 2, 3, and (4). This chapter discusses the integrated design (Section 5.1.1) and some preliminary testing (Section 5.2); some of these test results will need to be repeated with new pneumatic plates that have not arrived at the time of writing.

5.1.1 Overview

The primary contribution of this work is in the spiral oxygenator design; many other components of the platform, such as the pumping, pneumatic manifold design, and passive volume control (spillways) are technologies developed in the lab that have been demonstrated on other platforms [2, 6]. While the technologies may be proven, there are challenges and compromises involved in applying them to a new configuration.

The components of the revision 2 platform are shown in Figure 5-1, and in the photos of Figure 5-2. Each of six replicate lanes consists of a media exchange reser-

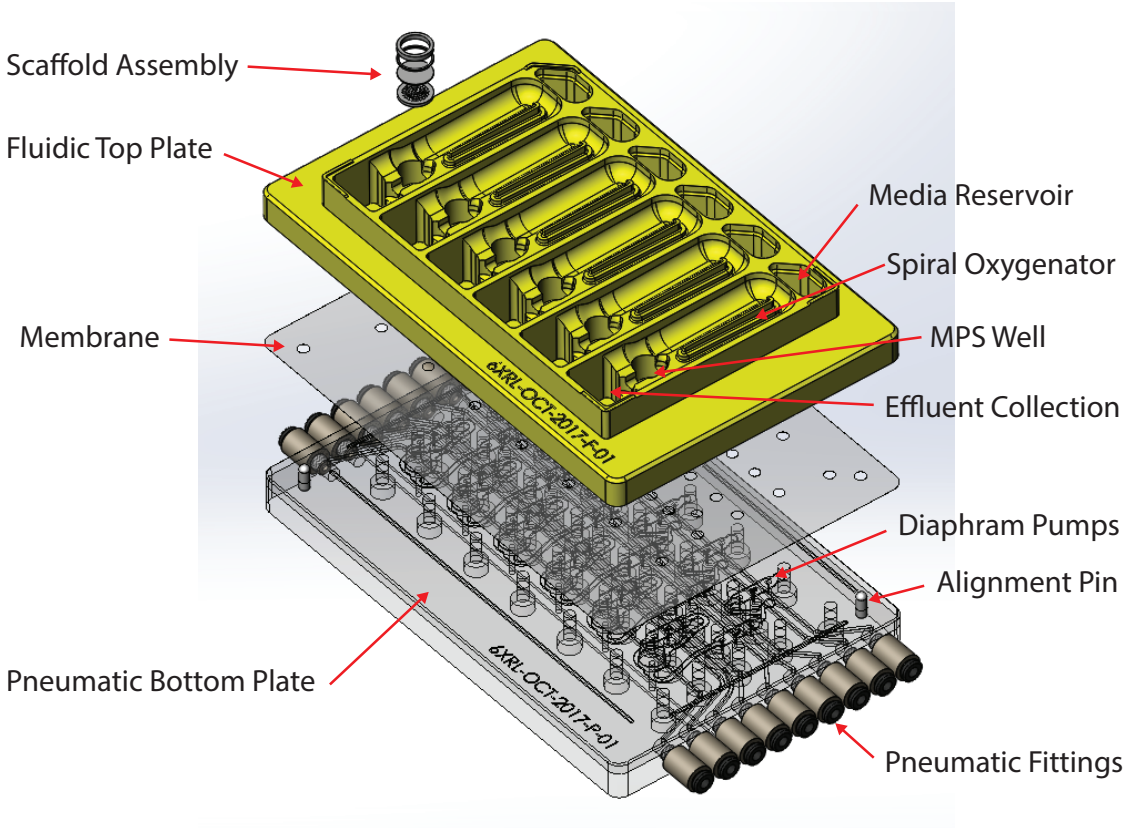

Figure 5-1: The platform consists of a fluidic top plate (polysulfone) and a pneumatic bottom plate (acrylic) separated by an elastomeric polyurethane membrane. Each of six replicate lanes consists of an oxygenator spiral, an MPS well, and a supply and effluent reservoir for the programmable media exchange. Three diaphragm pumps per lane control media exchange, oxygenator flow rate, and the MPS flow rate (perfusion rate through the scaffold), respectively. The pneumatic channels are coupled across lanes, so the flow rates in each lane are nominally the same for a given one of the three functions.

voir, an oxygenator spiral, a microphysiological system (MPS) culture well, and an effluent collection reservoir (Figure 5-3). The top plate is CNC machined from polysulfone, with open fluidic features on the top connected through vertical holes to closed passages and pumps on the bottom face. A polyurethane membrane (50 μm Aromatic Polyether Polyurethane film, extruded by American Polyfilm, Branford, CT) separates the top plate from the pneumatic bottom plate, where raised sealing lands seal the membrane against the bottom face of the top plate. Figure 5-3 shows a single lane of the top plate above the sealing land on the bottom plate, and Figure 5-4 shows how the sealing land seals around channels cut in the top plate to form the

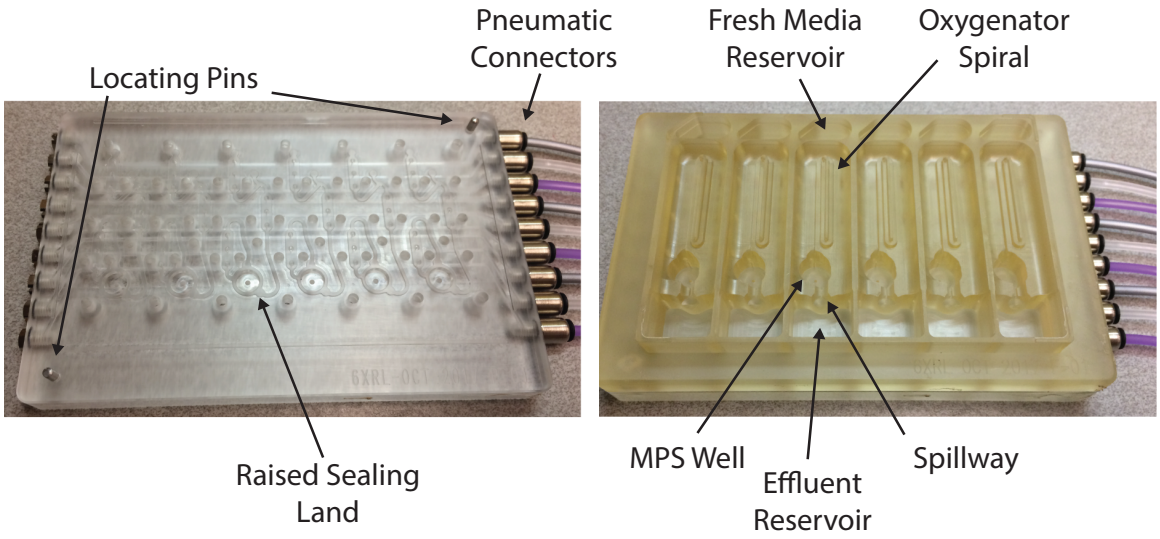

Figure 5-2: A photograph of the 6xRL revision 2 platform. The acrylic pneumatic plate is shown at left, and the fluidic top plate is shown at right. The polyurethane membrane is not shown.

diaphragm pumps and fluid channels. The diaphragm pumps are described in detail by Inman [19]. The platforms are held together by 1/2 in. long 4-40 screws with Belleville washers, which act as preload springs.

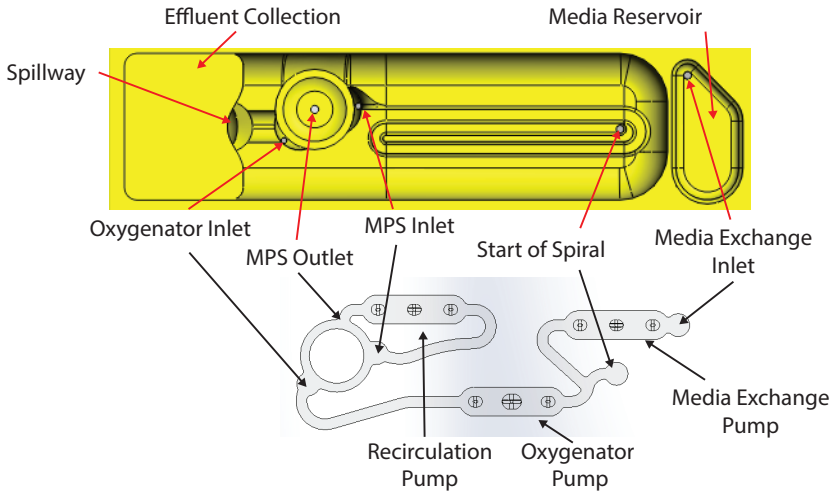

Figure 5-3: An overview of a single lane. The inlet and outlet holes (top) correspond to the indicated sealing points on the pneumatic sealing land (bottom).

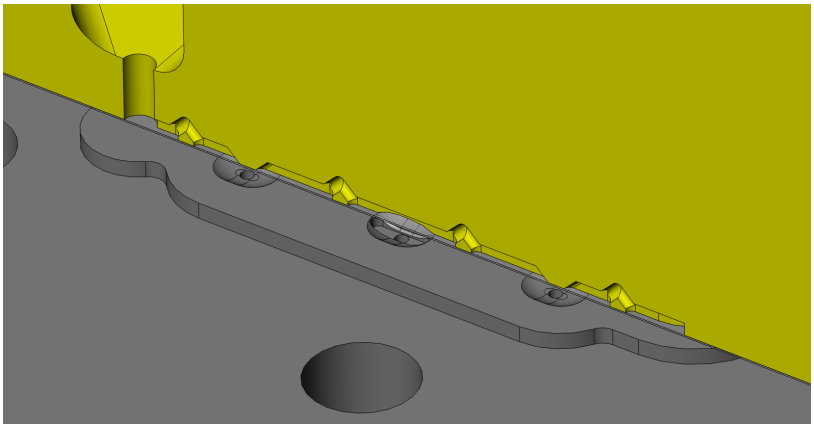

Figure 5-4: A section of the diaphragm pump geometry. A central pump chamber and two valves allow for bi-directional volume-determined flow. See Inman [19] for detail on the pump operating principle.

5.1.2 Programmable Media Exchange

Fresh media is stored in a reservoir designed to hold a maximum of 1 mL. The top of the reservoir has a sharp edge designed to constrain the meniscus and minimize the chance of fluid bridging between the reservoir and the oxygenator or neighboring reservoirs (Figure 5-5). The media exchange pump shown in Figure 5-3 feeds fresh media into the oxygenator channel. The resulting excess media volume is discharged from the MPS by passive spilling through the spillway and into the effluent collection (Chapter 6 discusses potential actively pumped designs). To predict the concentration of nutrients and waste products in the fluid leaving the MPS, we assume that the total circulating volume is well-mixed. If the media feed is continuous, and 500 μL are introduced each day, the media addition rate is .006 μL/s; comparing to the oxygenator and recirculation flow rates of 1 μL/s or greater, it is reasonable to assume the fresh media is well-mixed with the MPS volume.

5.1.3 Pump and Screw Layout

The Liverchip has 12 channels, with one pump per channel, each one in a straight line from one end of the lane to the other. The layout of the screws and the pneumatic channels is therefore relatively straightforward. The 6xRL, while it has only 6 lanes, has 3 pumps per lane, and the recirculation channel must double back. In

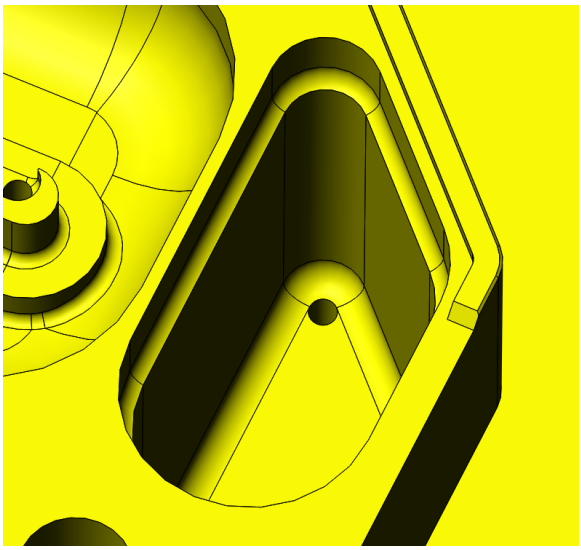

Figure 5-5: The 1 mL capacity fresh media reservoir features a sharp edge at the top to confine the meniscus, and an intake hole that is offset from the wall to allow flow rate measurement with the tool shown in Figure 5-9.

prototyping previous platforms with similar pumps and sealing lands, leaking had been a significant problem, and a rule of thumb was developed that no more than one sealing land should occur between two screws. The finite element study shown in Figure 5-6 helped to qualitatively assess the design. Because this sealing is critical to proper function, it may be worthwhile to fabricate an SLA model for leak testing before fabricating parts. A "polycarbonate-like" resin such as ACCURA 60 (3D Systems, Rock Hill, SC) should approximate the elastic modulus of polysulfone enough to make meaningful design decisions. The screw layout for revision 2 is likely conservative, and in fact initial fluid leak testing showed that one row of screws could be removed without resulting in leaking when the platform was left pumping water with food dye overnight. The clamping screws were tightened to 5 cNm. Tightening to 15 cNm prevented the pumps from actuating; we hypothesize that this is caused by the compressed polyurethane squeezing into the pump and valve chambers, causing the membrane in the chamber to buckle.

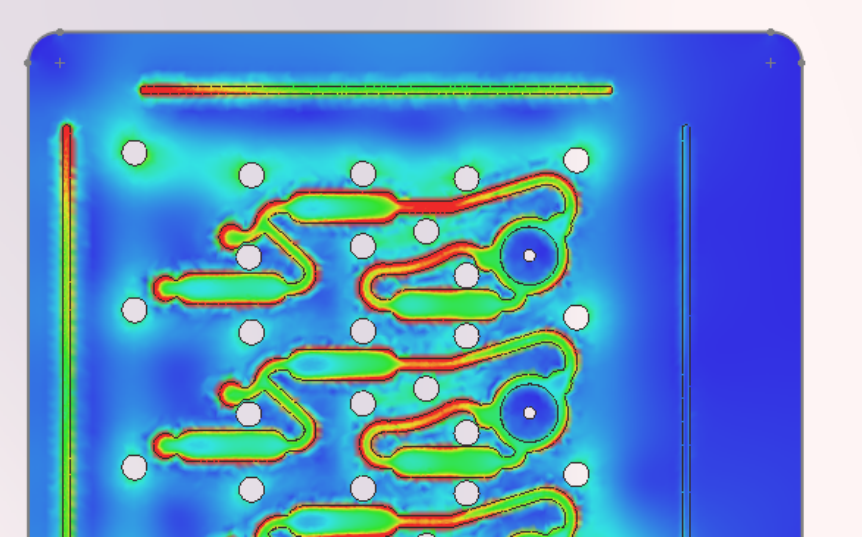

Figure 5-6: A pressure map of the sealing lands. In SolidWorks Simulation FEA of the bottom plate alone, the top surface of each sealing land was fixed and a force of 20 N applied to the counterbore of each screw hole (hidden). This was not meant as a quantitative measure of force, but helped to highlight any areas that might be leak-prone, and to show the general distribution of pressure.

5.1.4 Pneumatic Bottom Plate

The pneumatic bottom plate is separated from the culture medium by the membrane, and therefore does not have to be sterile or biocompatible. It is constructed from two acrylic plates that are solvent-bonded together, after the internal pneumatic channels are machined. These internal channels connect air and vacuum from the pneumatic fittings to the pump chambers.

Because of the high density of fasteners, and the presence of three pumps (each of which requires three distribution channels), there was a very thin wall between the screw clearance holes and the pneumatic channels on the Rev 2 pneumatic plate. These walls broke during manufacturing, and upon receipt of the platforms all of them leaked at multiple screw holes.

To resolve this issue, after the leak test described in Section 5.1.3 indicated that a row of screws could be removed, an altered revision with a thicker wall was sent for manufacture (the change is shown in Figure 5-7). The plates were not completed at the time of writing, preventing testing with them, but they are currently being

manufactured.

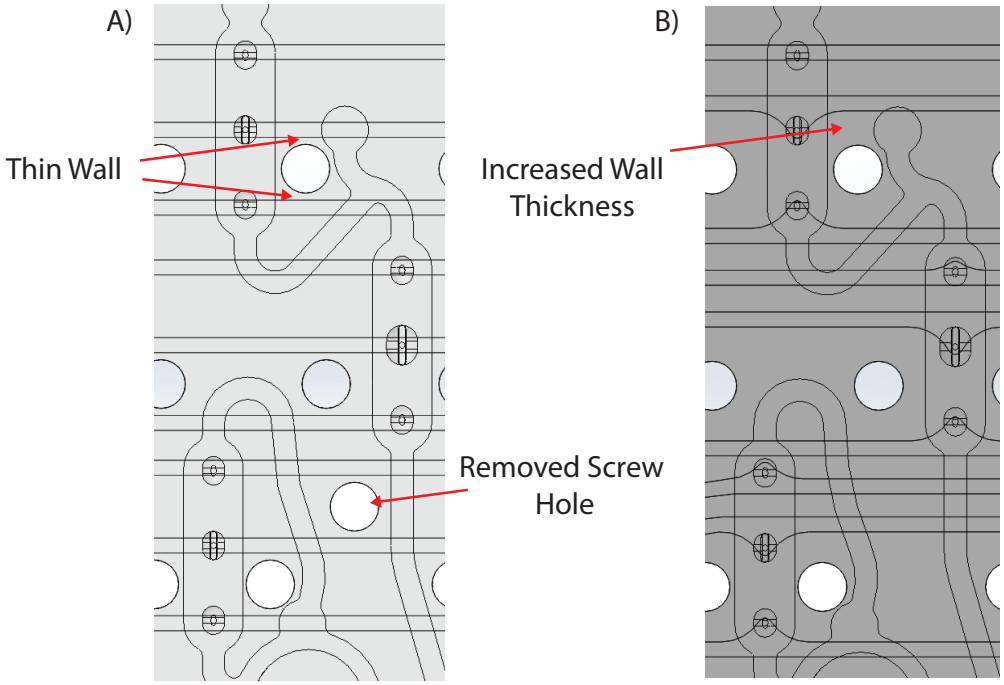

Figure 5-7: The revision 2 pneumatic manifold leaked between the horizontal pneumatic channels and the screw holes. The thin wall (470 μm thick, 1mm tall) separating the channels and screw holes fractured during manufacturing. The updated pneumatic platforms remove one set of screws to allow a thicker wall (2 mm wide, 1 mm tall).

After machining, the fluidic and pneumatic plates were deburred using a dry ice blasting service (Nitrofreeze, Worcester, MA). This freezes any small burrs from machining and breaks them off with the impact of fine dry ice pellets, leaving a clean surface without risk of grit remaining in the platforms. Figure 5-8 compares a pump chamber before and after this process.

5.2 Testing

The scope of testing was limited by the leaking pneumatic plates, but it appears that with a functional pneumatic plate the platform will meet the system-level requirements described in Section 1.5: (1) the device is made cell and drug compatible by using materials used and approved in existing platforms. For the short-term ex-

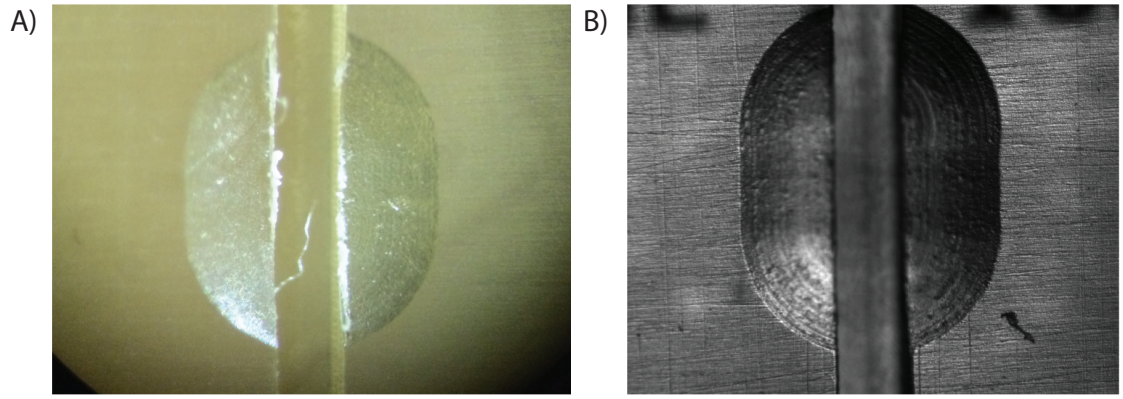

Figure 5-8: Inspection photos of pump chambers *A)* before and *B)* after cryo-deburring. In this process, the top and bottom plates are dry ice blasted to remove any burrs in the pumps or channels that might damage the membrane or dislodge and plug the scaffold.

periments planned, Viton does not appreciably adsorb the compounds measured, and absorption is entirely negligible. (2) The circulating volume is at the threshold of 500 μL, varying on the order of 7% from well to well; the precise value depends on measurement of the volume captured in the oxygenator, which is also flow-rate dependent. (3) Media exchange can be programmed and can store 1 mL of fresh media, and collect the waste by passive spilling. (4) The platform accommodates the same sterile technique that has been used on other platforms, and can be similarly moved between the incubator and Biological Safety Cabinet. (5) The platform accepts a commercially-available Costal universal lid. (6) The pneumatic manifold integrates with the existing hardware used in the Griffith lab.

5.2.1 Flowrate Measurement

To measure the recirculation flow rate, the tool shown in Figure 5-9 is inserted in the central hole in the MPS bottom and pressed down such that the o-ring seals. The MPS is filled with fluid such that the recirculation inlet does not run dry. Fluid is pumped up through the tool, paused, and pumped back down, to obtain measurements for upward and downward flow. The upward flow is therefore pushing against a pressure head of less than 100 mm of water, and the downward flow is assisted by

the same.

The inlet to the oxygenator does not allow the tool tip to seal, so the hole at the start of the oxygenator spiral (see figure 5-3) is plugged using a pipette tip (20-200 μL) that is plugged with silicone, and the flow rate is measured through the media exchange inlet. The media exchange pump and valves are actively held open during this test.

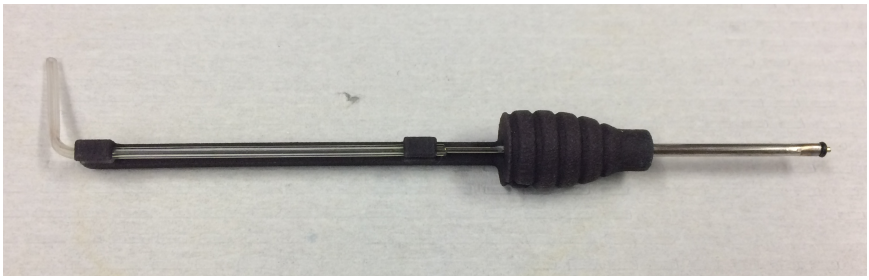

Figure 5-9: Flowrate test tool: the stainless tube is placed in 1mm fluid exit holes in the MPS and media supply reservoir, such that the o-ring seals against the platform. The time required for a fluid front to pass through the clear region of tubing between the two brown clips is measured using a stopwatch. The tube volume of 39.3 μL between the brown clips is divided by this time to obtain the flow rate.

The measured flow rates across the 6 wells are shown in Figure 5-10. All pumps measure about 10% lower than predicted based on nominal geometry. This may be due to the pump chamber geometry being smaller than expected, in which case a calibration factor can be added to the pump driving software, but it is necessary to re-measure these flow rates with a pneumatic plate that does not leak and can provide full actuation pressures.

5.2.2 Volume Recovery

To measure the circulating volume, the MPS and oxygenator are flooded with BSA solution until spilling occurrs, and allowed to sit in the incubator for 1.5 hrs to come to temperature. The pumps are off, and none of the scaffold assembly is present in the MPS. After spilling, the volume remaining in the MPS and oxygenator is pipetted onto a scale, and the mass remaining in each well was recorded. An average of 510$\pm$33 μL was recovered (95% confidence). Subtracting the volume of the retaining ring and

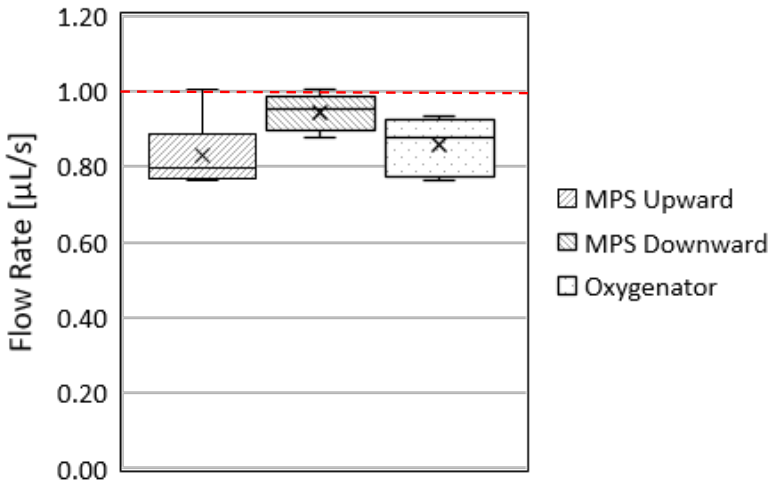

Figure 5-10: Measured flow rates, n=6: the MPS flow rate is measured in both directions, and the oxygenator is measured only in its normal forward operating direction. The intended flow rate was 1 μL/s.

gasket (39 μL), scaffold (25 μL), and scaffold support (54 μL), all measured calculated from 3D CAD models, and adding the fluid trapped in channels (55 μL, Figure 5-11) and an estimated 50 μL in the oxygenator when running, the circulating volume is 497±33 μL. This meets the 500 μL target closely. Note that this value depends on an estimate of the oxygenator volume. While pipetting 50 μL of BSA solution onto the oxygenator produces a profile comparable to that during flow at 2 μL/s, but stopping flow and immediately aspirating is only able to recover 10-15 μL. While the true volume is likely between these values, a reliable method of directly measuring trapped oxygenator volume directly would be valuable. Nonetheless, the oxygenator volume is small compared to the overall 500 μL volume.

5.2.3 Evaporation Test

Evaporation of media during cell culture is a critical consideration for an open well platform. As the water evaporates, the concentration of the nutrients and waste products increases, which will introduce error. Further, significant evaporation can lead to drying of the MPS, causing either direct drying of the cells or pulling air bubbles into the recirculation, either of which will adversely affect the cells.

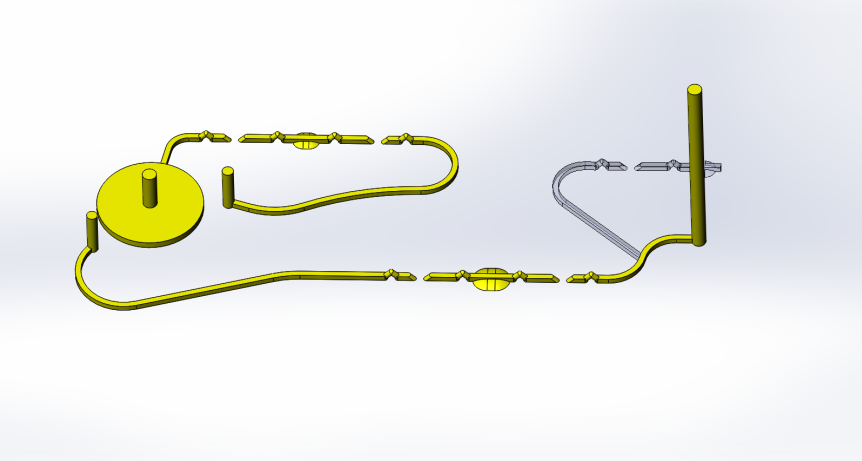

Figure 5-11: A 3D model of the fluid not measured by pipetting. The volume trapped in the channels is 55 μL. The volume in the media feed channel (grey) is not considered part of the circulating volume, though some nutrient exchange by diffusion will occur.

We attempted an initial test of the evaporation rate on the revision 2 platform by placing a silicone sheet over the bottom of the leaking pneumatic plate and wrapping the seam with electrical tape. The measured evaporation rate (shown in Figure 5-12) ranged from 144 to 220 μL/day, and the outer two lanes show the most evaporation. These values are much higher than the approximately 60 μL/day observed on the LiverChip (unpublished data). The increased evaporation at the edges is consistent with the leaking pneumatic plate introducing dry air into the incubator and lowering the relative humidity, as a gradient would develop between the humid environment under the culture lid and the drier air outside it. The test must be repeated with functioning pneumatic plates, but the updated revision 2B plates had not arrived at the time of writing. We predict a lower evaporation rate with a properly sealed peumatic plate.

5.3 Summary

Six replicate lanes are effectively packaged on a single platform that is compatible with a standard tissue culture lid. The layout of pumps, channels, and screws successfully seals the fluidic side while allowing separate pumping for perfusing the cell scaffold, flowing through the oxygenator, and providing fresh media. The waste

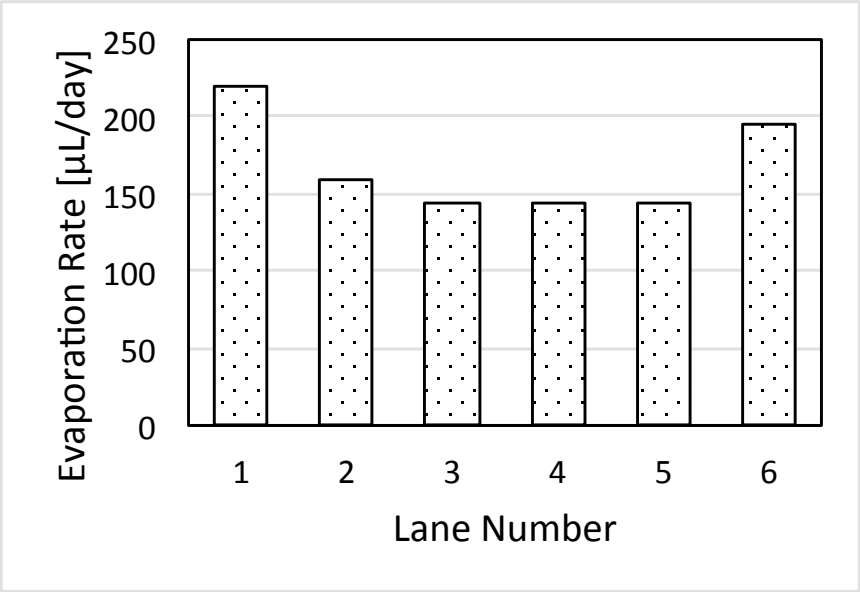

Figure 5-12: Evaporation test data: the evaporation rate appears significantly higher than the 60 μL/day seen on the LiverChip. The pneumatic plate was leaking dry air into the incubator, and the experiment should therefore be repeated with a sealed pneumatic plate when it is complete.

media spills passively into an effluent reservoir, which effectively controls fluid height, limiting the circulating to the 500 μL target. The peumatic plate fractured during manufacture due to a thin wall, causing critical air leaks, but a revision 2B bottom plate that is being manufactured at the time of writing is expected to resolve this issue. At that point the evaporation and flow rate tests will be repeated.

Chapter 6

Conclusions and Suggestions for Future Work

6.1 Summary

We have designed, fabricated, and tested a free-surface oxygenator that uses the tendency of fluid to wet corners in order to constrain the fluid flow with a short effective diffusion length. Relative to the CN Bio LiverChip, which uses a wide, open channel to oxygenate media, this method offers the advantages of self-emptying and robustness to sloshing at a fraction of the volume. The primary cost of this method is the extra circulation loop that it requires, but this cost brings other potential benefits, such as closed-loop oxygen control. The revision 2 oxygenator performs equivalently to the LiverChip oxygenation channel, though previous iterations show even better performance. Additional performance could be gained by increasing the length or total height of the oxygenator.

The additional oxygen circulation loop is designed to feed high-oxygen-concentration media exiting the oxygenator directly to the cells, while feeding low-oxygen-concentration media from the opposite side of the cell culture well directly into the oxygenator. During upward flow, this effect is observed at a flow rate of 2 μL/s. During downward flow, which is required for the first eight hours to seed the cells, the system is expected to behave like a fully mixed system, in which the oxygen concentration of

media flowing to the cells is lower than at the output of the oxygenator.

A short-term solution to challenge of fluid bypassing the cell scaffold has been developed, but it is limited in applicability due to concerns of Viton adsorbing certain compounds. Many alternative solutions are outlined above, and we suggest designing the scaffold attachment and the well geometry together, rather than designing an attachment method to fit the existing well.

The final experimental validation of the platform depends on an updated pneumatic plate, which has not arrived at the time of writing. This updated plate is designed to fix a thin wall that fractured during manufacture, rendering the original pneumatic plates non-functional. With the arrival of these plates, after validating the flow rates and measuring evaporation, we plan to run biological validation tests, and then the platform can be used to investigate differences in cell culture with three times lower circulating volumes.

6.2 Suggestions for Future Development

The suggestions below have two aims: first, to offer direction for the next steps this research might take, and second, to highlight the assumptions made and approaches taken during this work that should be revisited. While there is always an infinite supply of improvements to be made–the data could be more comprehensive, each behavior better characterized–we focus here on the end goal of providing a useful tool for answering biological questions.

6.2.1 Requirements

Some of the stated design requirements are educated guesses by the biology team, and the specific bounds of the necessary values are not definitively known. These are mostly biological research questions rather than mechanical design challenges, but there may be opportunities for mechanical design to support the experimental process. Specifically, the 150 μM oxygen concentration requirement is not rigorously determined, and there are questions regarding the optimal oxygen concentration for

hepatocyte culture (see, for example, Guo et al. [31]). In media lacking hemoglobin or some other oxygen carrier, the minimum concentration feeding the cells must be high enough that the down-stream cells are not hypoxic. This requirement could be eased with the use of media that has additional oxygen storage capacity, mimicking the role of hemoglobin in the blood.

The media exchange requirement also deserves assessment. The 6xRL platform described in this thesis incorporates media exchange that relies on active input pumping and passive output spilling. If media introduction flow rates are low enough (such as for continuous media exchange), then it is reasonable to assume that fresh media has been fully mixed into the system before the media mixture passively spills out into the effluent. However, if batch exchange is desired, or the implementation of a specific feeding schedule, a different media exchange system may be required. This could take the form of active media collection, or a volume-limited closed-well system, where introducing fluid volume at one end of the system must equal the fluid ejected at the other, and the amounts of fresh and old media can be specifically accounted for. Additionally, if the media source and effluent reservoirs are large enough, batch exchange can be achieved by flushing some or all of the old media before introducing new media.

The scaffold attachment sealing requirement of 40 kPa is likely excessive: the maximum pressure measured in the system with a fully occluded scaffold could provide a better upper-bound requirement, or alternatively the pressure drop across the scaffold at a 2 μL/s flow rate, which is the peak flow rate at the scaffold predicted by Inman [1] (p. 40).

6.2.2 Testing

As described above, additional work remains for testing the revised pneumatic bottom plate when it is completed for flow rates and evaporation. When the fluidics are proven to behave predictably, we should perform biological testing to validate the platform for cell culture and subsequent experiments to assess the effect of low-volume cell culture.

6.2.3 Scaffold Attachment

To provide scaffold sealing without using an elastomer, we recommend designing the sealing feature and well in tandem, rather than relying on a friction-based engagement with the existing well. Packaging elastic elements to generate adequate forces in both directions pushes the limits of available materials, at least for the 40 kPa sealing requirement used. While a lower sealing requirement may make the friction approach feasible, we recommend exploring the concepts outlined in Chapter 4 that we excluded due to scheduling constraints.

6.2.4 Spiral Oxygenator

Several aspects of the spiral oxygenator should be explored if it is to be used in further applications. First, we considered only polysulfone as a material, but plasma-activated polystyrene or some other wetting material may offer better performance and lower manufacturing cost. Further, the hypothesized effect of the corner radius limiting diffusion depth and improving performance over a sharp corner has not been tested. For machined prototypes, a small radius is required, but if parts are to be molded, it is worth further investigating this phenomenon. Finally, the addition of spontaneous capillary flow channels may be able to aid the initial wetting of the platform. The conditions for such channels are described by Berthier et al. [22].

6.2.5 Media Exchange

The media exchange system on the 6xRL platform is actively pumped from a fresh media reservoir, and the waste media passively spills over into an effluent collection reservoir. If the flow rate of fresh media into the system is significantly lower than the circulation and oxygenation flow rates, then it is reasonable to assume that the system is fully mixed, and that the fluid spilling into the effluent is a uniform mixture of old and new media. For continuous media exchange, where the media feed rate is orders of magnitude lower than the recirculation rate, this fully-mixed assumption applies.

For media feeding protocols other than continuous exchange, however, it is not clear what ratio of old to new media is spilling over. Nor is it clear at what feed rate we would observe a change from this fully mixed regime to only partial mixing. A combination of modeling and experimental investigation (for example, by introducing fluorescein dye with the fresh media) might reveal a safe operating range, where the mixing assumption applies and the cell's exposure to fresh media can be appropriately predicted.

Another pumping channel for effluent collection could actively evacuate old media, though care would need to be taken to ensure that a difference in flow rate between the source and effluent pumps does not cause accumulation or depletion of media in the system. An effluent intake similar to the MPS and Oxygenator inlets shown in Figure 5-3 could avoid depleting the MPS by drawing air when the volume dropped lower than the intake. This can also be solved by including and effluent spillway as well as an effluent pump, and ensuring that the media input rate is slightly higher than the media extraction rate.

Storing the fresh and effluent media off-platform could allow large enough volumes to flush the system with fresh media, thereby achieving batch exchange, if this is desired experimentally.

6.2.6 Closed-loop Oxygen Control

One advantage of having an oxygenator in a separate flow loop from the recirculation/perfusion pump, is that the oxygenator flow rate can be adjusted to adjust the concentration of a mixed system to a desired level. An oxygen probe, such as those made by Lucid Scientific (Atlanta, GA), could be integrated with the platform to sense the oxygen concentration, which would feed back to the pump controller to adjust the concentration. The concentration would be varied by increasing or decreasing the oxygenator flow rate. Questions such as where to place such a probe, how to account for concentration differences across wells if the oxygenator pumps are coupled, and what model to use for the oxygenator-cells system would all need to be addressed.

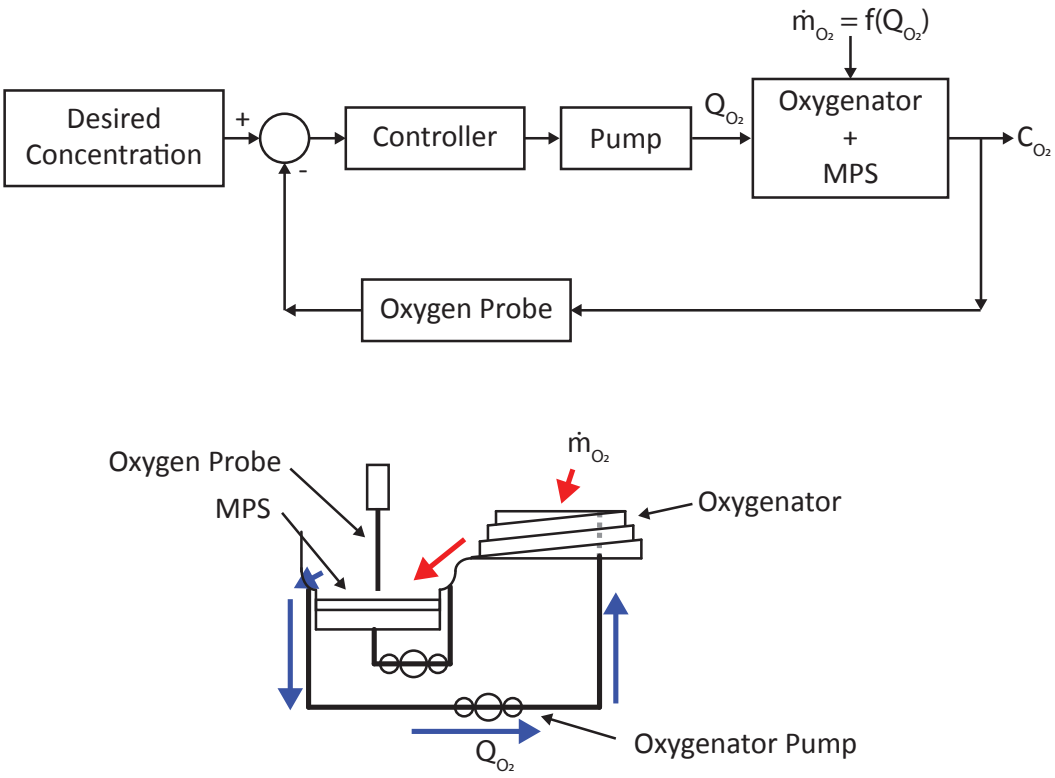

Figure 6-1: *Top)* A block diagram of the proposed oxygen concentration feedback control. A controller uses the error between measured and desired oxygen concentrations to adjust the oxygenator pump flow rate and thereby controll the oxygen concentration in the MPS. *Bottom)* A schematic of the oxygenator and MPS, with the oxygen probe measuring oxygen concentration in the MPS. Placement of the probe requires careful consideration of local oxygen micro-environments, and depends on experimental need.

6.2.7 Clamping and Sealing

One of the practical limitations of the 6xRL platform is the number of screws holding the pneumatic and fluidic plates together. A significant improvement would be an alternate clamping method using no screws or a substantially reduced number of screws.

One reason for having so many screws in the present design is that because the polyurethane membrane is so thin, it is stiff enough in compression that bending of the acrylic and polysulfone plates becomes a consideration. For more details on the stiffness characteristics of thin elastomer sheets, see [32]. If a thicker elastomer gasket

is placed under the membrane, deformation occurs primarily in the gasket, allowing a less even distribution of forces, and potentially fewer screws. This gasket approach was designed by Continuum Innovations (Boston, MA) and has been used in the Griffith lab for some prototype platforms that did not seal adequately without them. The main challenge is achieving deterministic and repeatable pump volumes: Continuum addressed this with acrylic protrusions that hold the pump and valve geometry, but that are surrounded by an elastomer to provide fluidic sealing. Such a gasket configurations, if the sealing lands are significantly more compliant in compression than the platform is in bending, could allow the use of significantly fewer screws, or even a custom clamp. In a disposable platform, the plates could be temporarily clamped, compressing the gasket, and then bonded, either ultrasonically or with adhesive. After clamping is released, the bond would maintain a pressure seal. This might enable use of membrane materials that cannot be effectively bonded.

6.2.8 Further Reducing Volume: a Closed Fluidic System

The 6xRL Rev2 volume of 500 μL appears to be close to the lower limit achievable in an open-well system. We believe that achieving substantially lower fluid volumes with the same liver cell count will likely require a closed system without free surfaces, where the volume is constrained and free of surface forces, and all constraints are fully wetted. Design concepts for such a system are described below.

Overview

The platform proposed here is intended to be reusable, using the same basic structure of a fluidic and pneumatic plate sandwiching a polyurethane membrane that the 6xRL and LiverChip platforms use. We advise reusable platform for initial development of the hardware itself, and for the iterative process of presenting a new tool to biologists as it has lower cost and faster development time. A single-use device can then be designed from the resuable design, incorporating new understanding and user feedback. If the platform design is sufficiently solidified, the platform can be

adapted to a disposable design, and work adapting the diaphragm pumps to a bonded COC format is ongoing [33].

The membrane oxygenator, discussed in more detail below, uses a single in-line circuit much like the CN Bio LiverChip. This feeds media directly from the oxygenator to the cells in both flow directions. There are three main differences betwen this platform and the LiverChip: (1) The use of a membrane oxygenator, (2) a media exchange system, and (3) a cap that seals the MPS but can be removed to accommodate the existing cell seeding protocol. A cross section of one embodiment of this proposed platform is shown in Figure 6-2, and a top level view is shown in Figure 6-3.

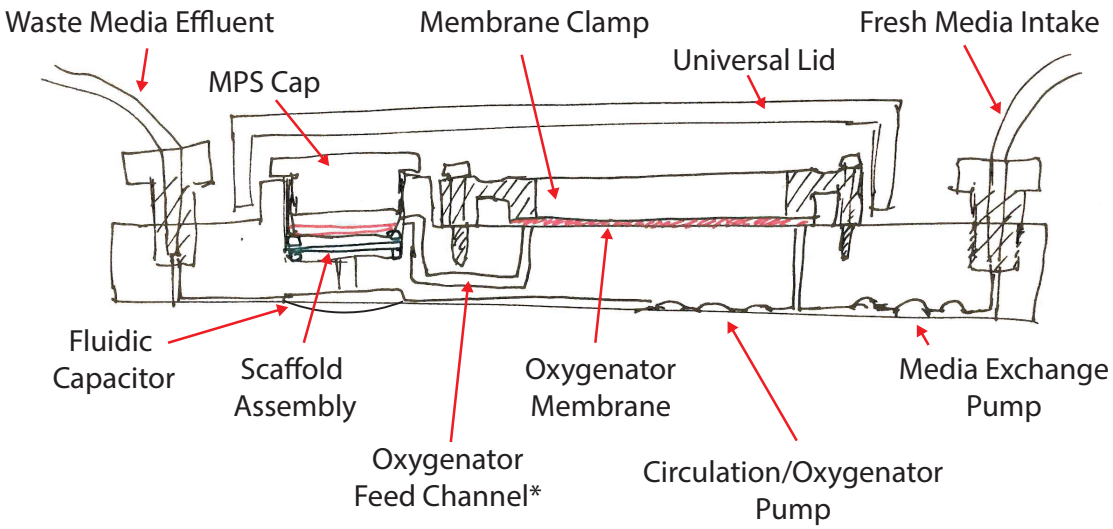

Figure 6-2: Each lane of the proposed closed-volume platform has media exchange pulling from an external reservoir, an oxygenator membrane that is clamped in place to provide a confined fluid path, an MPS cap to limit volume, and on-board pumping (pneumatic plate not shown). The MPS cap and membrane are placed under a lid for sterility, but this may be uncessary, depending on the sterile workflow. *Note that oxygenator feed channel would actually be on the bottom plane with the other flow channels. It is shown higher in this illustration for visibility.

We estimate that a circulating volume of 100-150 μL is achievable with this configuration. The volume trapped in circulation and the fluidic capacitor [1] is 55 μL for the 6xRL, as shown in Figure 5-11; this could likely be reduced to about 40 μL. The example oxygenator described below has a volume of 10 μL, and for 8 mm diameter

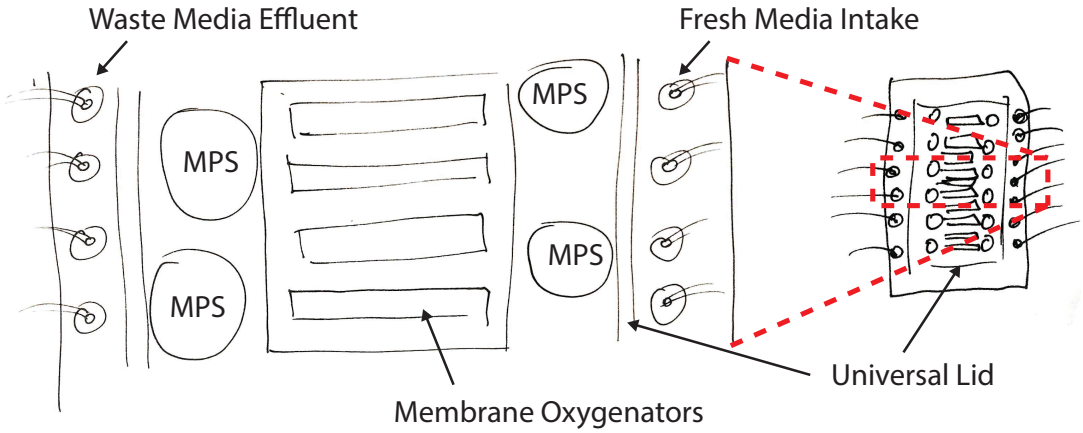

Figure 6-3: A top view of the proposed platform. We expect to accommodate 12 liver cell culture wells on a single platform by staggering the oxygenators and MPS wells.

of exposed scaffold, we add an additional 50 μL. Assuming the vertical fluid space above the scaffold and through the scaffold support is 1 to 2 mm, a reasonable total is 100 to 150 μL. This is potentially down to one tenth of the LiverChip volume, which is more likely to reveal autocrine biomarkers than the 50 to 60% reduction achieved with the 6xRl.

One additional consideration in this design is the height of the effluent, which sets the system pressure, and avoiding a negative pressure on that line. The hydrophobic membrane will resist fluid leaving the system, but may allow gas to enter if the system is at lower than atmospheric pressure. The effluent exit to atmosphere should therefore be located some amount above the system level.

Membrane Oxygenator

Membrane oxygenation is the only method we have found that would allow for a volumetrically confined system. Hydrophobic nanoporous membranes (pore sizes 100 to 450 nm) made from polypropylene, polycarbonate, and PTFE appear to have mass transfer coefficients exceeding that of a free surface, likely due to the velocity profile near the membrane reducing the diffiusion boundary layer thickness [34]. Mass transfer is reported to increase with contact angle; a higher oxygen transfer rate was

observed with more hydrophobic materials.

As a conservative lower bound, we take the transfer rate through a free surface and use the models described in Chapter 2. At 1 μL/s , equation 2.21 suggests a diffusion depth to exposed surface area ratio $\frac{h}{A}$ of .0005 [mm^{-1}] will give an oxygenation potential of 1.00 (i.e. fluid leaves the oxygenator fully saturated). Assuming a 2 mm wide two-sided oxygenation channel 100 μm tall, that is oxygenated from top and bottom, a 50 mm length is required to achieve $\frac{h}{A} = .0005$ [mm^{-1}]. The same dimensions, but oxygenated from one side, would still give an oxygenation potential of 0.998 (the model over-predicts the oxygenation potential, but this gives a rough guide to appropriate dimensions). The hydraulic resistance R_h can be approximated by

$$R_h = \frac{12L\mu}{wh^3} \tag{6.1}$$

where L is the oxygenator length (0.050 m), $\mu$is the dynamic viscosity (0.78 mPa*s for DMEM/F12 Medium at 37 °C) [35], w is the channel width (0.002 m) and h is the channel height (0.0001 m) Multiplying by a flow rate of 1 μL/s (1×10^{-9} m^3/s) gives a pressure drop of less than 0.2 kPa, which the pneumatic pumps can easily accommodate [19], and well below the pressure required to drive liquid across a suitable membrane (for a 1 μm pore diameter EPTFE membrane this pressure was found to be on the order of 100 kPa [36]). The volume of fluid in the oxygenator would be 10 μL. This is just a representative example, but it shows that this approach is quite feasible. Equation 2.21 allows quick prediction of oxygenator efficiency for a wide range of channel dimensions.

One advantage of the membrane oxygenation method, in addition to allowing a closed-volume system, is that flow is reversible, and the inline flow configuration can be used. This reduces the number of pumps required, and feeds media from the oxygenator directly to the cells when flowing upwards or downwards. While it does not allow for real-time oxygen control by changing the flow rate–changing the perfusion rate would change local shear stresses and might inadvertently alter cell function–such control could potentially be achieved by controlling the local gas

environment outside the membrane. A further advantage of micro- or nano-porous membranes is that the oxygenator should act as a bubble trap, allowing gas to flow out through the membrane, while retaining the fluid.

To allow removable fluidic sealing of the membrane, a clamping block with an elastomeric gasket can compress the membrane in long channels, confining flow to the uncompressed region. Potential configurations for such a design are shown in Figure 6-4. Depending on the stiffness of the membrane relative to the width of the channel, the channel height could be defined by deflection of the membrane alone, or by a spacer. To make the system more compact, the oxygenator could have a membrane on the top and bottom, but this results in a leak path that is challenging to seal. For a single-sided oxygenator, two potential clamping plate configurations are shown in Figure 6-5. In each of these clamped configurations, the membrane hydrophobicity is advantageous. Even if there is a very small gap, surface tension forces will prevent fluid from penetrating if the pressure differential is not extreme.

To gain the benefits of a double-sided oxygenator, while mitigating the leak path shown in Figure 6-4-D, the membrane might be bonded to a secondary plug which would seal to the platform. Such a configuration is shown in Figure 6-6. The top membrane could then be bonded to this bottom membrane, eliminating the need for a clamping block.

Media Exchange

If the media exchange inlet and outlet connect to the circulating fluid path on either side of the recirculation pump, as shown in Figure 6-7, this allows greater control over the media being added. Continuous media exchange, because the addition flow rate is orders of magnitude smaller than the recirculation flow rate, will result in a fully mixed system, so the fresh media exposure of the cells can be modeled straightforwardly. Batch exchange is also possible, unlike in the 6xRL Rev2, by sealing the recirculation pump while fresh media flushes the system. This system would also allow programmed feeding schedules, so that a set amount of media could be dosed at discrete times. This approach in general offers an easier system to model

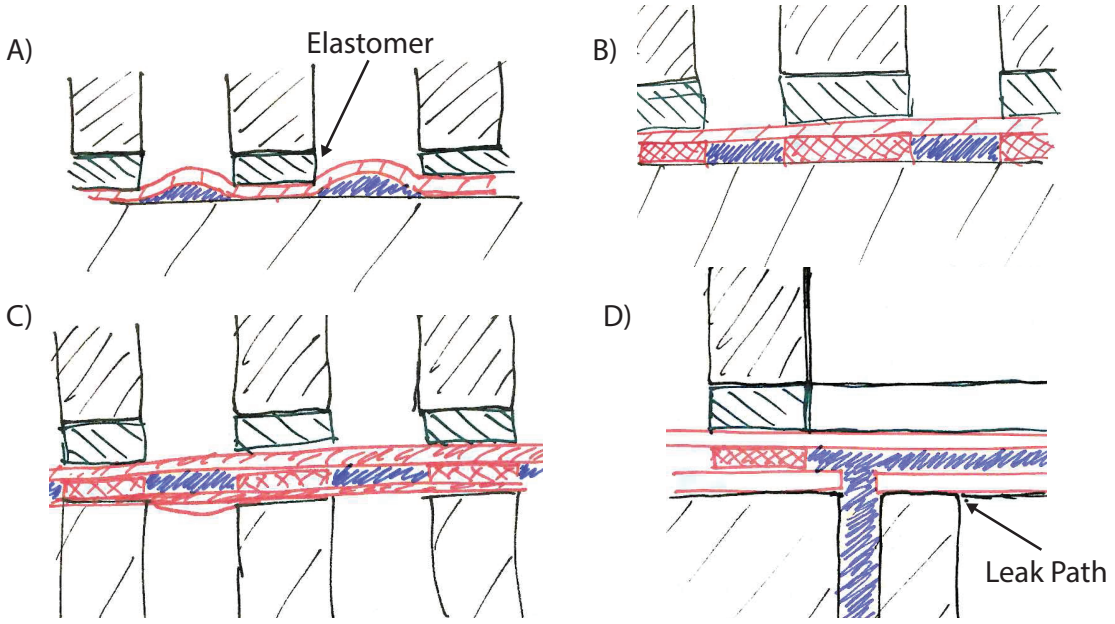

Figure 6-4: Membrane oxygenator cross sections with membrane shown in red and fluid in blue: *A)* The fluid path width is defined by a clamping plate with an elastomeric gasket to distribute pressure. The fluid path height is defined by deflection of the membrane under pressure. *B)* If the membrane is stiff relative to the path width, a spacer (crosshatched red) can be used. *C)* To halve the diffusion length and make a more compact oxygenator, a double-membrane method could be used. *D)* This double-membrane method does create a potential leak path that is challenging to seal by clamping alone.

than an open system, allowing biologists to answer questions that depend on these different dosing schemes. The inlet and outlet tubes are shown using standard HPLC fittings, but other connectors could work as well. In packing multiple replicates on a chip it may be advantageous to ensure that the effluent ports and the fresh media supply ports are on opposite sides of the platform if they have to connect to an external supply. Depending on packing and the relevant volumes, the reservoirs could also be on the platform itself.

MPS Cap

The MPS must be sealed for this to be a closed-volume system, but in the current seeding protocol, the hepatocytes are pipetted over the scaffold and allowed to settle. This protocol could be accommodated by using a sealing cap, with either a solid

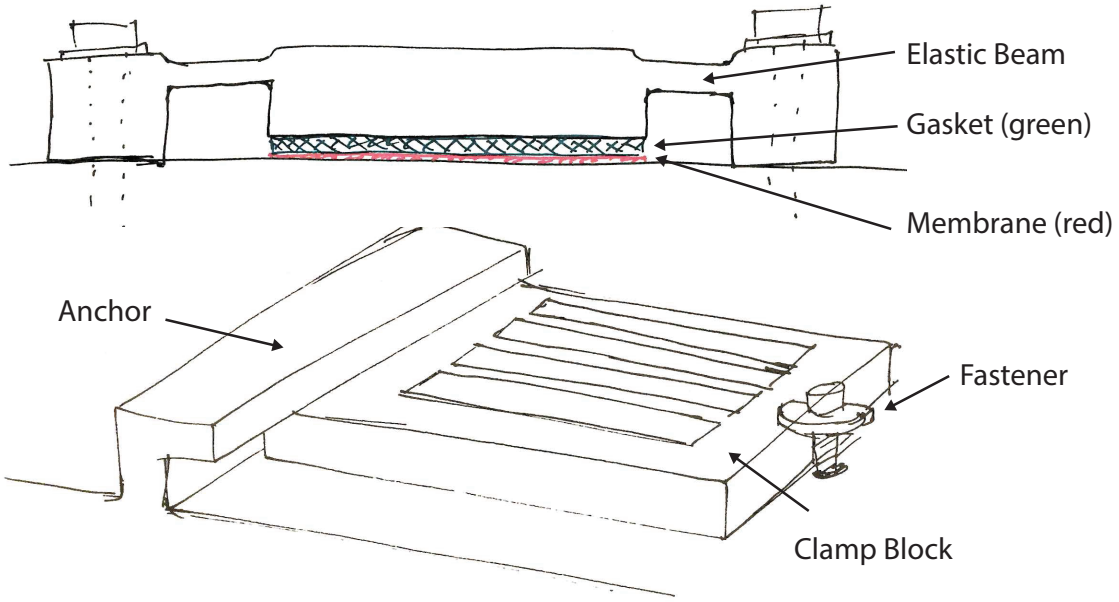

Figure 6-5: *Top)* A membrane (shown in red) could be clamped by a plate that has narrow elastic beams connecting to posts that are bolted to the platform. The beams would provide a spring element that would minimize bowing of the clamping plate, and an elastomer gasket above the membrane would distribute the force to provide an even sealing pressure to the membrane. *Right)* Such a clamping block, consisting of several bars that confine fluid flow to the empty regions, could also be secured by means of a fixed anchor at one end and an easy-to-use pivoting fastener (or multiple of these) at the other end.

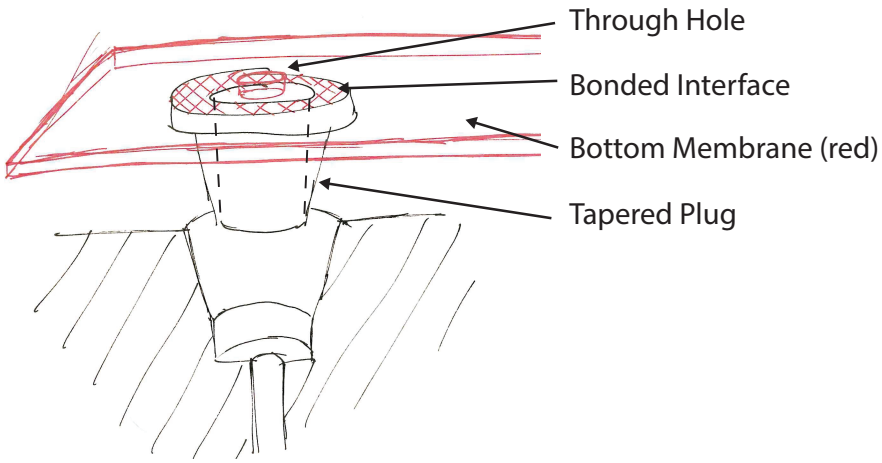

Figure 6-6: The lower membrane (shown in red) of a two-membrane oxygenator could potentially be bonded to a tapered plug, which would seal to the platform below. The top membrane could then be bonded or clamped to this bottom membrane. In a disposable platform, the membrane might be bonded directly to the lower platform. This depends on having a thermoplastic membrane material, such as polypropylene.

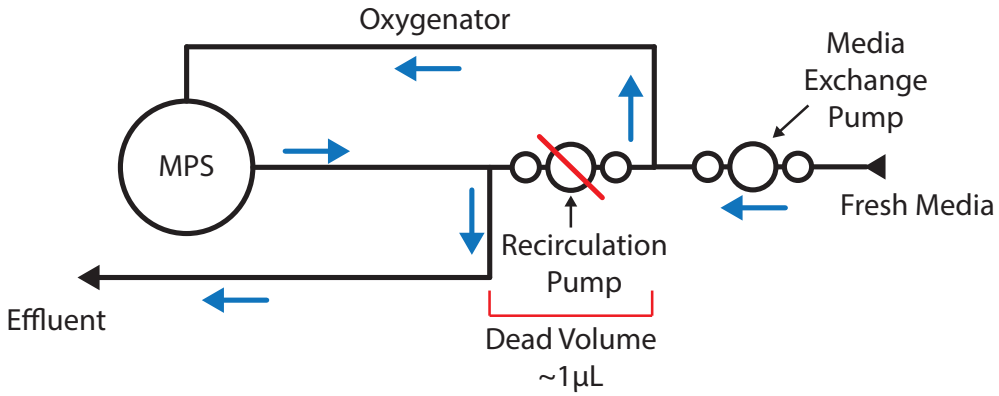

Figure 6-7: This media exchange configuration has media inlet and effluent on either side of the recirculation pump. To feed media in, all chambers of the recirculation pump are closed, blocking this path. The media exchange pump then adds the desired amount of media through the oxygenator path. If media is flushed through the system, the dead volume in the channels around the recirculation pump is on the order of 1 μL. This could also be eliminated by pumping backwards for one or two cycles. Some mixing between old and new media may occur in the MPS well.

surface or oxygenation membrane, that is placed into the well after the cells are seeded. Two example caps are shown in Figure 6-8, one which inserts downward, and another which slides from the side. It is important to ensure that the cap can be applied without introducing bubbles, and that any fluid displaced by the cap can exit either around the cap or out the effluent tube, so as not to creat flow or pressure pulses that could displace the cells. The hepatocytes sink fairly quickly, so we expect that either cap can safely be applied without significant risk of displacing the hepatocytes with the media, but it would be necessary to confirm this empirically.

6.3 Conclusions

The 6xRL platform described in this thesis offers one solution to the challenge of culturing relatively large numbers of hepatocytes in low fluid volumes. We conclude that while the 6xRL volume could be further reduced, achieving volumes much less than 400-500 μL while using the same scaffold may require a closed-volume approach

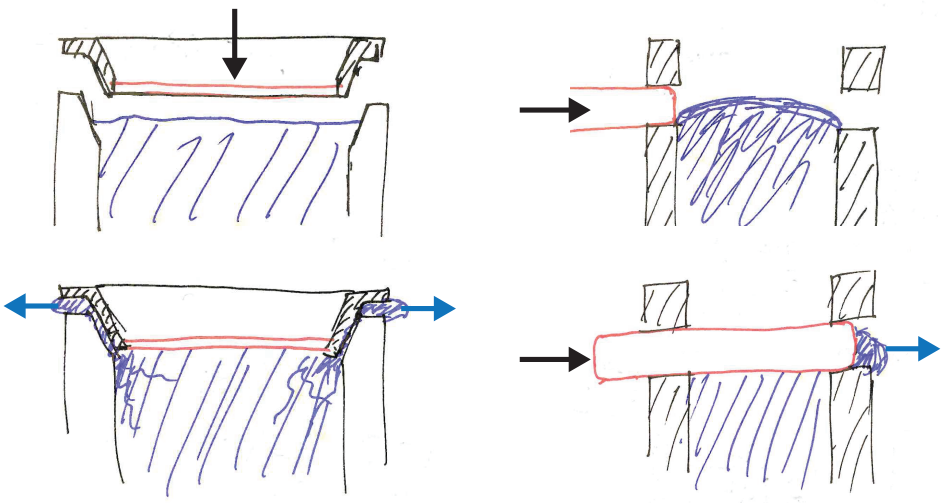

Figure 6-8: Caps for sealing the MPS volume after cells are added to the scaffold. *Left)* A cap that is inserted downward will displace fluid around the sides, which can be aspirated. Once seated, the cap will also push fluid out through the effluent channel, which must remain open. The cap seals in place by a locking taper (shown), screw threads, or a bayonet mount. *Right)* Alternatively, a sliding cap can cause less disturbance to the fluid, pushing a fluid front off the top as it slides in place.

as described above.

The spiral oxygenator offers a novel method for achieving adequate oxygenation at lower fluid volumes, and the downhill slope prevents the oxygenator from accumulating fluid and depleting the MPS well. It is resistant to physical disturbances and bubbles. It requires no extra parts and can be injection molded into a disposable platform.

In addition to documenting the development process of this oxygenator and the 6xRL platform, this thesis provides a broad concept-space to consult when considering oxygenator designs for other open-well fluidic applications, as well as methods for improved scaffold sealing without the use of elastomers. These ideas, combined with feedback from biological testing, will inform the design of future iterations of the reduced volume liver cell culture platform.

Bibliography

[1] S. W. Inman, "Development of a high throughput 3D perfused liver tissue bioreactor," Masters Thesis, Massachusetts Institute of Technology, 2006.

[2] K. Domansky, W. Inman, J. Serdy, A. Dash, H. M. Lim, and L. G. Griffith, "Perfused Multiwell Plate for 3D Liver Tissue Engineering," *Lab Chip*, no. 10, pp. 51–58, 2010.

[3] S. W. Inman, "Integration of Real Time Oxygen Measurements with a 3D Perfused Tissue Culture System," PhD Thesis, Massachusetts Institute of Technology, 2011.

[4] E.-M. Dehne, T. Hasenberg, and U. Marx, "The ascendance of microphysiological systems to solve the drug testing dilemma," *Future Science OA*, vol. 3, 2017. [Online]. Available: http://www.future-science.com/doi/pdf/10.4155/fsoa-2017-0002

[5] L. A. Low and D. A. Tagle, "Microphysiological Systems ("Organs-on-Chips") for Drug Efficacy and Toxicity Testing," *Clinical and Translational Science*, vol. 10, no. 4, pp. 237–239, jul 2017. [Online]. Available: http://www.ncbi.nlm.nih.gov/pmc/articles/PMC5504483/

[6] C. D. Edington, W. Li, K. Chen, E. Geishecker, T. Kassis, and L. R. Soenksen, "Interconnected Microphysiological Systems for Quantitative Biology and Pharmacology Studies," *Scientific Reports*, In Press.

[7] Z. Tao and P. P. Ghoroghchian, "Microparticle, nanoparticle, and stem cell-based oxygen carriers as advanced blood substitutes," *Trends in Biotechnology*, vol. 32, no. 9, pp. 466–473, 2014. [Online]. Available: http://dx.doi.org/10.1016/j.tibtech.2014.05.001

[8] F. T. Barbosa, M. J. Jucá, A. A. Castro, J. L. Duarte, and L. T. Barbosa, "Artificial oxygen carriers as a possible alternative to red cells in clinical practice," *Sao Paulo Medical Journal*, vol. 127, no. 2, pp. 97–100, 2009.

[9] P. E. Oomen, M. D. Skolimowski, and E. Verpoorte, "Implementing oxygen control in chip-based cell and tissue culture systems," *Lab Chip*, vol. 16, no. 18, pp. 3394–3414, 2016. [Online]. Available: http://xlink.rsc.org/?DOI=C6LC00772D

[10] A. A. Gimbel, E. Flores, A. Koo, G. García-Cardeña, and J. T. Borenstein, "Development of a biomimetic microfluidic oxygen transfer device," *Lab Chip*, vol. 16, no. 17, pp. 3227–3234, 2016. [Online]. Available: http://xlink.rsc.org/?DOI=C6LC00641H

[11] D. M. Hoganson, H. I. Pryor II, E. K. Bassett, I. D. Spool, and J. P. Vacanti, "Lung assist device technology with physiologic blood flow developed on a tissue engineered scaffold platform," *Lab Chip*, vol. 11, no. 4, pp. 700–707, 2011. [Online]. Available: http://xlink.rsc.org/?DOI=C0LC00158A

[12] R. H. W. Lam, M.-C. Kim, and T. Thorsen, "A Microfluidic Oxygenator for Biological Cell Culture," in *Transducers and Eurosensors*, 2007, pp. 2489–2492.

[13] A. P. Vollmer, R. F. Probstein, R. Gilbert, and T. Thorsen, "Development of an integrated microfluidic platform for dynamic oxygen sensing and delivery in a flowing medium," *Lab Chip*, pp. 1059–1066, 2005.

[14] M. Busek, S. Gruenzner, T. Steege, F. Schmieder, U. Klotzbach, and F. Sonntag, "Design, characterization, and modeling of microcirculation systems with integrated oxygenators," *Journal of Sensors and Sensor Systems*, vol. 5, no. 1, pp. 221–228, 2016.

[15] M. W. Toepke and D. J. Beebe, "PDMS absorption of small molecules and consequences in microfluidic applications," *Lab on a Chip*, vol. 6, no. 12, p. 1484, 2006. [Online]. Available: http://xlink.rsc.org/?DOI=b612140c

[16] W.-I. Wu, N. Rochow, E. Chan, G. Fusch, A. Manan, D. Nagpal, P. R. Selvaganapathy, and C. Fusch, "Lung assist device: development of microfluidic oxygenators for preterm infants with respiratory failure," *Lab on a Chip*, vol. 13, no. 13, p. 2641, 2013. [Online]. Available: http://xlink.rsc.org/?DOI=c3lc41417e

[17] J. Blackie, P. Wu, and D. Naveh, *Membrane Oxygenation of Mammalian Cell Culture Fermenters Using Dupont Teflon AF-2400 Tubing*. Dordrecht: Springer Netherlands, 2002, pp. 299–301. [Online]. Available: https://doi.org/10.1007/0-306-46875-1{_}66

[18] T. L. Place, F. E. Domann, and A. J. Case, "Limitations of oxygen delivery to cells in culture: An underappreciated problem in basic and translational research," *Free Radical Biology and Medicine*, vol. 113, no. October, pp. 311–322, 2017. [Online]. Available: https://doi.org/10.1016/j.freeradbiomed.2017.10.003

[19] W. Inman, K. Domansky, J. Serdy, B. Owens, D. Trumper, and L. G. Griffith, "Design, modeling and fabrication of a constant flow pneumatic micropump," *Journal of Micromechanics and Microengineering*, vol. 17, no. 5, pp. 891–899, 2007.

[20] J. A. Potkay, "The promise of microfluidic artificial lungs," *Lab Chip*, no. August, 2014. [Online]. Available: http://dx.doi.org/10.1039/C4LC00828F

[21] P. Concus and R. Finn, "On the behavior of a capillary surface in a wedge," *Proceedings of the National Academy of Sciences of the United States of America*, vol. 63, no. 2, pp. 292–299, 1969.

[22] J. Berthier, K. A. Brakke, and E. Berthier, "A general condition for spontaneous capillary flow in uniform cross-section microchannels," *Microfluid Nanofluid*, no. 16, pp. 779–785, 2014.

[23] J. F. Oliver, C. Huh, and S. G. Mason, "Resistance to spreading of liquids by sharp edges," *Journal of Colloid and Interface Science*, vol. 59, no. 3, pp. 568–581, may 1977. [Online]. Available: file: //www.sciencedirect.com/science/article/pii/0021979777900522

[24] E. M. Liston, L. Martinu, and M. R. Wertheimer, "Plasma surface modification of polymers for improved adhesion: a critical review," *Journal of Adhesion Science and Technology*, vol. 7, no. 10, pp. 1091–1127, jan 1993. [Online]. Available: https://doi.org/10.1163/156856193X00600

[25] K. Asano, *Mass transfer: from fundamentals to modern industrial applications*. Weinheim: Wiley-VCH, 2006.

[26] L. R. Glicksman and J. H. V. Lienhard, *Modeling and Approximation in Heat Transfer*. New York: Cambridge University Press, 2016.

[27] M. Ruiz-Peña, R. Oropesa-Nuñez, T. Pons, S. R. W. Louro, and A. Pérez-Gramatges, "Physico-chemical studies of molecular interactions between non-ionic surfactants and bovine serum albumin," *Colloids and Surfaces B: Biointerfaces*, vol. 75, no. 1, pp. 282–289, 2010.

[28] N. Tygstrup, K. Winkler, K. Mellemgaard, and M. Andreassen, "Determination of the Hepatic Arterial Blood Flow and Oxygen Supply in Man by Clamping the Hepatic Artery During Surgery," *Journal of Clinical Investigation*, vol. 41, no. 3, pp. 447–454, 1962.

[29] P. F. Bruning, K. M. Jonker, and A. W. Boerema-Baan, "Adsorption of steroid hormones by plastic tubing," *Journal of Steroid Biochemistry*, vol. 14, no. 6, pp. 553–555, 1981.

[30] S. Smith, B. Norris, and L. Peebles, *Older Adult Data: the Handbook of Measurements and Capabilities of the Older Adults: Strength Data for Design Safety*. London: Department of Trade and Industry, 2002.

[31] R. Guo, X. Xu, Y. Lu, and X. Xie, "Physiological oxygen tension reduces hepatocyte dedifferentiation in in vitro culture," *Scientific Reports*, vol. 7, no. 1, pp. 1–9, 2017. [Online]. Available: http://dx.doi.org/10.1038/s41598-017-06433-3

[32] A. Barton, "Rubber Bearings For Precision Positioning Systems," Masters, Massachusetts Institute of Technology, 2005.

[33] B. Bushan, "Development of electro-magnetic pump and hardware for human physio-mimetic platforms," Masters, Massachussetts Institute of Technology, 2018.

[34] R. Balgobin, "Bubble-free oxygen and carbon dioxide mass transfer in bioreactors using microporous membranes," Masters, University of Western Ontario, 2012.

[35] C. Wang, H. Lu, and M. A. Schwartz, "A novel in vitro flow system for changing flow direction on endothelial cells," *Journal of Biomechanics*, vol. 45, no. 7, pp. 1212–1218, apr 2012. [Online]. Available: http://www.ncbi.nlm.nih.gov/pmc/articles/PMC3327813/

[36] T. P. Maxwell, "Passive Gas-Liquid Separation Using Hydrophobic Porous Polymer Membranes: A Study on the Effect of Operating Pressure on Membrane Area Requirement," Masters, University of North Florida, 2012.

[37] R. Wenger, V. Kurtcuoglu, C. Scholz, H. Marti, and D. Hoogewijs, "Frequently asked questions in hypoxia research," *Hypoxia*, vol. 3, p. 35, 2015. [Online]. Available: https://www.dovepress.com/frequently-asked-questions-in-hypoxia-research-peer-reviewed-article-HP

[38] R. Sander, "Compilation of Henry's law constants (version 4.0) for water as solvent," *Atmospheric Chemistry and Physics*, vol. 15, no. 8, pp. 4399–4981, 2015. [Online]. Available: https://www.atmos-chem-phys.net/15/4399/2015/

Appendix A

Oxygen Saturation

A.1 Oxygen Partial Pressure

The partial pressure of oxygen in the incubator—and therefore the dissolved oxygen concentration in the media—depends on ambient total pressure and the partial pressures of other gases present, such as CO_2 and water vapor. These calculations assume the media is water, and follow Wenger et al. [37], except that the humidity in the incubators is near 80% relative humidity. The saturation vapor pressure at 37 °C is 6.28 kPa and and the room oxygen content is 20.9% by volume [37]. Incubator CO_2 is regulated at 5%, and atmospheric pressure is assumed to be 101.3 kPa. The water vapor partial and CO_2 pressure are therefore

$$P_{\mathrm{H_2O}_g} = (80\%)6.28\ [\mathrm{kPa}] = 5.024\ [\mathrm{kPa}] \tag{A.1}$$

$$P_{\mathrm{CO}_2} = (5\%)101.3\ [\mathrm{kPa}] = 5.065\ [\mathrm{kPa}]. \tag{A.2}$$

The balance of the partial pressures is taken up by oxygen and nitrogen, in the same ratio as outside the incubator. The oxygen partial pressure in an incubator at 80% humidity, 5% CO_2, 1 atm, and 37 °C is then

$$P_{\mathrm{O}_2} = (20.9\%)(101.3 - 5.065 - 5.024)\ [\mathrm{kPa}] = 19.1\ [\mathrm{kPa}]. \tag{A.3}$$

A.2 Dissolved Oxygen Concentration

Henry's law relates the aqueous concentration C_{aq} of a gas to the partial pressure P by a constant $H^{(cp)}$:

$$C_{aq} = H^{cp} \times P. \tag{A.4}$$

This constant H^{cp} is temperature dependent, and can be calculated [38] by

$$H^{cp} = H_{ref} \times \exp\left[1700\left(\frac{1}{T} - \frac{1}{T_{ref}}\right)\right], \tag{A.5}$$

where

$$H_{ref} = 1.3 \times 10^{-3}\ \left[\frac{\mathrm{M}}{\mathrm{atm}}\right] = 12.8 \times 10^{-6}\ \left[\frac{\mathrm{M}}{\mathrm{kPa}}\right] \tag{A.6}$$

$$T_{ref} = 298\ [\mathrm{K}] \tag{A.7}$$

The saturated concentration of dissolved oxygen in water at 37 °C (310 K) is therefore

$$C_{sat} = 10.2\ \left[\frac{\mu\mathrm{M}}{\mathrm{kPa}}\right] \times 19.1\ [\mathrm{kPa}] = 195\ \mu\mathrm{M}. \tag{A.8}$$

Appendix B

Fourier Number and One-Term Model

The equations describing diffusion of heat through a solid of uniform properties can be used by analogy to characterize mass diffusion. For unsteady heat transfer in one dimension, without heat generation, the temperature profile in a material of uniform thermal diffusivity α is described by the heat equation:

$$\frac{\partial T}{\partial t} = \alpha \frac{\partial^2 T}{\partial x^2} \tag{B.1}$$

For mass transfer, the analogous one-dimensional equation without species formation is known as Fick's Second Law:

$$\frac{\partial C}{\partial t} = D \frac{\partial^2 C}{\partial x^2} \tag{B.2}$$

where D is the diffusivity of the relevant species in the specific medium ($D_{O_2} = 3 \times 10^{-3} [\frac{\text{mm}^2}{\text{s}}]$ is the diffusion coefficient for oxygen in water at 37 °C).

Non-dimensionalizing with the characteristic time τ, depth h, and saturation and

intitial concentrations C_{sat} and C_o yields

$$t^* = \frac{t}{\tau}, \tag{B.3}$$

$$x^* = \frac{x}{h}, \tag{B.4}$$

$$\Phi = \frac{C - C_{sat}}{C_o - C_{sat}}. \tag{B.5}$$

Note that Φ is distinct from ϕ, the oxygenation potential, and

$$\phi = 1 - \Phi. \tag{B.6}$$

The non-dimensionalized diffusion equation is then

$$\frac{\partial \Phi}{\partial t^*} = \frac{D\tau}{h^2} \frac{\partial^2 \Phi}{\partial x^{*2}}. \tag{B.7}$$

The non-dimensional cluster $\frac{D\tau}{h^2}$ is known as the Fourier number, notated for mass transfer here as Fo_m. The Fourier number describes the ratio of the diffusive transport rate ($\frac{D}{h^2}$) to the species storage rate ($\frac{1}{\tau}$). For the oxygenator described in Chapter 2, the relevant time is the advection time constant τ_a

$$\mathrm{Fo}_m = \frac{D_{O_2}\tau_a}{h^2} = \frac{D_{O_2}A}{2Qh} = \frac{Dw}{2Qh}L \tag{B.8}$$

where A is the gas-liquid interface area, w is the interface width, Q is the oxygenator flow rate, and L is the oxygenator length. The factor of two comes from the triangular cross-section.

Glicksman and Lienhard [26] describe the normalized average temperature Θ using a one-term approximation of the Fourier series that describes the developing concentration profile for a rectangular slab:

$$\bar{\Theta} = \frac{\bar{T} - T_\infty}{T_o - T_\infty} = D_1 e^{-\lambda_1 \mathrm{Fo}} \tag{B.9}$$

where D_1 and λ_1 are coefficients that depend on the Biot number Bi, which describes

the ratio of the heat transfer rates outside and inside the medium of interest. In the case of oxygen mass transfer, the rate of oxygen transport through air is orders of magnitude greater than that through water, so the Biot number is essentially infinite, meaning that the concentration at the liquid surface is instantaneously brought to saturation. We can similarly define a normalized averate concentration,

$$\bar{\Phi} = \frac{\bar{C} - C_{sat}}{C_o - C_{sat}}, \tag{B.10}$$

where $\bar{C}$ is a concentration spatially averaged from the interface at $x = 0$ to the opposite wall at $x = h$. Drawing an analogy between $\bar{\Theta}$ and $\bar{\Phi}$, and using the tabulated coefficients [26] for Bi$\rightarrow \infty$ and plate geometry,

$$\bar{\Phi} = \frac{\bar{C} - C_{sat}}{C_o - C_{sat}} = 0.8106e^{-2.47\mathrm{Fo}_m}. \tag{B.11}$$

Using equation B.6 the oxygenation potential of the oxygenator is then

$$\phi = \frac{\bar{C} - C_o}{C_{sat} - C_o} = 1 - 0.8106e^{-2.47\mathrm{Fo}_m}. \tag{B.12}$$

For a very large Biot number, Glicksman and Lienhard suggest that the one-term approximation is appropriate for a Fourier number above 0.2. For the PSU spiral oxygenator flowing at 1 μL/s,

$$\mathrm{Fo}_m = \frac{Dw}{2Qh}L \approx \frac{(3 \times 10^{-3})(1)}{2(1)(0.3)} \times L \tag{B.13}$$

$$\mathrm{Fo}_m = 0.2 \Rightarrow L \approx 40 \text{ [mm]}. \tag{B.14}$$

For an oxygenator length of 175 mm, this suggests that the one-term solution is appropriate for approximately 77% of the length.

Appendix C

LiverChip Oxygenation Measurement

To measure oxygen consumption rates on the CN Bio LiverChip platform, we designed and fabricated a custom lid that holds fiber optic probes (Lucid Scientific, Atlanta, GA) submerged in the tail and 1 mm above the scaffold. To protect the oxygen probes during sterilization, we assembled an acrylic shield, shown in Figure C-1.

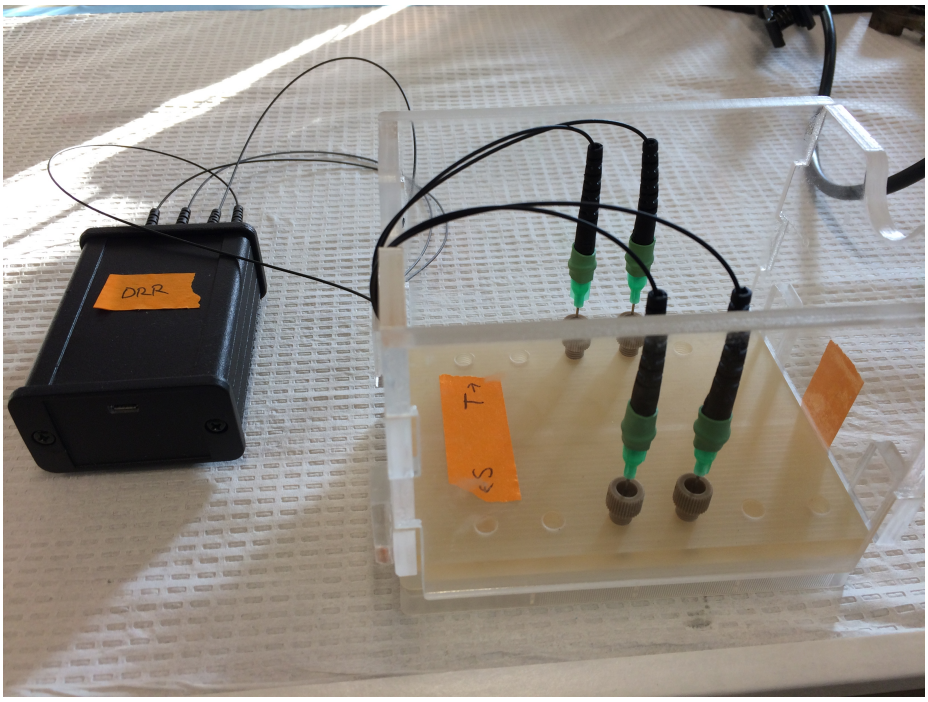

Figure C-1: A simple lid holds oxygen probes at the proper position and depth with HPLC ferrule fittings. An acrylic shield prevents bending or other damage to the probes during ETO sterilization of the assembly shown.

Rat hepatocytes (250k) were seeded on the LiverChip, and assembled with the custom lid. The oxygen readings over time are shown in Figure C-2. This was a simple pilot test of only one channel to validate the sterilization process of the oxygenation lid and obtain a ballpark figure for the consumption rates.

1 kPa partial pressure in the incubator environment corresponds to 10.2 μM (see Appendix A). Multiplying the concentration differences between tail and scaffold by the flow rates, we see an oxygen consumption rate of approximately 100 pmol/s. Two ubsequent measurements of 600k human hepatocytes from two different donors showed a consumption rate of approximately 60 and 80 pmol/s (unpublished data).

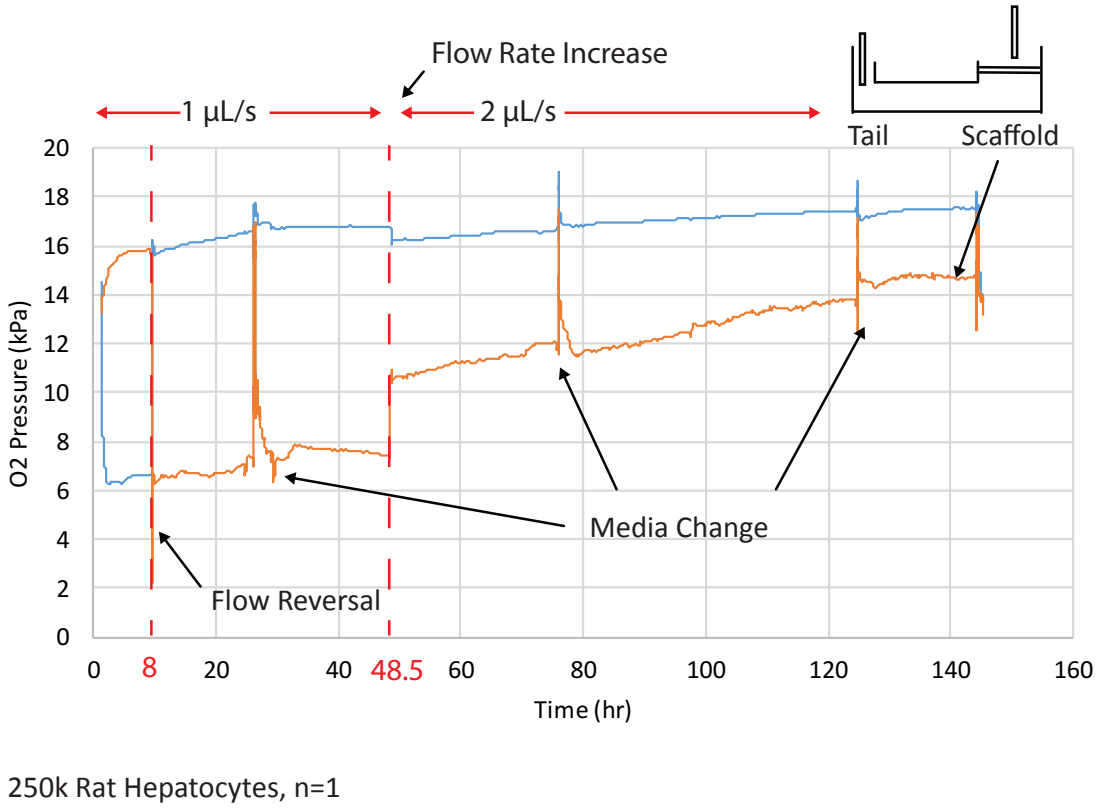

Figure C-2: Oxygenation measurments from one well of the LiverChip with 250k Rat hepatocytes. Flow was downward through the scaffold for the first 8 hours, then reversed to flow upward for the remainder of the experiment. After 48.5 hrs, the flow rate was increased to 2 μL/s.